Okura Wēiti Marine Receiving Environment Modelling

Calibration Report – Hydrodynamics, Waves, Sediment Transport and Metal Accumulation Models

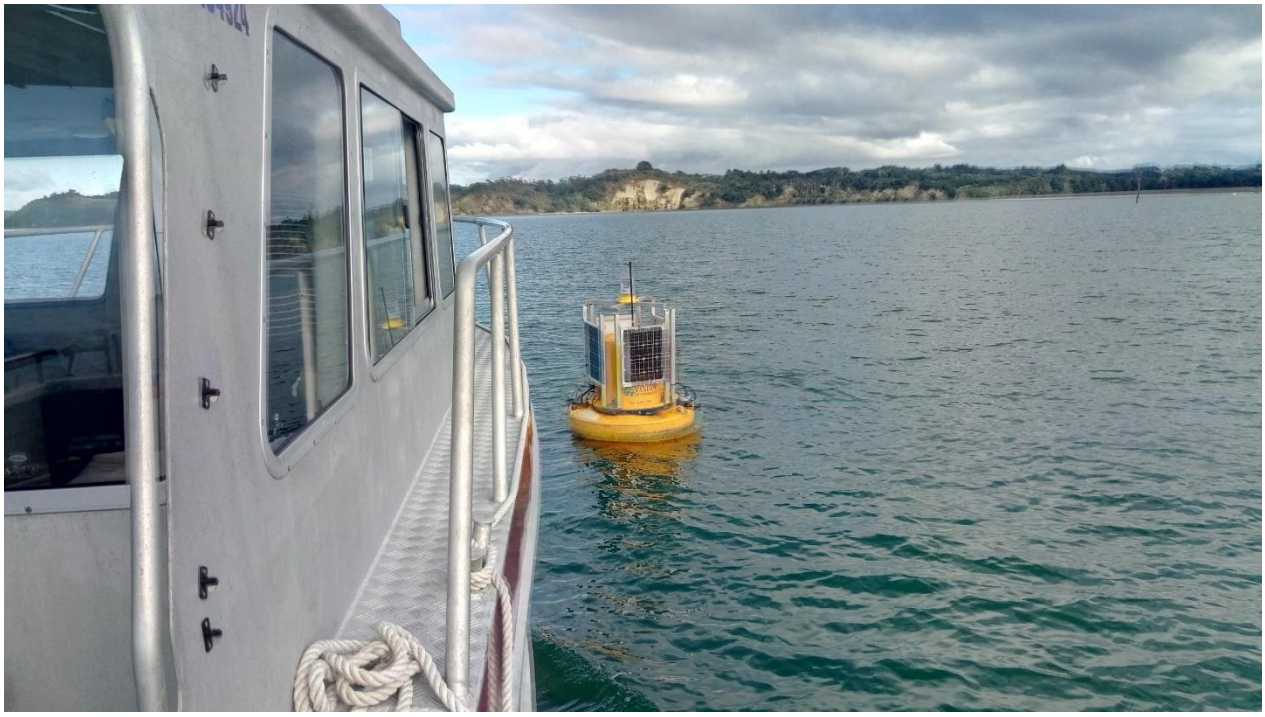

Auckland Council

Report 44801163/03

June 2019

Okura Wēiti Marine Receiving Environment Modelling

Calibration Report – Hydrodynamics, Waves, Sediment Transport and Metal Accumulation Models

Prepared for	Auckland Council
Represented by	Tom Porter

Instrument buoy, Vision Environment

Project manager	John Oldman

Project number	44801163
Approval date	12th June 2019
Revision	Final

DHI Water and Environment Ltd• B:HIVE, Smales Farm• Takapuna 0622 Auckland• New Zealand•
Telephone: +64 9 912 9638 • Telefax: • info.nz@dhigroup.com• www.dhigroup.com

CONTENTS

1 Introduction

There is pressure for significant future development within the catchments which surround the Wēiti and Okura estuaries to have an accumulative effect on the marine receiving environment which, to date, has not been studied in detail. The ecology value of the area is recognised by the creation of the Long Bay - Okura Marine Reserve and its designation as a Significant Ecological Area Marine 1 in the Auckland Unitary Plan.

Previous studies have focused on development within the Okura catchment and its potential ecological effects within Okura estuary itself. There has been limited work to date to assess the potential for combined effects of future developments within the Okura and Wēiti catchments. In addition, previous sediment transport models have not included a wave model and have been used to model schematic events (i.e. constant freshwater flow and suspended sediment concentrations at catchment outlets and fixed tide range and wind speeds and directions).

In this context, Auckland Council (AC) commissioned DHI to undertake the numerical modelling of hydrodynamics, waves and sediment transport in Karepiro Bay and the Wēiti and Okura estuaries, to assess the impact of future development on the marine receiving environment. For this purpose, input data derived from the Freshwater Management Tool (FWMT) developed by Morphum Environment (ME) were used to feed the coastal numerical models. *In situ* data collected by Vision Environment (VE) and presented in (DHI, 2018) were compared to the model outputs to quantify the confidence in the predictions of the marine receiving environment models.

This report describes the numerical modelling approach applied for this study and provides the results of the validation process for the existing level of development in the catchment and current land use (Table 1-1). Details of the scenarios are provided in Morphum Environment (2019).

A further report will be provided which summarises the marine receiving environment model results for Scenarios 1-14 in the context of the Existing Development within the catchment (Scenario 0, Table 1-1).

Table 1-1. FWMT scenario conditions modelled.

	Scenario description	Long Bay Structure Plan Development	Wēiti Bay Growth Area Development	Future Growth Area Development
Scenario 0	Land use prior to recent development within Long Bay	✗	✗	✗
Scenario 1	Completion of Long Bay Structure Plan development (2017-2018)	✓	✗	✗
Scenario 2	550 home Wēiti Bay Development	✓	550 home	✗
Scenario 3	1200 home Wēiti Bay Development	✓	1200 home	✗
Scenario 4	Future Growth Development	✓	✗	✓
Scenario 5	Future Growth + 550 Wēiti Bay Development	✓	550 home	✓
Scenario 6	Future Growth + 1200 Wēiti Bay Development	✓	1200 home	✓
Scenario 7	Scenario 6 with less Cu/Zn build-up wash-off	✓	1200 home	✓
Scenario 8	Scenario 6 more Cu/Zn build-up wash-off	✓	1200 home	✓
Scenario 11	Scenario 5 with inert roofing materials Wēiti Bay	✓	550 home	✓
Scenario 12	Scenario 6 with inert roofing materials Wēiti Bay	✓	1200 home	✓
Scenario 13	Scenario 5 with inert roofing materials Wēiti Bay and Future Growth	✓	550 home	✓
Scenario 14	Scenario 6 with inert roofing materials Wēiti Bay and Future Growth	✓	1200 home	✓

2 Methodology

This section describes the methodology applied to undertake the hydrodynamic, wave, sediment transport and metal accumulation models. It details the numerical model modelling strategy, model domain and bathymetry, boundary conditions, atmospheric forcing, river discharges, sediment loads and sea bed characteristics.

2.1 Numerical Model

The MIKE 21 & 3 systems were used in this study to simulate the wave, hydrodynamic and sediment transport processes. For this purpose, four modules were coupled on a unique unstructured mesh grid to simulate the numerous interactions between the physics and the morphodynamics. For coastal areas such as estuaries or bays, unstructured mesh grids provide an optimal degree of flexibility in the representation of complex geometries. It allows increasing the computational resources on areas where more precision is required, while also maintaining an acceptable level of details elsewhere in the domain.

The Hydrodynamic Module (HD) included in MIKE 3 (DHI, 2017a) was used to simulate the three-dimensional (3D) flows, surface elevation, sea temperature and salinity over the domain solving the 3D incompressible Reynolds-averaged Navier-Stokes equations subject to the assumptions of Boussinesq and of hydrostatic pressure. The model consists of continuity, momentum, temperature, salinity and density equations and it is closed by a turbulent *k-epsilon* closure scheme.

The Spectral Wave Module (SW) was applied to simulate the generation and propagation of waves from the global scale to the local scale. MIKE 21 SW captures the following physical processes:

- Wave growth by wind action
- Non-linear wave-wave interaction
- Dissipation due to whitecapping, bottom friction and depth-induced wave breaking
- Refraction and shoaling due to depth variations
- Wave-current interactions
- Effect of time-varying water depth

Further details about the SW module are provided in (DHI, 2017b).

The transport of cohesive fine-sand, silt and clay particles is modelled in the present study using the Mud Transport (MT) module (DHI, 2017c). This add-on module to MIKE 3 allows simulating the processes of flocculation, hindered settling and consolidation while calculating the rates of erosion, deposition and resuspension of fine particles under current and wave actions. This tool is particularly well-adapted for areas where the suspended riverine silt particles enter the ocean characterised by increasing water depths, multi-directional waves and currents.

2.2 Modelling Approach

The numerical model has been first calibrated against measurements of water elevations, currents, waves and bed changes in Karepiro Bay between March and July 2018. The main

purpose was to determine the capability of the model in capturing the dominant coastal processes. Because of the lack of information regarding the existing sea bed characteristics, the initial thickness of the sea bed was determined using a morphological spin-up simulation to distribute the sediments based on the forcing represented in the model.

Once calibrated, the model was set up without any initial bed thickness over the domain to examine the riverine sediment deposition process only over a 6-month period (January – June 2018). The choice of the period has been made based on an analysis of winds, predicted freshwater inflows and contaminant loads delivered to the system.

2.3 Model Domain and Bathymetry

The model domain covers the entire Hauraki Gulf.

The mesh grid used in MIKE 21 SW and MIKE 3 is composed of 14,916 triangular elements relatively coarse in both the northern and the eastern regions of the domain and refined in Karepiro Bay, Okura River and Wēiti River (Figure 2-1). A 43 km wide open boundary has been applied between Takatu Point and Port Jackson on the western and eastern sides of the Hauraki Gulf entrance, respectively.

The model bathymetry has been generated combining chart data from C-MAP (DHI, 2017d) and 2013 Auckland Council LIDAR data. A classic linear method has been used to interpolate the Chart Datum referenced water depths on the triangular mesh-grid. Details of the model bathymetry within both the Hauraki Gulf and the Karepiro Bay are shown in Figure 2-2.

The water depth varies from 50 m at the open-ocean boundary to 4 m at the entrance to Karepiro Bay. The western margin of the Karepiro Bay is characterised by relatively wide inter-tidal areas. Alternating inter-tidal areas and shallow margin channels compose both the Okura Estuary and the Wēiti Rivers.

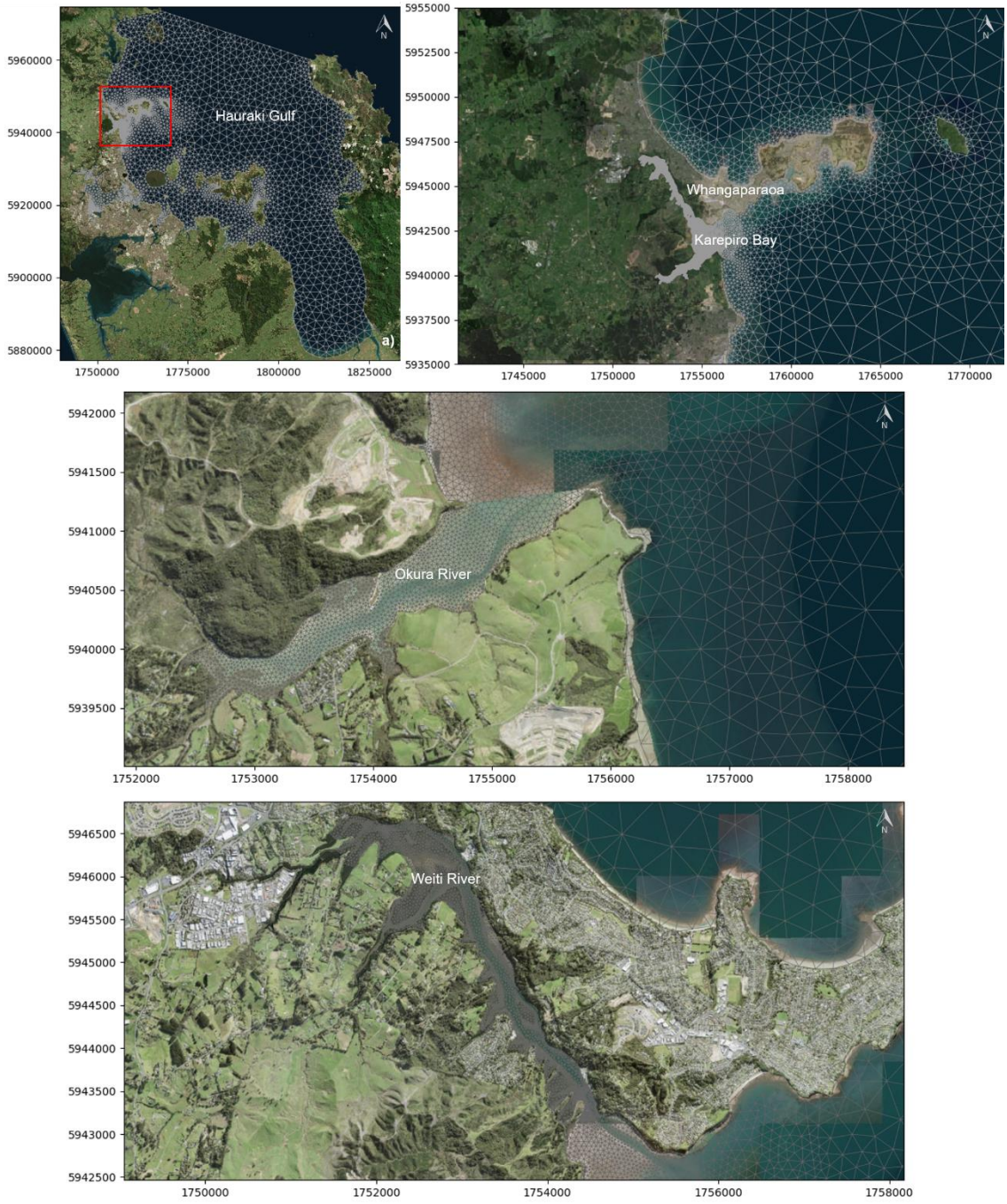

Figure 2-1. Triangular mesh grid used in MIKE 3 to simulate wave, hydrodynamic and sediment transport processes. Top left panel shows full extent of grid, top right shows detailed grid around Long Bay/Whangaparoao. Middle panel shows detailed grid within the Okura estuary and the bottom panel shows the detailed grid within the Wēiti River.

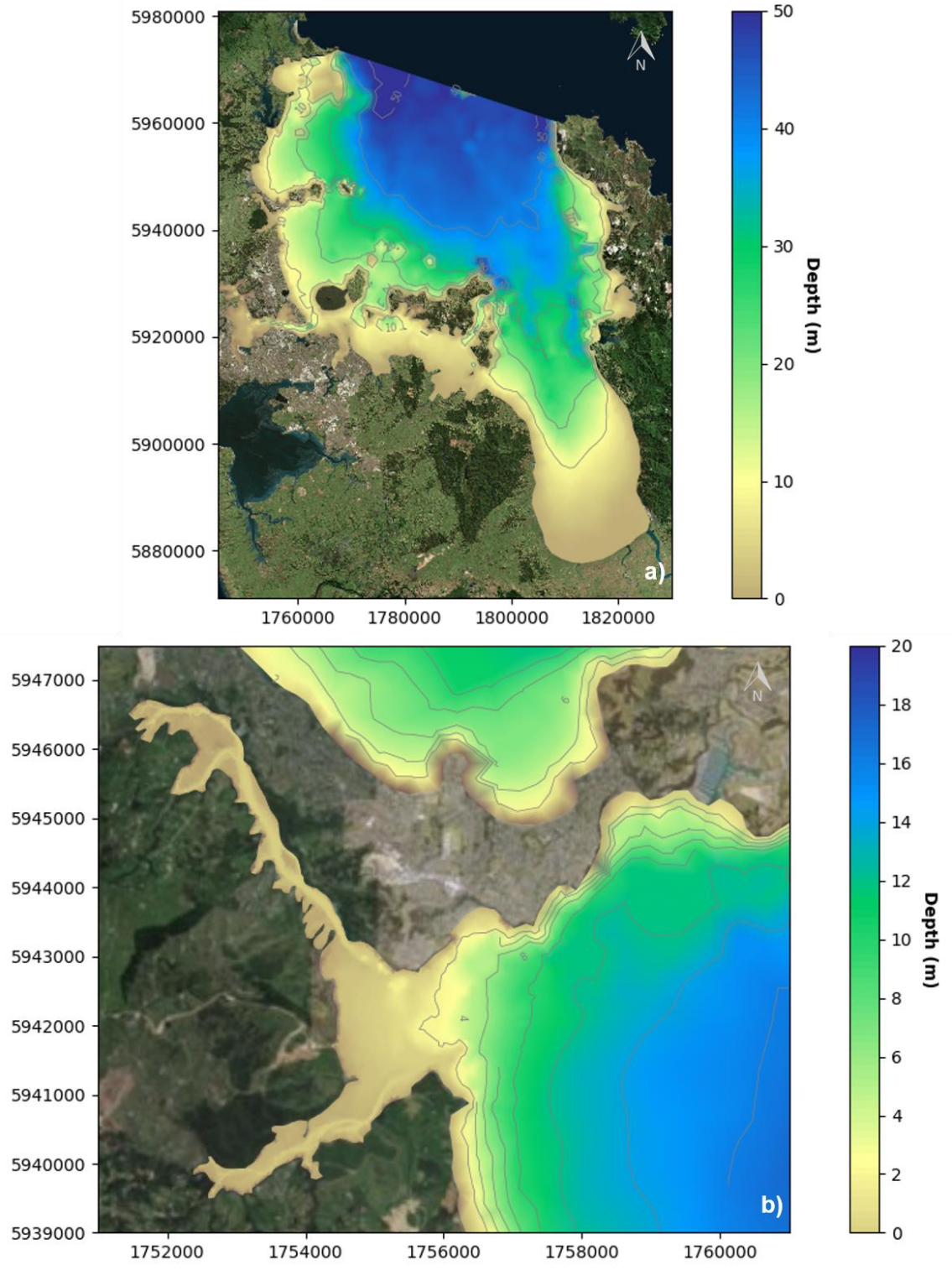

Figure 2-2. Bathymetry (Chart Datum) over the entire model domain (top panel) and within Karepiro Bay (bottom panel) and the Okura and Wēiti Rivers.

2.4 Wind Forcing

Regional 6-hourly nowcast surface winds (supplied by WeatherRadar) were applied to force both the hydrodynamic and the wave models. Comparisons between this product and wind measurements at Whangaparaoa and Whenuapai have been presented in DHI (2018). The results showed the spatial variability of the wind speed was well represented in the dataset. However, the model wind direction exhibited a slight shift in the prevailing direction that might influence the local hydrodynamics and waves. The mean, 90th percentile and 99th percentile of the spatial surface wind field calculated between 01/01/2018 and 01/10/2018 are presented in Figure 2-3. Model wind statistics, timeseries and wind rose are provided at Whangaparaoa in Table 2-1, Figure 2-4 and Figure 2-5.

As shown in Figure 2-3, the model wind field exhibits a notable spatial variability over the Hauraki Gulf caused by the complex topography. Such results justify the use of spatial wind field for the numerical modelling rather than space-constant measured wind data. At Whangaparaoa, the mean and maximum wind speed between 01/01/2018 and 01/10/2018 is 5.69 m/s and 17.24 m/s, respectively. Prevailing winds come from the south-western direction while the strongest wind events are dominated by wind directions in the north-eastern quadrant.

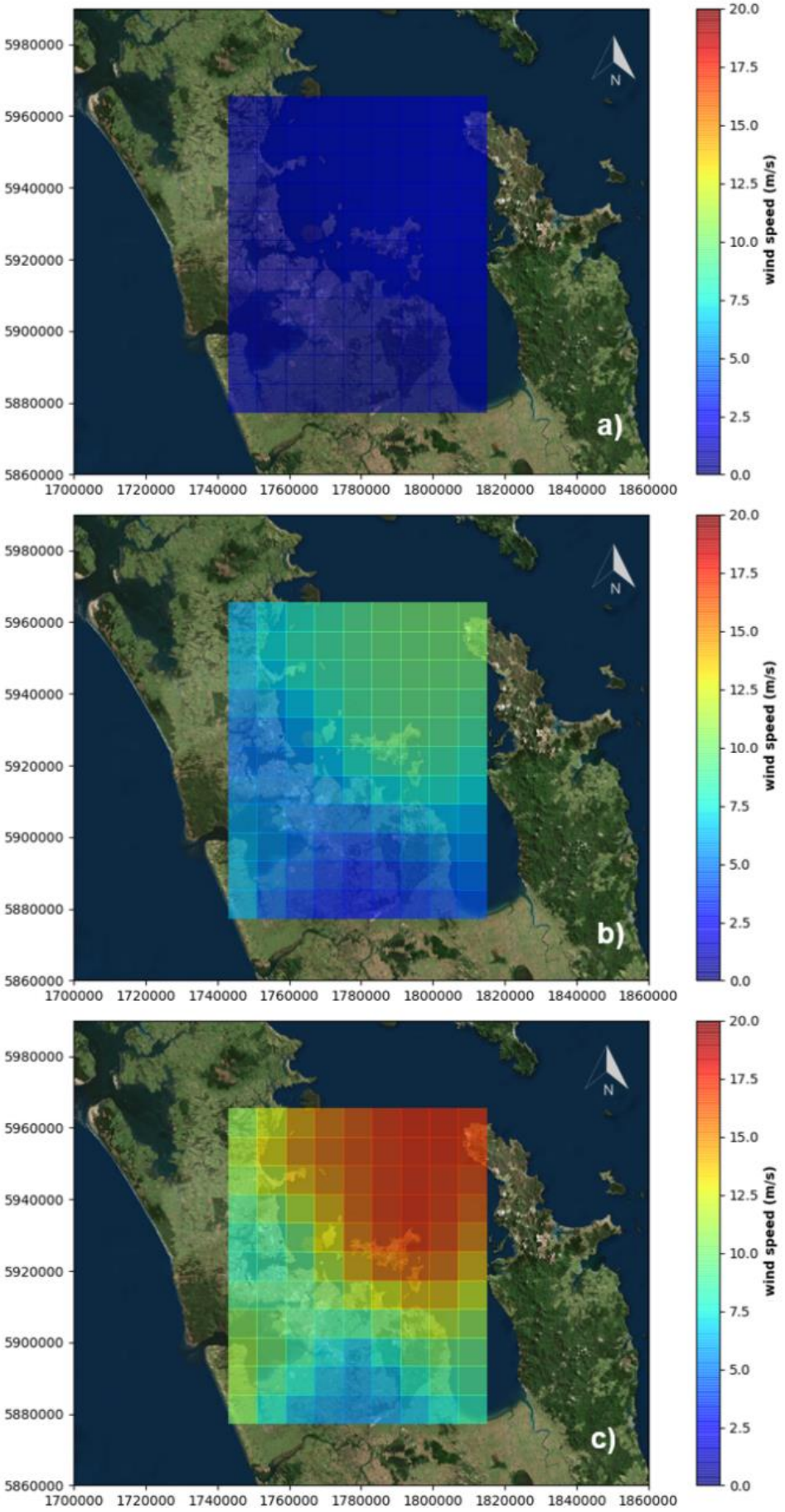
5980000
5960000
5940000
5920000
5900000
5880000
5860000
1700000 1720000 1740000 1760000 1780000 1800000 1820000 1840000 1860000
N
a)
b)
c)
20.0
17.5
15.0
12.5
10.0
7.5
5.0
2.5
0.0
wind speed (m/s)

Figure 2-3 Map showing the mean (a), percentile 90th (b) and percentile 99th (c) of the wind speed field extracted from the nowcast dataset between January and October 2018.

Table 2-1 Wind statistics at Whangaparaoa between January and October 2018.

Wind speed statistics	
(m/s)	
Mean	5.69
Maximum	17.48
P25	3.51
P50	5.22
P75	7.42
P90	9.86
P95	11.14
P99	13.64

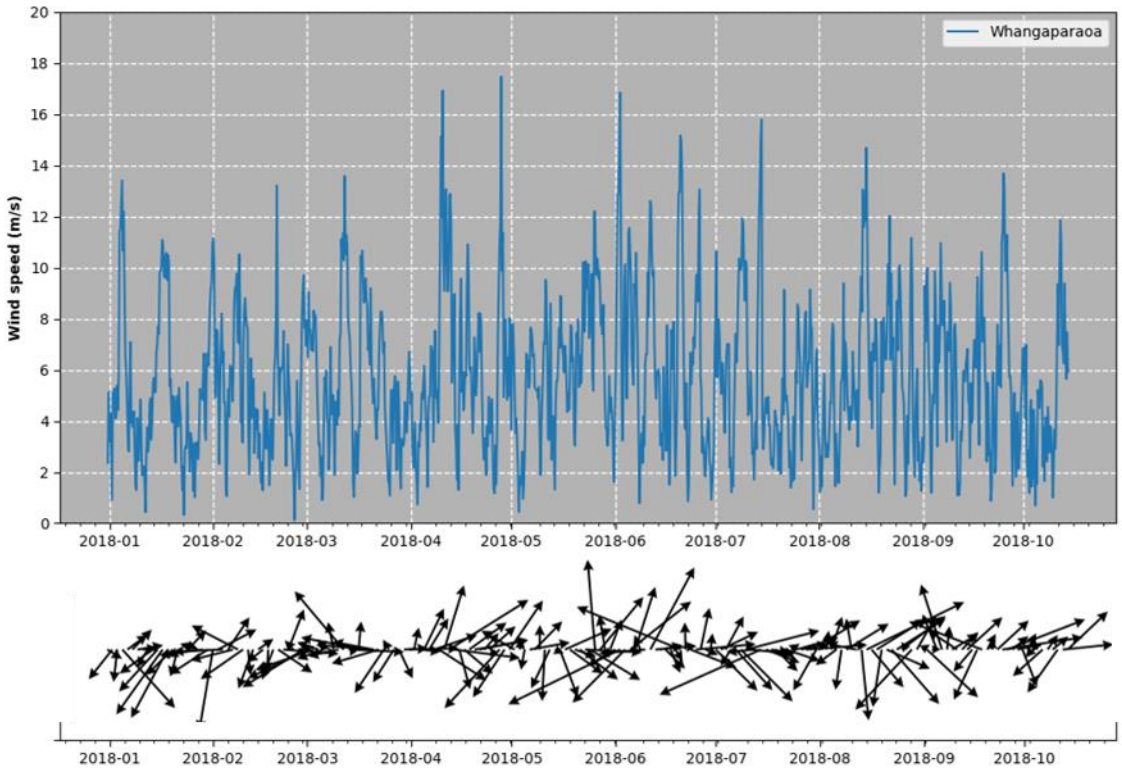

Figure 2-4 Wind speed and direction ("going to") extracted from the nowcast dataset at Whangaparaoa between January and October 2018.

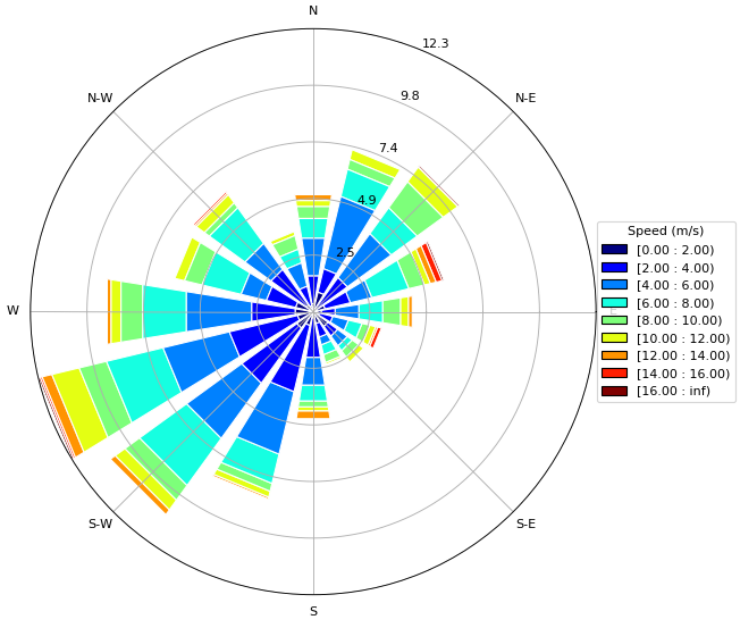

Figure 2-5 Wind rose produced from the nowcast dataset at Whangaparaoa between January and October 2018.

2.5 Boundary Conditions

Open boundary conditions for both the hydrodynamic and the spectral wave models are defined between Takatu Point and Port Jackson (Figure 2-6) at the Hauraki Gulf entrance.

As described in Greig (1990), the Hauraki Gulf is not influenced by consistent, largescale patterns of flow. The net southward flow occurring through the Jellicoe Channel to the North of the Hauraki Gulf is typically deflected toward the Colville Channel without appreciably penetrating the inner gulf. In this context, it is considered that the hydrodynamics within the Hauraki Gulf are dominated by tidal and locally wind-induced currents. For this reason, the hydrodynamic model has been forced at the open boundary using timeseries of tidal water elevation predicted at Port Jackson. The timeseries of water elevation in Figure 2-7 exhibits variations between -1.42 m and 1.44 m, with the Mean Sea Level (MSL) estimated to 1.48 m.

Regarding the wave boundary conditions, the Hauraki Gulf spectral wave model was nested into the New Zealand (NZ) spectral wave model produced by DHI providing hourly two-dimensional (2D) wave spectra at the gulf entrance (Figure 2-8). The timeseries of the model significant wave height and wave rose extracted at the centre of the open boundary from the NZ wave model between 01/01/2018 and 15/09/2018 are shown in Figure 2-9 and Figure 2-10. Although the wave climate within the Hauraki Gulf is dominated by short period sea-waves generated by local wind action, including incoming swells through the narrow gulf entrance improved somewhat the performance of the wave model. Results of the model validation are provided in Section 3.1.

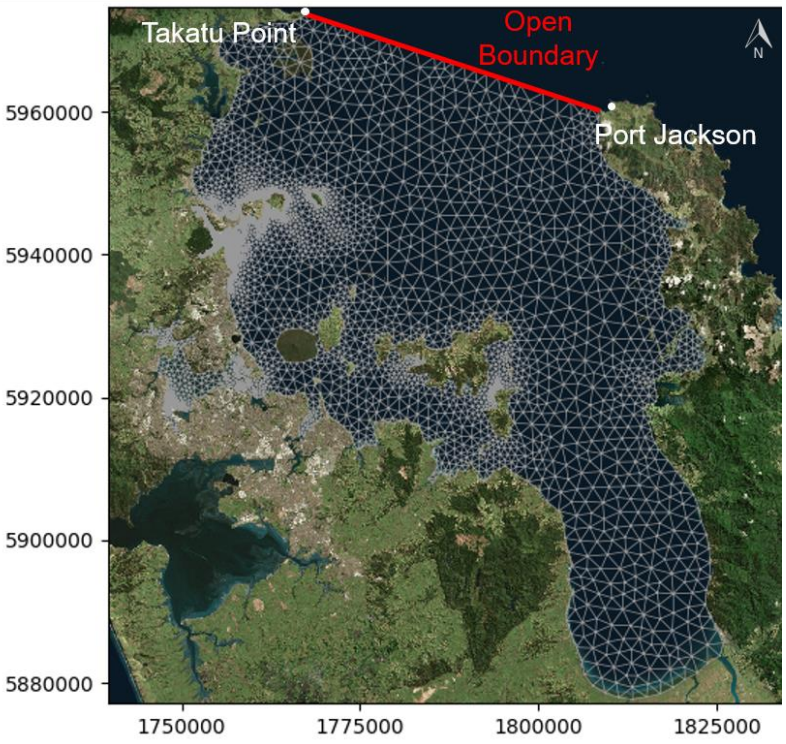

Figure 2-6 Mesh grid including the location of the open boundary forced by tidal water elevations in the hydrodynamic model. The white dot indicates the location of Port Jackson where tidal water elevations have been predicted.

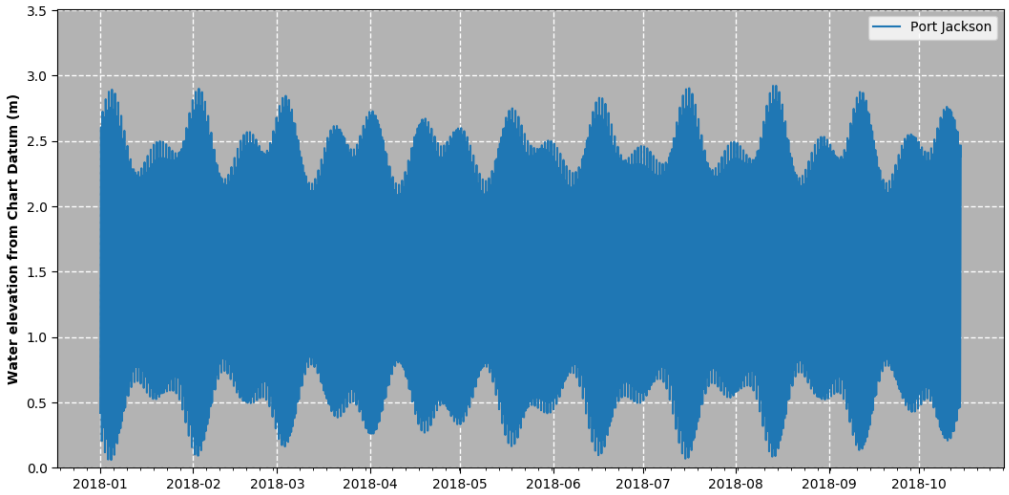

Figure 2-7 Water elevation predicted at Port Jackson between January and October 2018.

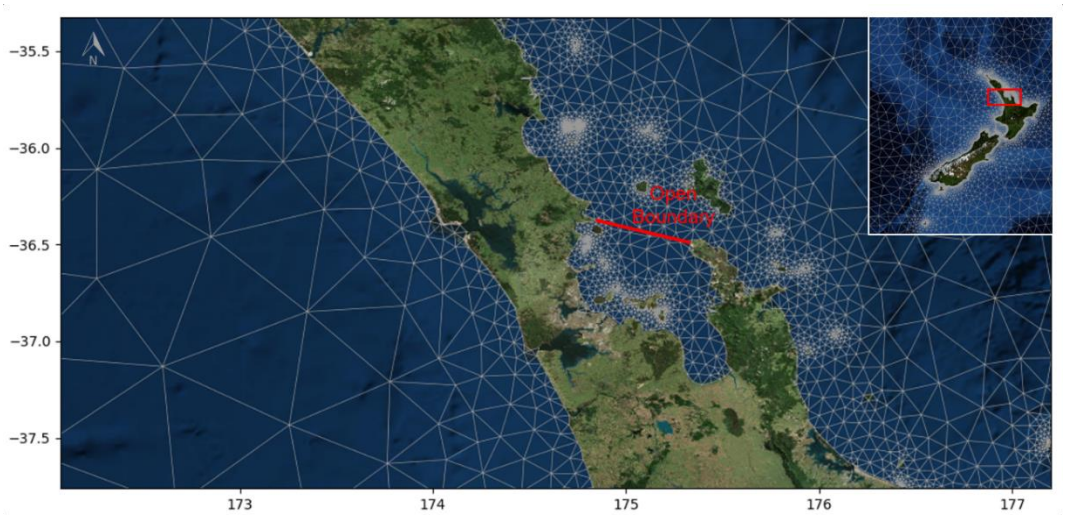

Figure 2-8 Coarse mesh grid used in MIKE 21 SW to provide the spectral wave conditions along the open boundary of the fine Hauraki Gulf wave domain presented in Figure 2-6.

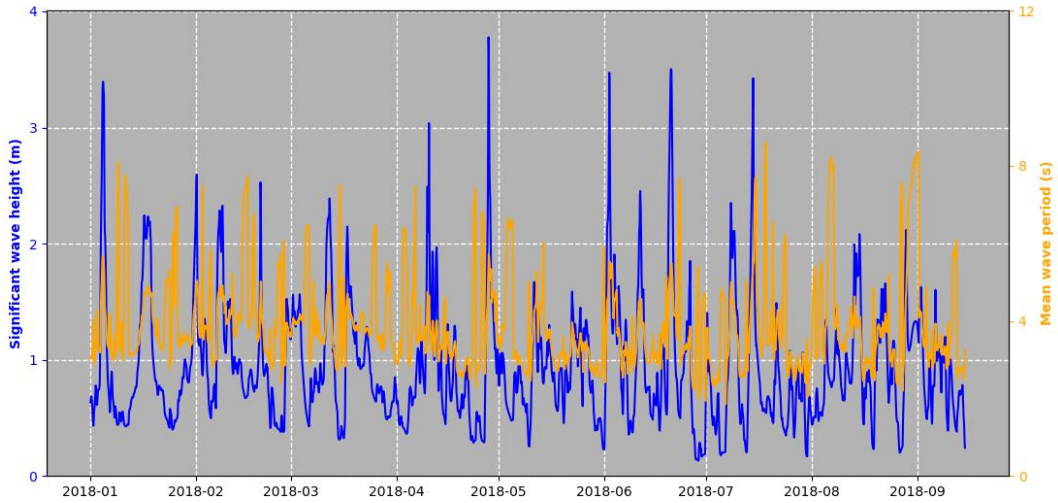

Figure 2-9 Timeseries of the model significant wave height and mean wave period extracted from the NZ wave model at the centre of the open-boundary.

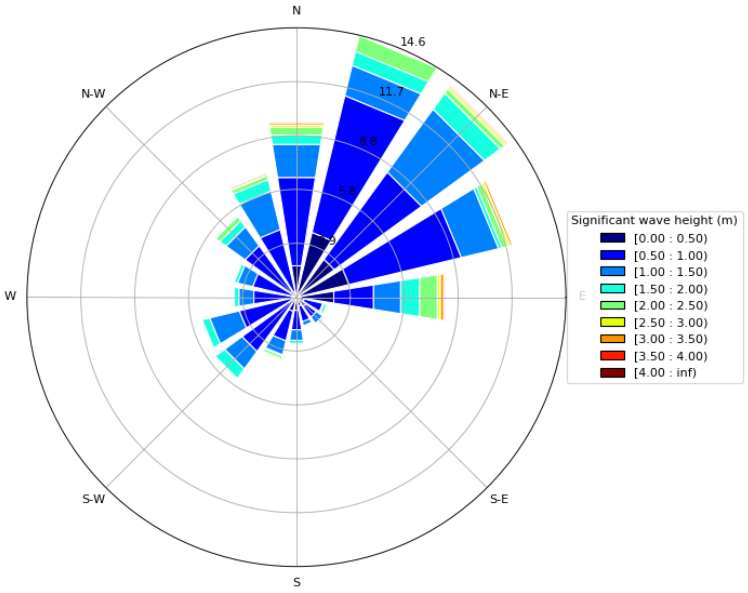

Figure 2-10 Wave rose produced from the NZ wave model data at the centre of the open boundary. between January and October 2018.

2.6 Catchment Inputs

Based on the FWMT outlet data a total of nineteen discharge locations were defined for the marine model (Figure 2-11). The linkages between the FWMT nodes and the marine receiving environment catchment outlets are given in Appendix A.1.

The summary of the FWMT data for each of these outlets are detailed in Table 2-2 and Table 2-3 were introduced into the model domain to simulate the inputs of freshwater and suspended sediments associated with the river discharges. In addition, the predicted loads of metals were used to determine the source concentrations (i.e. mg of metal to kg of sediment) of both Zinc and Copper at each of the catchment outlets.

Some of the discharge locations were moved or merged to avoid any problem related to the wet and dry conditions. Model river flows and SSC were processed combining the river flows provided at 43 sites (Figure 2-11) between 2002 and 2018 by ME. Total flows and SSC at the discharge sites in MIKE 3 were calculated adding and weighted-averaging, respectively, multiple catchment discharges provided at 43 sites (Figure 2-11) .

Timeseries of river flows and total SSC for all locations are provided in Figure 2-13 to Figure 2-24.

Table 2-4 summarises the load and runoff data from the FWMT for Scenario 0.

The Okura catchment includes the North Shore, North Arm, Redvale, SS Inner, SS Mid-West, SS Mid-East SS Outer outlets. The Wēiti catchment Wēiti North, Silverdale, Wēiti South, Duck Creek and Stillwater outlets. The Marine Reserve includes the Long Bay, North Outlet and Awaruku outlets and Karepiro Bay refers to the Arkle Bay, Karepiro and Karepiro Beach outlets.

Note the mean annual sediment load derived from the FWMT tool for the Okura estuary catchment is much lower than the previous estimates from catchment modelling which range from a mean annual sediment loads of between 2263 and 2926 tonnes/yr (Stroud et al. 1999, Hicks et al., 2011 and Yalden and Moores, 2014)), through to 4416 tonnes (for a 1-year return period load, Pritchard et al. 2009). This is in part due to the fact the FWMT uses a fully developed snapshot of land use, it does not consider the temporary effects of non-compliant discharges and (at this stage of its development) does not consider streambank erosion processes or sediment generation associated with post development realignment of stream networks.

Figure 2-12 shows the high degree of inter annual variability which is driven by the magnitude and frequency of rainfall events during the period 2002-2016 and the runoff response of the catchment as modelled by the FWMT.

Table 2-2 Location, mean runoff and sediment load for each of the catchment outlets.

Catchment Outlet	Coordinates (NZTM)		Mean Annual Runoff	Mean Annual Sediment Load	Percentage of mean annual sediment load
	X (m)	Y (m)	($m^3 \times 10^3$)	(tonnes)	(%)
North Outlet	1756863	5938307	466	17.7	0.78%
Awaruku	1756624	5939521	1810	53.1	2.34%
Long Bay	1755378	5941180	2042	129.3	5.70%
SS Outer	1754790	5940522	369	16.9	0.74%
SS Mid-East	1753984	5940238	477	35.8	1.58%
SS Mid-West	1752822	5939834	428	26.7	1.18%
SS Inner	1752822	5939834	463	27.1	1.20%
Redvale	1752822	5939834	6622	589.9	26.03%
North Arm	1753813	5940216	3327	186.1	8.21%
North Shore	1754732	5941732	379	10.1	0.44%
Karepiro	1754521	5942391	930	26.1	1.15%
Karepiro Beach	1753566	5944512	1508	29.9	1.32%
Stillwater	1752856	5945947	852	28.2	1.25%
Wēiti South	1752847	5946365	2970	205.7	9.07%
Silverdale	1756426	5943305	13451	801.7	35.37%
Arkle Bay	1754090	5943912	677	23.7	1.04%
Whangaparaoa	1753112	5945715	463	12.9	0.57%
Wēiti North	1756335	5939989	463	12.9	0.57%
Duck Creek	1752856	5945947	723	32.9	1.45%

Table 2-3 Summary of load data for sand, silt and clay fractions plus Zinc and Copper loads and concentrations (expressed as mg of metal per kg of sediment).

Catchment Outlet	Mean Annual Load (tonnes)			Annual Load (kg)		Metal Source Concentration (mg Metal/kg Silt)	
	Sand	Silt	Clay	Zinc	Copper	Zinc	Copper
North Outlet	0	7.261	10.452	1.1	0.6	157.7	78.4
Awaruku	0.006	24.458	28.653	54	7.9	2208.9	322.1
Long Bay	37.334	36.912	55.045	13.4	3.9	363.9	106.3
SS Outer	0	6.802	10.057	1.3	0.6	195	82.4
SS Mid-East	0.022	15.965	19.804	4.5	1.3	281.9	82.5
SS Mid-West	0.007	14.366	12.357	3.5	1	242.9	69.2
SS Inner	0	12.755	14.373	6.9	1.4	540.9	110.6
Redvale	110.706	320.572	158.668	49.5	15	154.3	46.9
North Arm	49.599	70.237	66.293	14.9	5.4	212.2	76.6
North Shore	0	8.124	1.939	0.4	0.2	52.5	26
Karepiro	0	21.022	5.045	1.1	0.6	54.2	26.6
Karepiro Beach	1.329	19.771	8.771	2.2	0.9	110.8	46.1
Stillwater	0	22.301	5.938	11.4	1.8	511.2	78.9
Wēiti South	61.004	69.825	74.853	16.6	6.1	238.2	86.9
Silverdale	131.515	345.868	324.286	115.1	33.8	332.8	97.8
Arkle Bay	2.02	15.151	6.493	15.2	2.2	1002.4	142.3
Whangaparaoa	0	9.007	3.9225	6.55	1.15	729.2	127.5
Wēiti North	0	9.007	3.9225	6.55	1.15	729.2	127.5
Duck Creek	0	17.258	15.63	6.1	1.7	353.8	97.7

Table 2-4 Summary of contaminant loads and runoff for Scenario 0 land use (Table 1-1).

	Okura catchment	Wēiti catchment	Karepiro Bay	Marine Reserve
Sediment Load (tonnes/year)	893	1094	80	200
90th percentile daily load (tonnes/day)	0.5	1.2	0.1	0.2
95th percentile daily load (tonnes/day)	3.4	8.5	0.1	0.8
99th percentile daily load (tonnes/day)	52.4	74.8	4.6	13.6
99.9th percentile daily load (tonnes/day)	347.2	321.8	32.8	68.2
Runoff (m^3 x 10^3/yr)	12065	18922	3115	4318

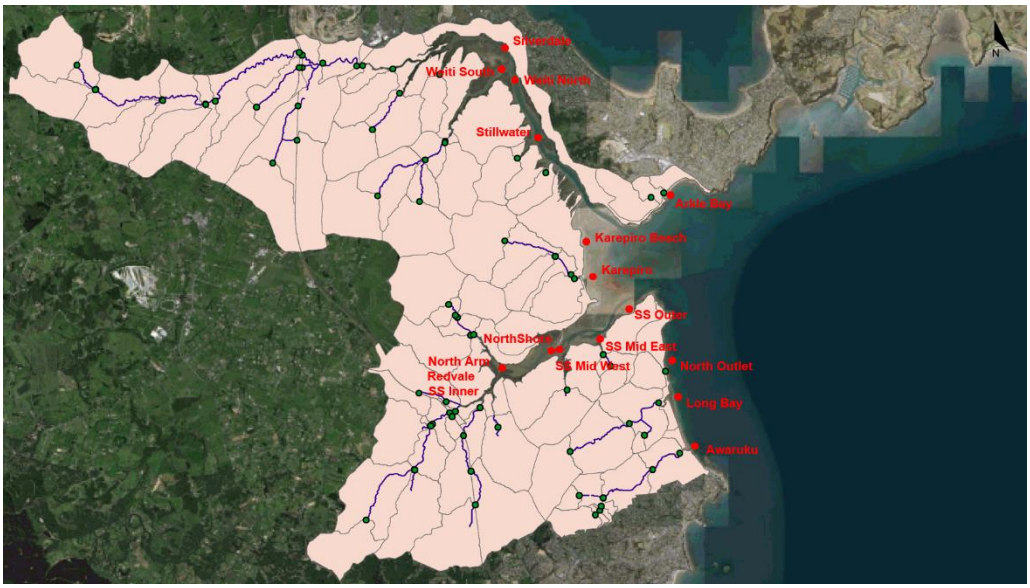

Figure 2-11. Location of the 19 discharge points in Karepiro Bay, Okura River and Wēiti River.

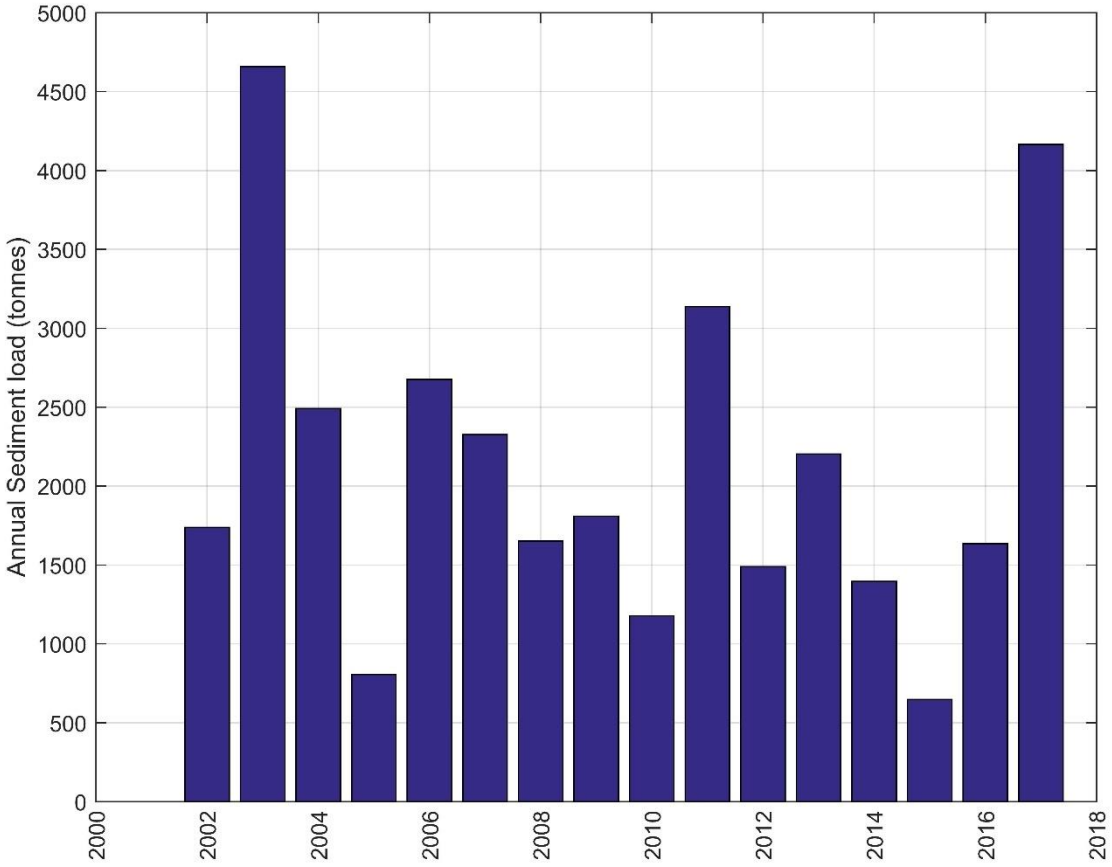

Figure 2-12. Annual sediment load (tonnes/yr) delivered to the Okura/Wēiti marine receiving environment.

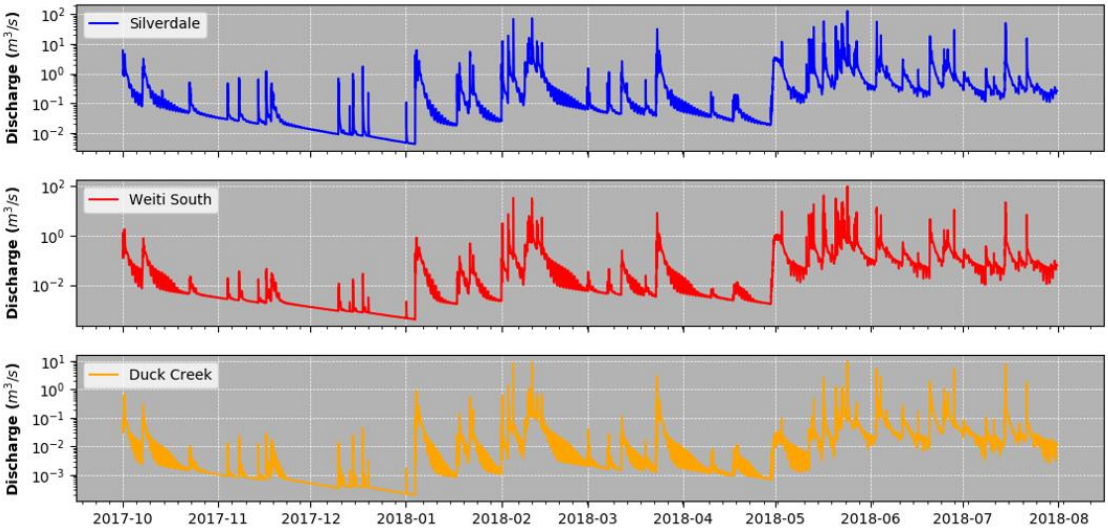

Figure 2-13. River discharges (m^3/s) at the Silverdale, Wēiti South and Duck Creek sites between 01/10/2017 and 31/07/2018.

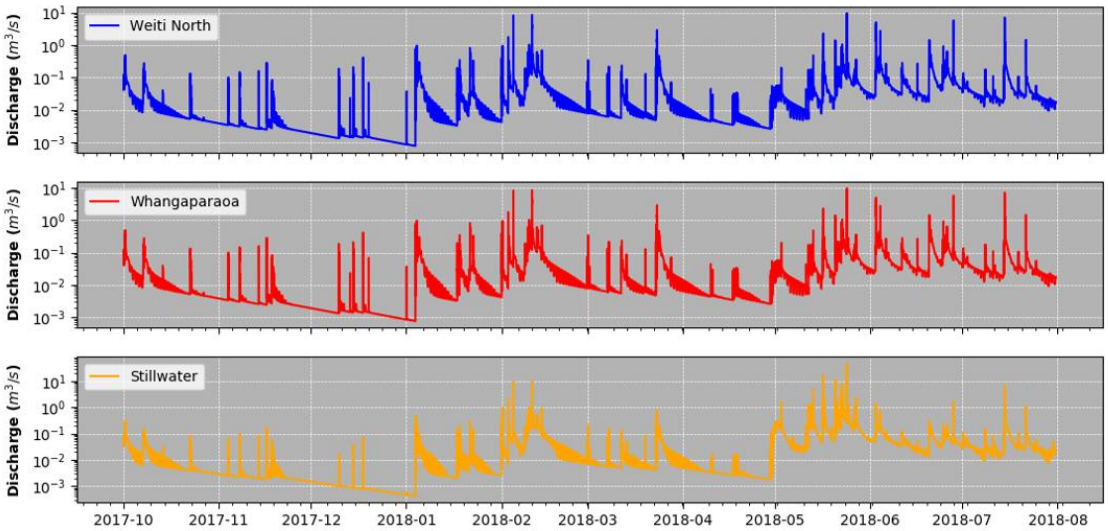

Figure 2-14. River discharges (m^3/s) at the Wēiti North, Whangaparaoa and Stillwater sites between 01/10/2017 and 31/07/2018.

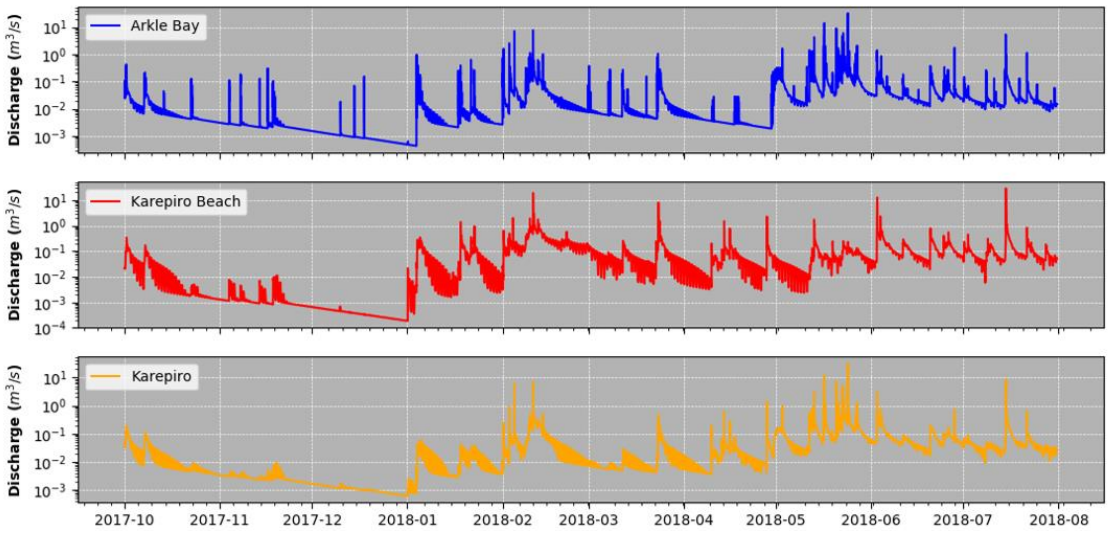

Figure 2-15. River discharges (m^3/s) at the Arkle Bay, Karepiro beach and Karepiro sites between 01/10/2017 and 31/07/2018.

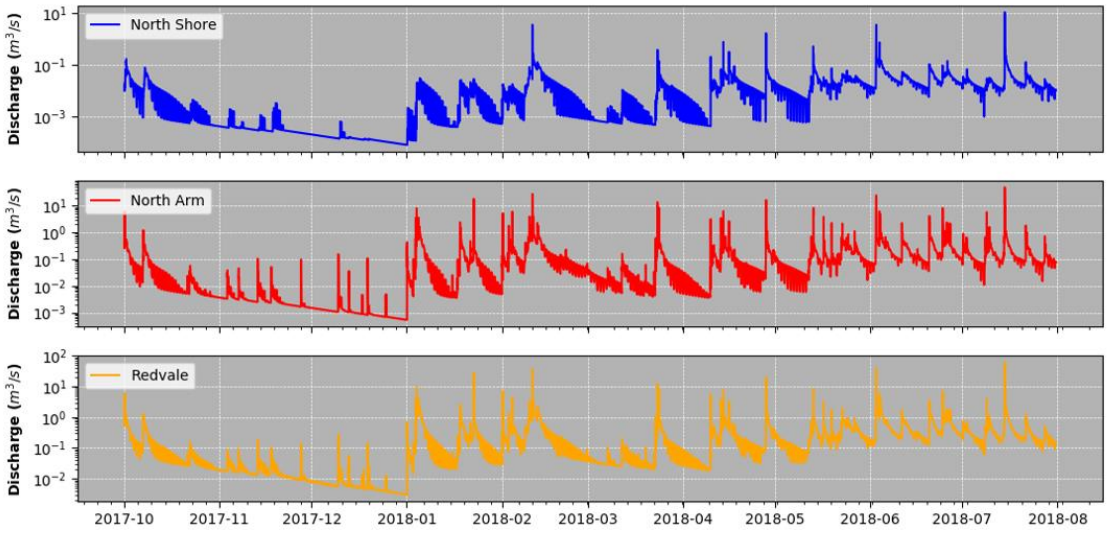

Figure 2-16. River discharges (m^3/s) at the North Shore, North Arm and Redvale sites between 01/10/2017 and 31/07/2018.

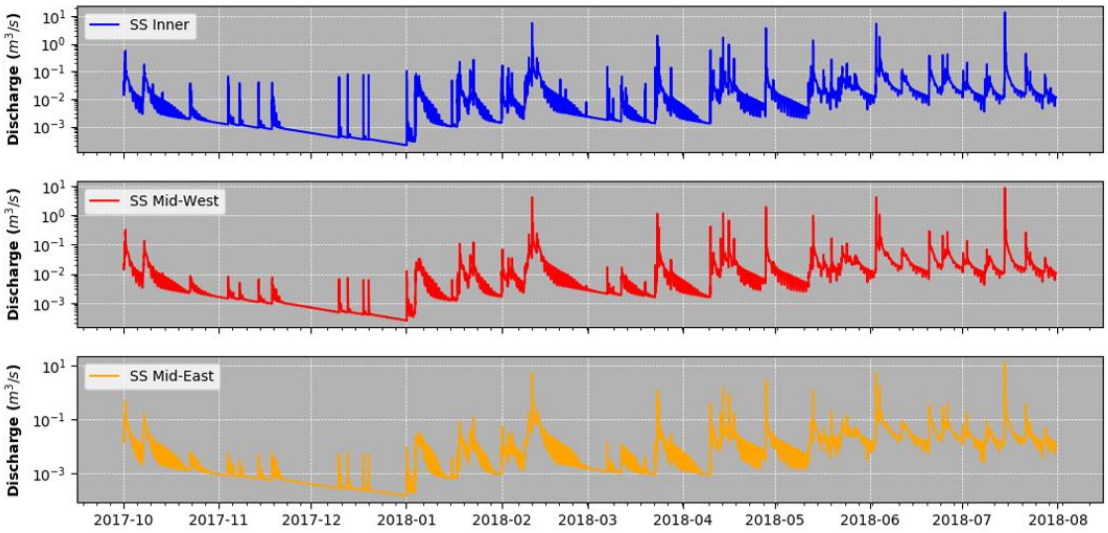

Figure 2-17. River discharges (m^3/s) at the SS Inner, SS Mid-West and SS Mid-East sites between 01/10/2017 and 31/07/2018.

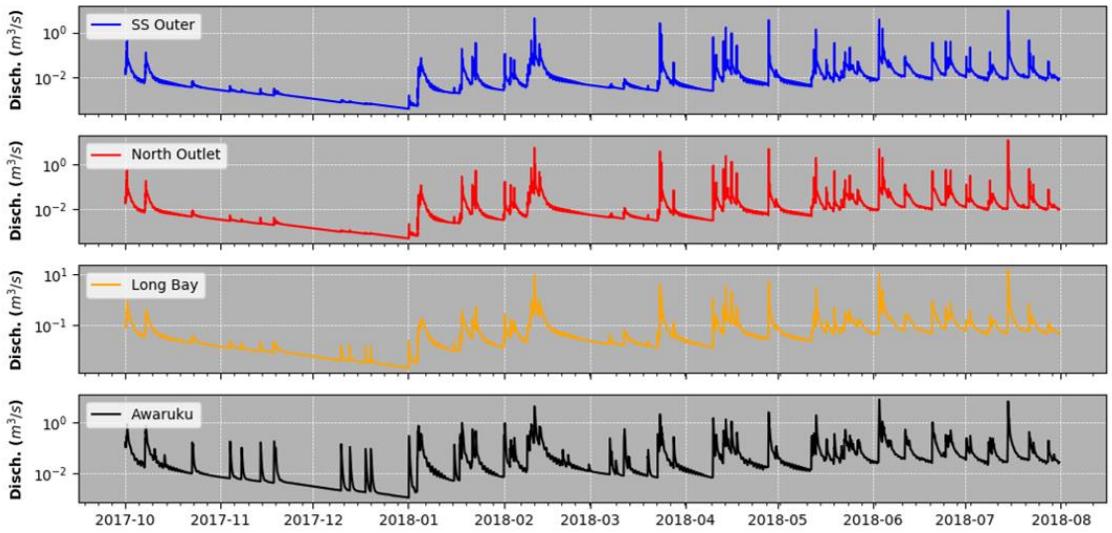

Figure 2-18. River discharges (m^3/s) at the SS Outer, North Outlet, Long Bay and Awaruku sites between 01/10/2017 and 31/07/2018.

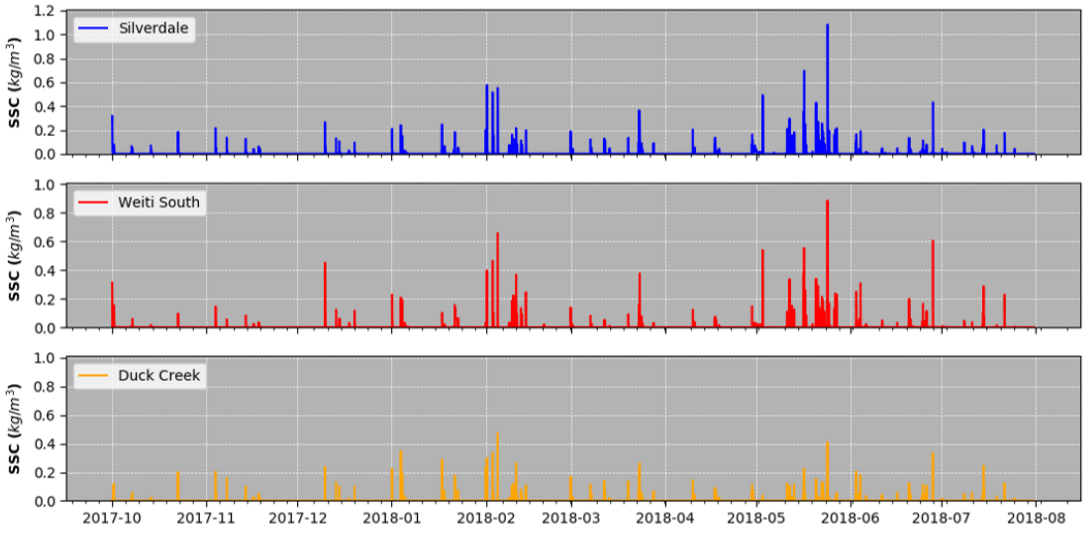

Figure 2-19. Total river suspended sediment concentration (SSC) at the Silverdale, Wēiti South and Duck Creek sites between 01/10/2017 and 31/07/2018.

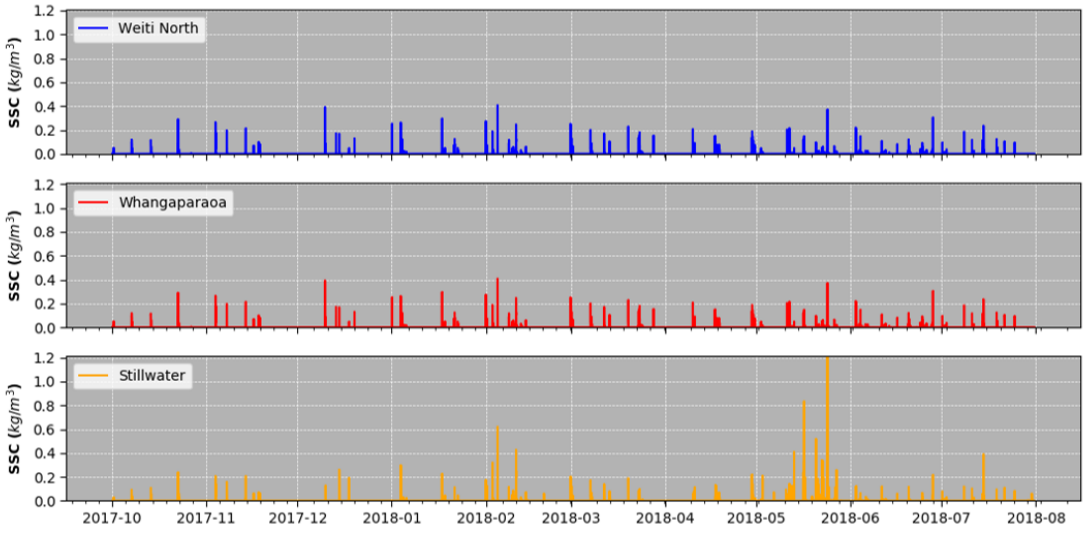

Figure 2-20. Total river suspended sediment concentration (SSC) at the Wēiti North, Whangaparaoa and Stillwater sites between 01/10/2017 and 31/07/2018.

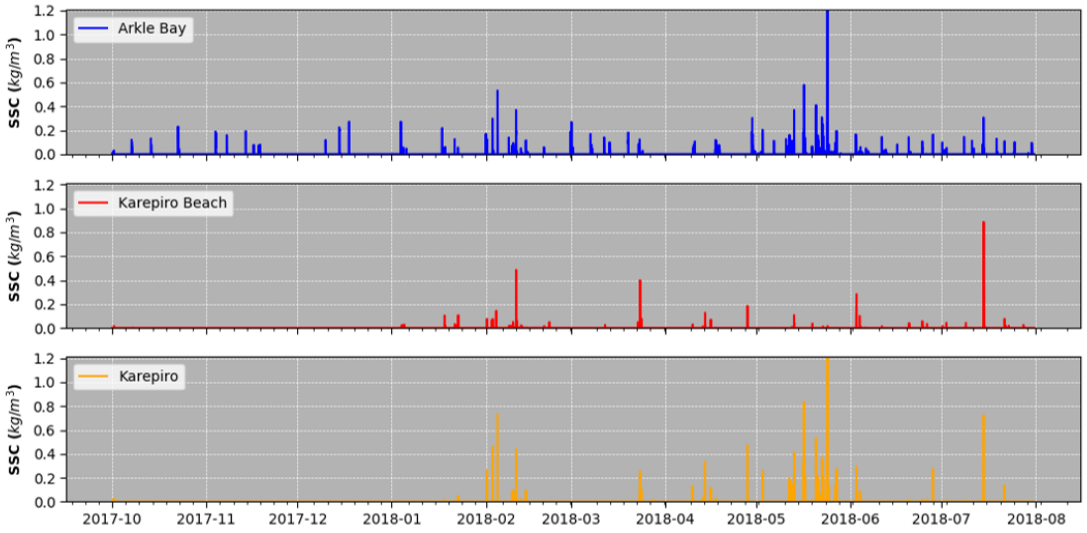

Figure 2-21. Total river suspended sediment concentration (SSC) at the Arkle Bay, Karepiro beach and Karepiro sites between 01/10/2017 and 31/07/2018.

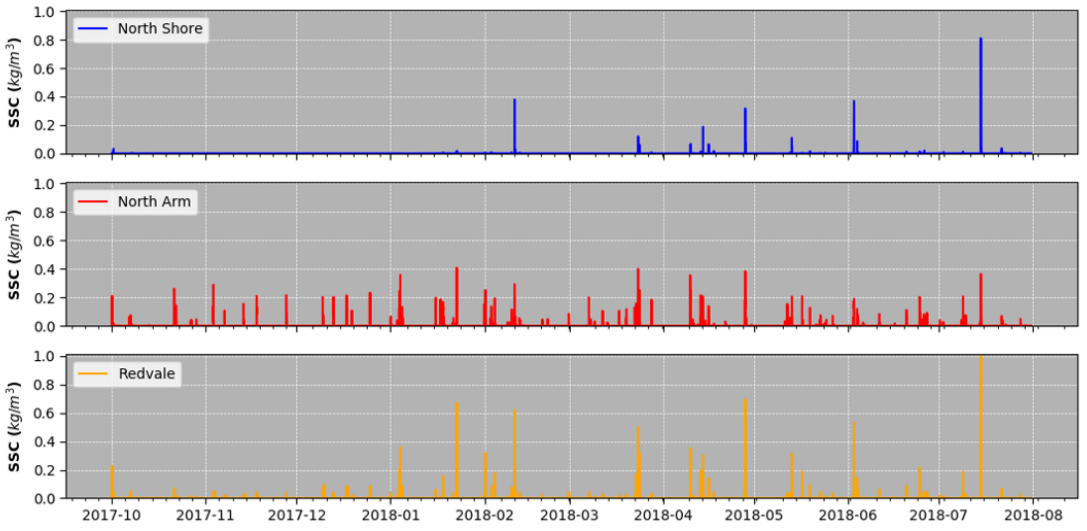

Figure 2-22. Total river suspended sediment concentration (SSC) at the North Shore, North Arm and Redvale sites between 01/10/2017 and 31/07/2018.

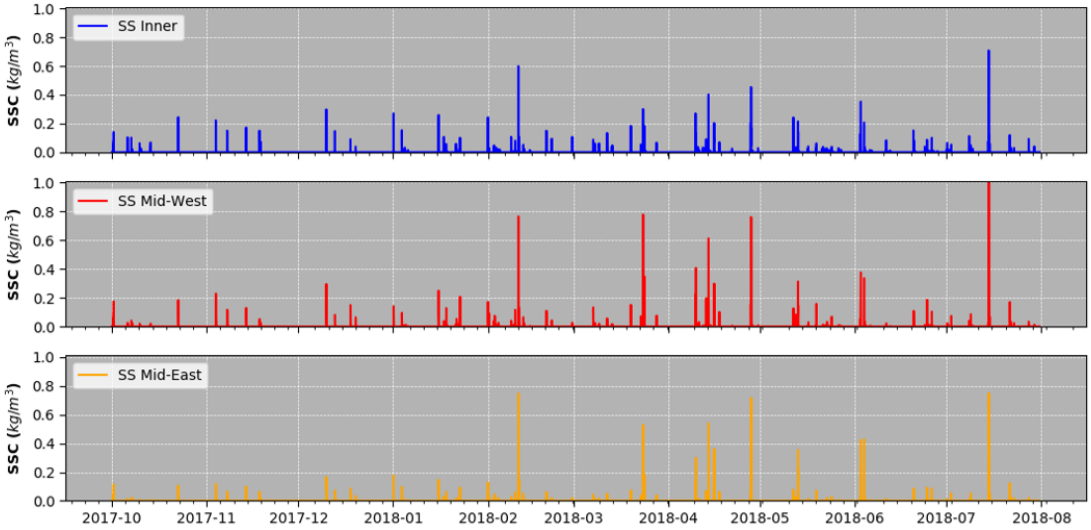

Figure 2-23. Total river suspended sediment concentration (SSC) at the SS Inner, SS Mid-West and SS Mid-East sites between 01/10/2017 and 31/07/2018.

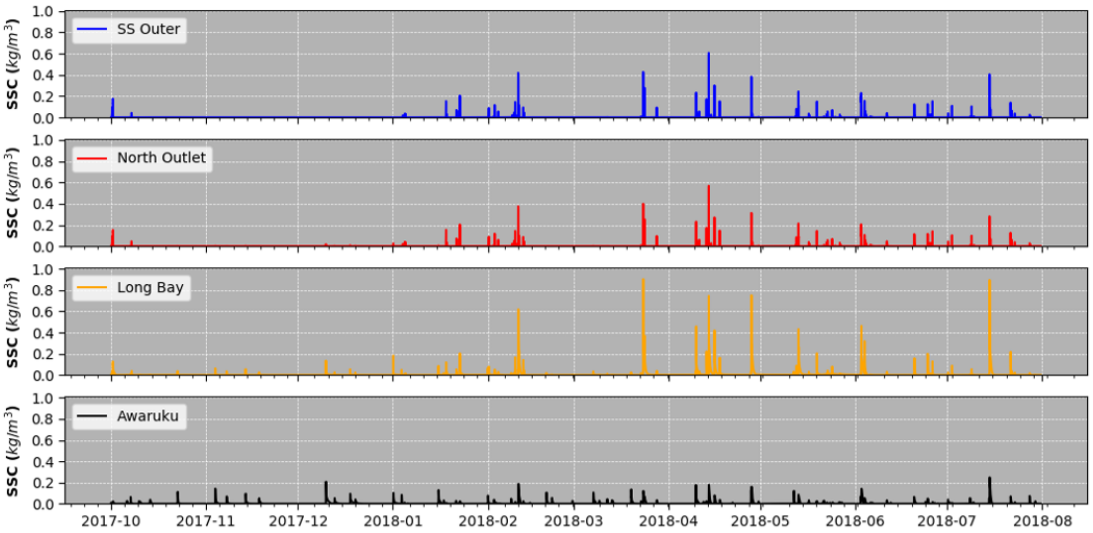

Figure 2-24. Total river suspended sediment concentration (SSC) at the SS Outer, North Outlet, Long Bay and Awaruku sites between 01/10/2017 and 31/07/2018.

2.7 Characteristics of the Sea Bed

The MIKE 3 Mud Transport (MT) model was setup based on the analysis of the sediment sampling presented in NIWA (2008).

Sediment samplings at three positions within Karepiro Bay showed the sea bed was primarily composed of fine sand (>80%) and mud (<20%), with the presence of organic and abundant shell material. The dry density of the muddy-sand in the surface layers was found to be higher than 400 kg/m^3. The dry density of the sea bed combined with the sand-mud-shell mixture highlighted a partly consolidated sea bed.

Based on this information, MIKE 3 MT was setup using the Partheniades (1965) formulation for the erosion of dense mud and a unique space-varying bed thickness layer with a constant density of 450 kg/m^3. An erosion coefficient of 0.00016 kg/m^2/s was defined accordingly to the recommended values provided in (DHI, 2017c, p. 3) for dense mud. The power of erosion was set to 1 (default value). The critical shear stress for erosion was defined in the range 0.125 – 0.425 N/m^2 as shown in Figure 2-25 (bottom panel) to represent the space-varying level of consolidation related to the water depth. The initial bed thickness was determined combining the bed thickness used in Swales et al. (2008) with a 3-month morphological spin-up. This approach aimed to avoid unrealistic erosion patterns caused by inconsistencies between the sea bed characteristics and the model forcing, particularly in areas where organic and shell material may be present which would lead to less bed erodibility than assumed in the model.

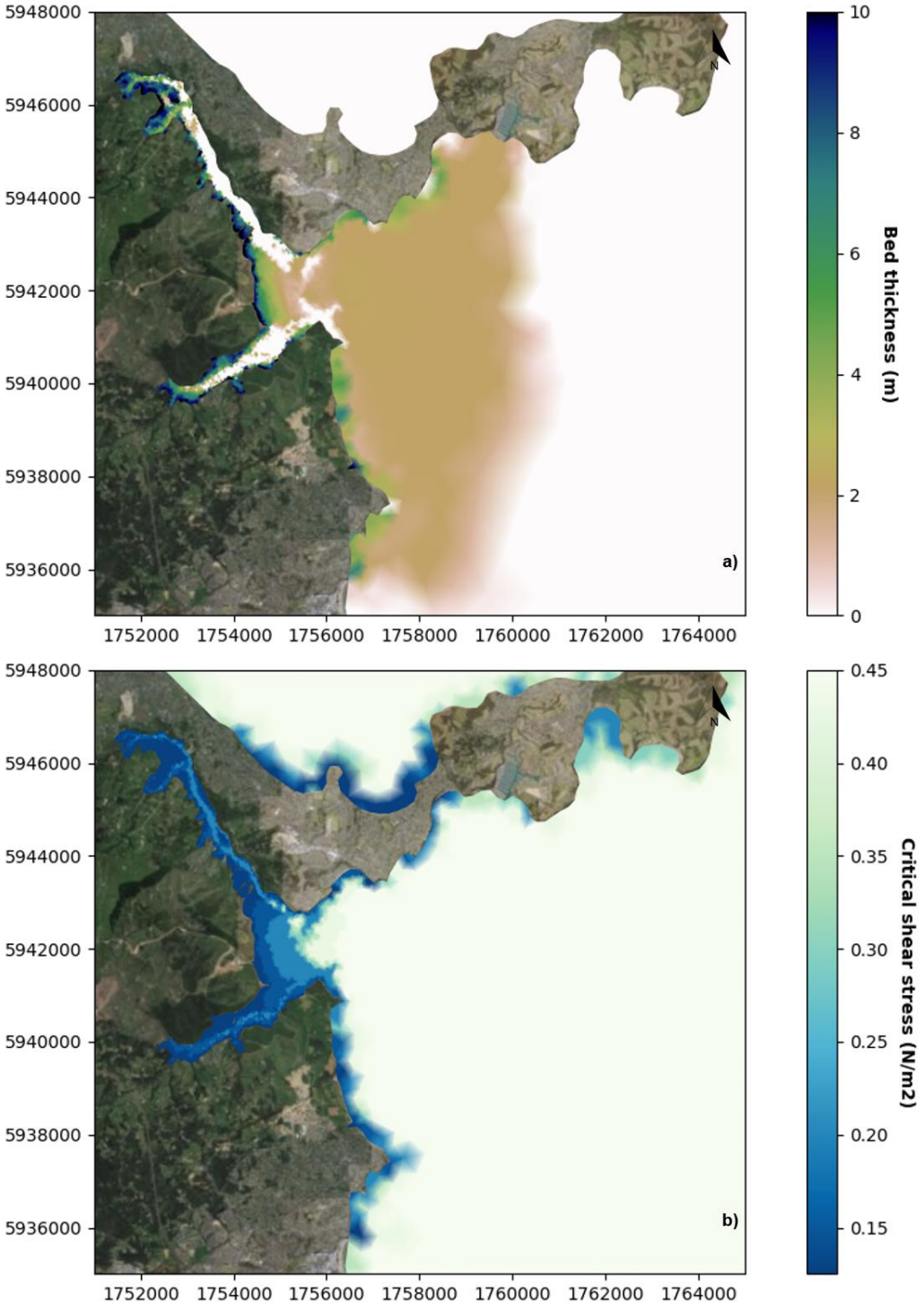

Figure 2-25. Initial bed thickness (top) and spatially varying critical bed shear stress for erosion (bottom) used within Mud Transport model.

2.8 Representativity of the Simulation Period

Based on an analysis of the long-term river data and the Whangaparaoa wind record a representative period was chosen for which to run the calibrated coupled model. This period was chosen to ensure that predicted deposition rates could be related to annual accumulation rates and so that predicted suspended sediment concentrations occur for a broad range of sediment inputs, wind and wave conditions.

It was found that the first 6 months of 2018 provided such conditions.

Daily and accumulated total sediment loads for this period are shown in Figure 2-26.

Figure 2-27 shows the distribution of daily loads for the Okura catchment (SS Outer, SS Mid-East, SS Mid-West, SS Inner, Redvale, North Arm and NorthShore in Figure 2-11), Wēiti catchment (Stillwater, Wēiti South, Silverdale, Whangaparaoa, Wēiti North and Duck Creek in Figure 2-11), Karepiro inputs (Karepiro, Karepiro Beach and Arkle Bay outlets, Figure 2-11) and loads direct to the Marine Reserve (Awaruku, Long Bay and North Outlet outlets, Figure 2-11).

From January to June 2018, the total load delivered during this period is 3,107 tonnes. This period therefore delivers more than the annual average sediment load of 2,267 tonnes (Table 2-4) but includes a number of days when the daily load exceeds 100 tonnes of sediment are delivered and a maximum daily load in excess of 650 tonnes.

As shown in Figure 2-28, the scatter plot of the daily mean freshwater inflow and daily sediment load indicate that the 2018 period is representative of the longer-term distribution for medium to higher flows and loads but does not include periods of very low flows and sediment load. Such periods are not significant in terms of determining the long-term pattern of deposition and elevated suspended sediment concentrations associated with the delivery of catchment derived sediments.

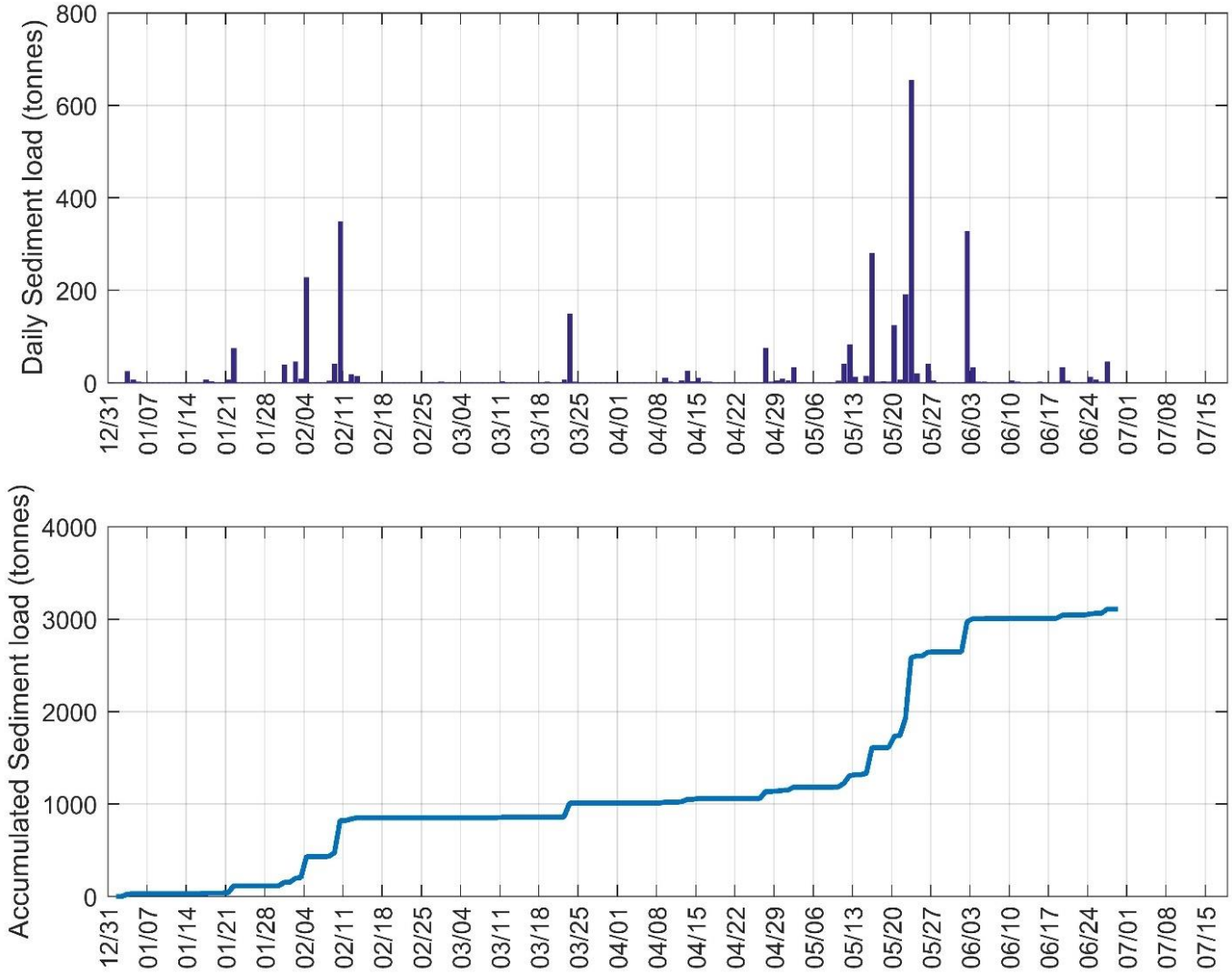

Figure 2-26. Time-series of daily sediment load (tonnes) and accumulated sediment load (tonnes) for the first 6 months of 2018.

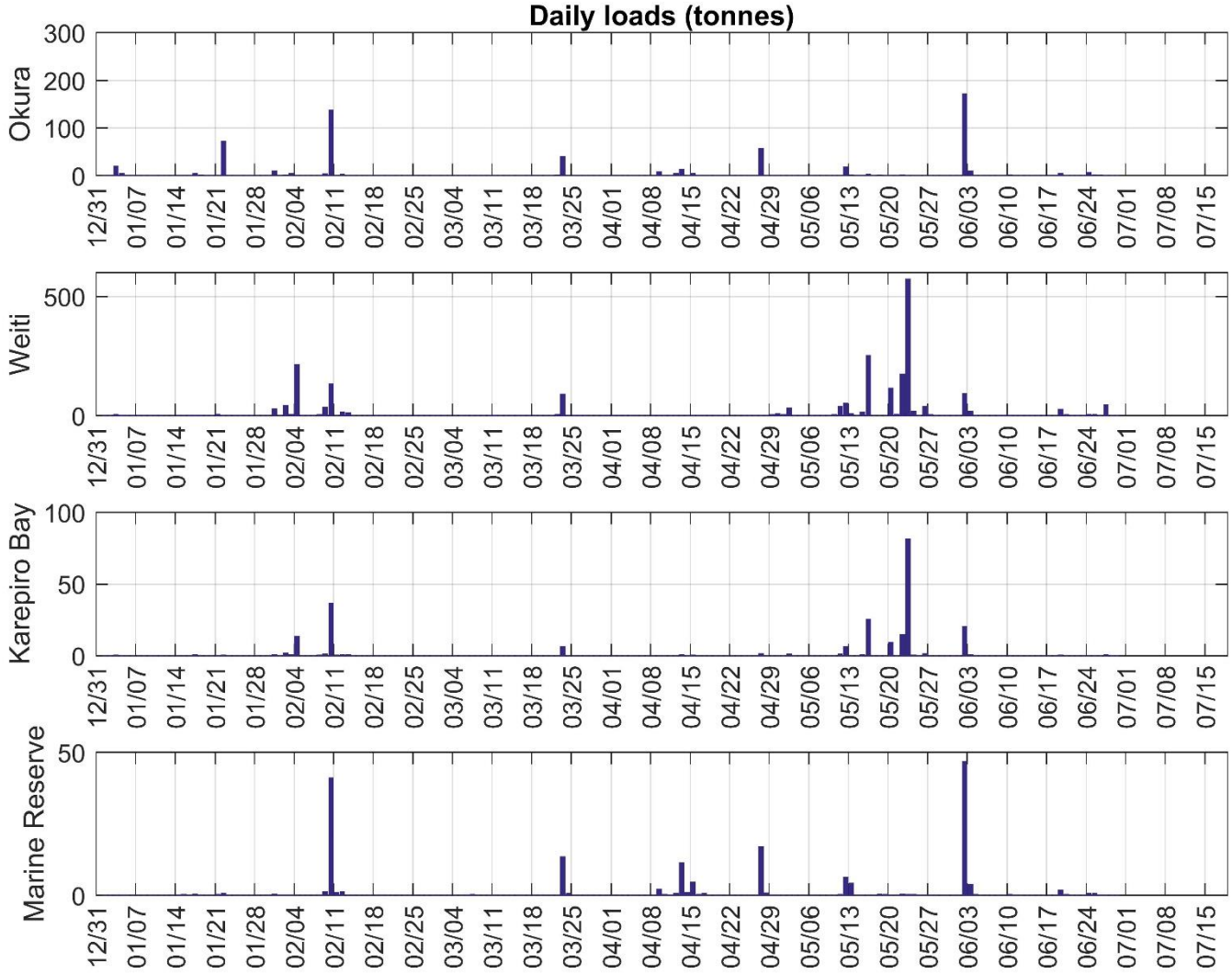

Figure 2-27. Time-series of daily loads from the Okura catchment, Wēiti catchment, Karepiro Bay catchments (Karepiro, Karepiro Beach and Arkle Bay, Figure 2-11) and direct to the Marine Reserve (Awaruku, Long Bay and North Outlet, Figure 2-11) for the first 6 months of 2018.

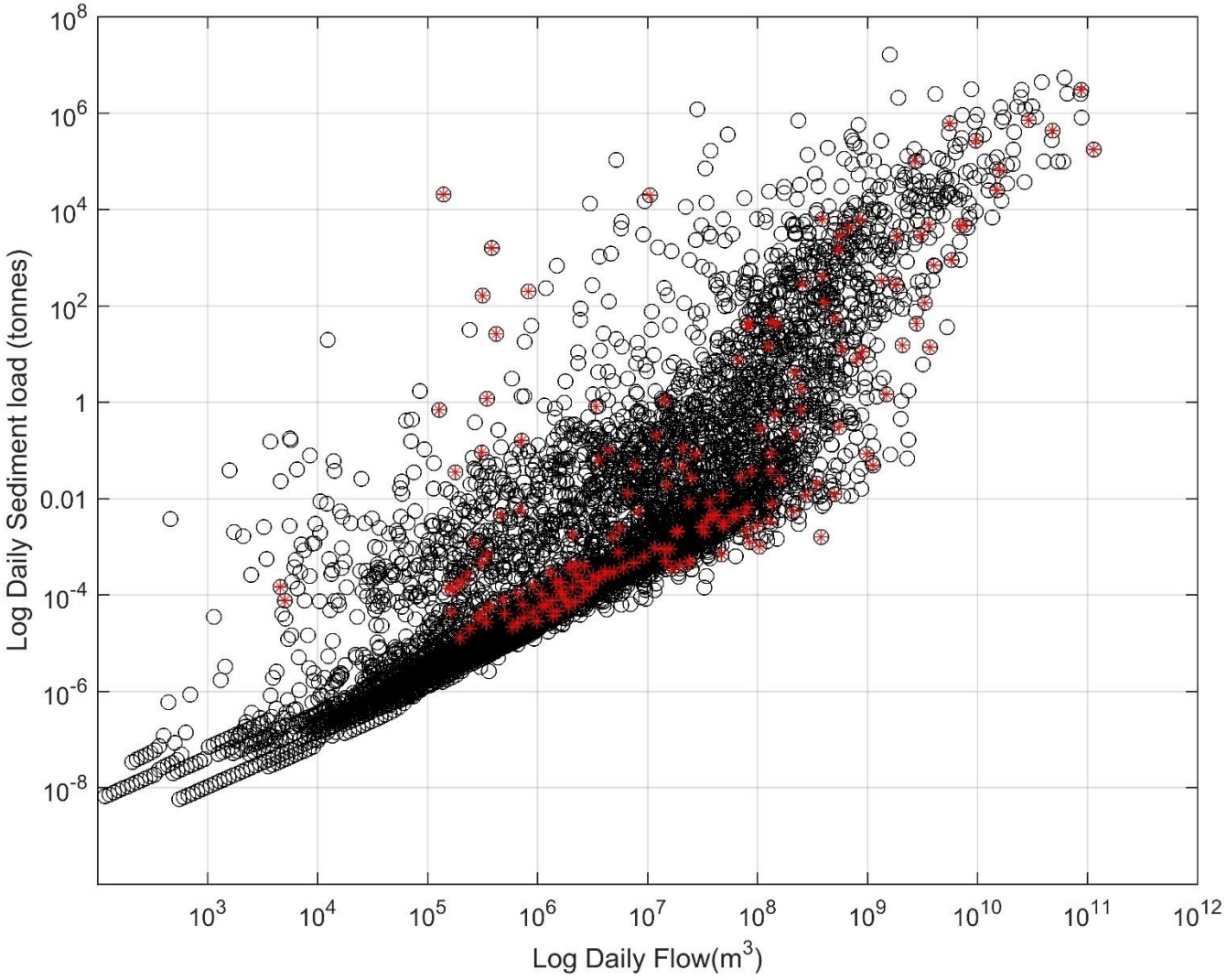

Figure 2-28. Scatter plot of daily freshwater flow (m^3) and sediment load (tonnes) for the full FWMT record from January 2002-July 2018 (black symbols) and for the 6-month period from January 2018 (red symbols).

2.9 Metal Accumulation Model

The metal accumulation model is based on the methodology adopted in a number of studies in the Auckland Region (Green, 2008, Green 2016).

One of the major assumptions in the metal accumulation model is the current day metal concentrations in the sediments. These are a function of historic land use and deposition patterns and rates over many decades.

To fully calibrate the metal accumulation model, it needs to be run in hindcast mode (i.e. from some point in the past to current day) using historic sediment and metal load data. This allows the model parameters to be adjusted to provide good estimates of the current day metal concentrations in the sediments.

Results from a calibrated metal accumulation model (and of course, long term monitoring data) give an indication if current day metal concentration are at or near an equilibrium state or are still increasing due to historic inputs of metals and sediments into the system.

One of the major parameters used to calibrate the metal accumulation model is a Metal Reduction Factor (Green, 2008). This factor (which can vary between 40 and 70%, Green 2008) removes a certain fraction of the metal load to account 1) for a dissolved fraction at source and 2) for the movement of metals from the particulate to dissolved phase once they deposit on the seabed. The other parameters used in the metal accumulation model are the depth to which sediments are mixed in the top few centimetres of the seabed and the mass of new sediment (and metal) arriving within a given subestuary in a given year.

The approach used for the development of the FWMT is to use a snapshot of load generation for a particular land use. Thus, historic sediment and metal load data based on past land use were not available. To carry out the model calibration against current date metal concentrations in the receiving environment, we assumed a Metal Reduction Factor of 50% and assumed a gradual exponential increase in metals loads over the last 100 years to the current predicted metal loads.

Such an approach provides quantification of the relative changes in future metal accumulation due to differing sediment and metal loads under the land use scenarios being considered.

In addition to a current day metal concentration, the metal accumulation model assumes there is a surface mixed layer of sediments that is uniformly mixed to a certain depth (the surface mixed layer depth - SML) during the course of each year. Effectively, it is assumed that at the end of each year, sediment in the surface mixed layer consists of a combination of new sediment deposited during the course of the year mixed uniformly with previously deposited sediments.

At the beginning of the simulation period the metal concentration in the surface mixed layer is assumed to be C_0 (defined in units of mg metal/kg sediment). This value is either assumed to be a constant (sometime in the past) or the spatially averaged value derived from the calibration of the hindcast model.

Outputs from the sediment transport model are used to quantify the sediment accumulation rate (SAR) within a given subestuary. The model data is post-processed to only consider the SAR due to catchment derived sediments and not the transport of pre-existing sediment from other parts of the harbour into the subestuary being considered. To do so would require a full process-based model that tracked the exchange of sediments and metals between subestuaries as well as the sediments and metals from the catchment. This is not feasible over the time-frame considered for the metal accumulation. In terms of the metal accumulation results, this means that there would some “smoothing out” of the model results at a subestuary level. The exchange of pre-existing sediments between a subestuary with higher predicted metal accumulation and one with a lower level of metal accumulation would result in slightly higher levels in the “low”

subestuaries and an equivalent reduction in the “high” subestuary. In a similar way, within each subestuary there will be areas with higher rates of deposition than the subestuary-wide SAR. Here, higher levels of metal accumulation will occur than predicted by the metal accumulation model. Conversely, there will be areas with lower rates of deposition than the subestuary wide SAR where lower levels of metal accumulation will occur than predicted by the metal accumulation model. Finally, there will be areas within each subestuary where there will be net erosion where the build-up of metals is unlikely to be of concern. Thus, the metal accumulation model provides an indication of which subestuaries may, over time, be more susceptible to metal accumulation but not the absolute level of metal accumulation or the spatial distribution of metal accumulation within that subestuary.

The predicted change in bed-level due to the catchment derived sediments at the end of the 2010 model simulation were then averaged over a given subestuary to provide the mean sedimentation rate within that subestuary.

Information from the catchment load data is used to define the metal concentration associated with the new sediment arriving into the subestuary each year (C_c defined in units of mg metal/kg sediment).

Based on a mass balance approach, the following can be derived. Details of the approach are given in Appendix A.4. Where C_i is the concentration in a given year and C_{i-1} is the metal concentration in the previous year.

$$C_i = [SML*Cc + (SML-SAR)*C_{i-1}]/SML$$

Thus, for year one of the metal model simulation the metal concentration in the SML is

$$C_1 = [SML*Cc + (SML-SAR)*C_0]/SML$$

In year two of the metal model simulation the metal concentration in the SML is

$$C_2 = [SML*Cc + (SML-SAR)*C_1]/SML$$

Essentially, the sediment transport model is used to define the connectivity of each of the subestuaries to each of the catchment sources and to define the mass of new sediment that is arriving in each subestuary. This then provides the necessary inputs to the metal accumulation model at the subestuary scale.

3 Model Validation

To ensure the capability of the model to appropriately simulate the sediment transport in the study area, the model outputs were compared against measurements of significant wave heights, water elevations, 3D current velocities, turbidity and bed thickness changes. The main purpose of the validation was to demonstrate the present model was a suitable tool to assess the effect of the discharges from the Wēiti and Okura catchments. For this purpose, both hydrodynamics and sediment dynamics were investigated. Results of the validation are presented in this section.

Appendix A.2 provides a summary of the model setup, assumptions and inputs compared to the earlier modelling carried out in the Okura estuary (Pritchard et al. 2009).

3.1 Waves

Predicting wave heights in semi-enclosed environments such as the Hauraki Bay is challenging as it requires the use of accurate wind conditions to force the spectral wave model. To verify the accuracy of the hindcast, the model significant wave heights were compared against the wave measurements at position AK1 (Figure 3-1) between March and July 2018. As shown in Figure 3-2 and Figure 3-3, the model represents very well the local wind-induced peak wave events characterised by waves higher than 1 m. The 6-hour wind forcing does not allow capturing the rapid variations of the sea state leading to wave heights in the range 10 – 25 cm. However, timeseries of measured bed level changes at the entrance to Karepiro Bay (DHI, 2018) showed that sediment transport was mostly occurring during storm events. The shear stresses induced by 10 – 50 cm waves are therefore negligible in this context.

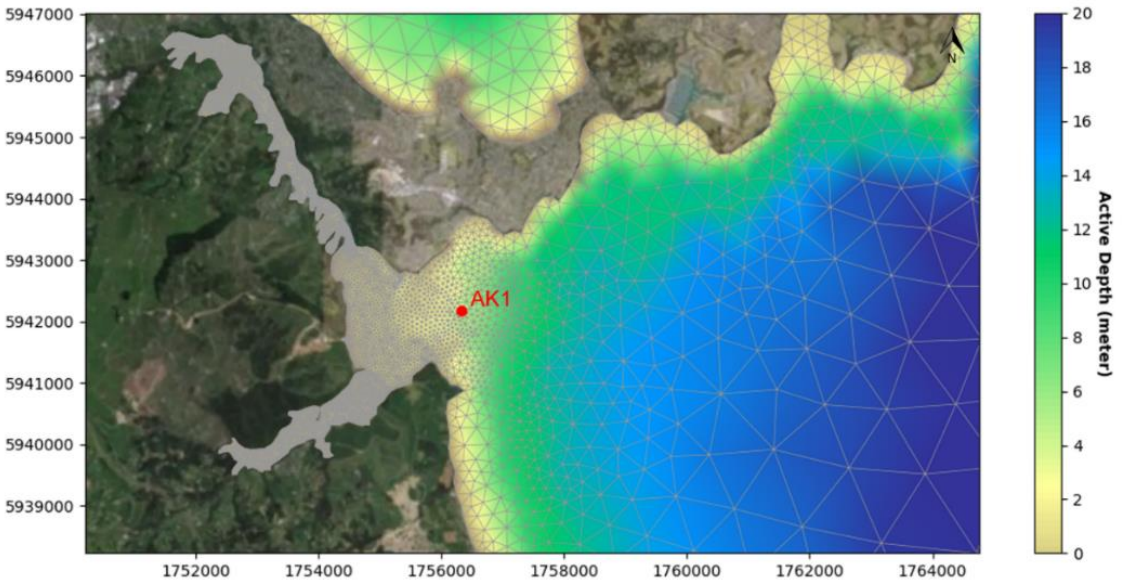

Figure 3-1. Bathymetry map with the location of the ADCP deployed at Position AK1 at the entrance to Karepiro Bay.

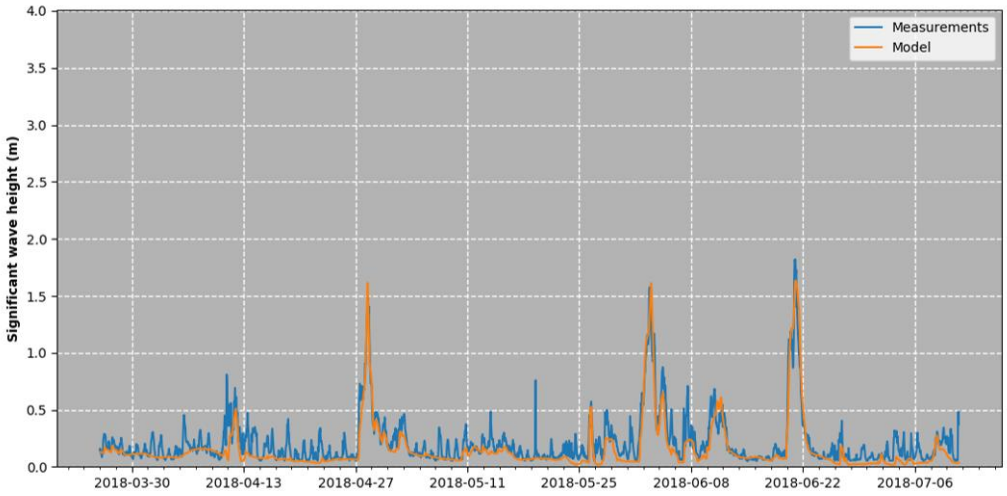

Figure 3-2. Measured and model significant wave heights at Position AK1 at the entrance to Karepiro Bay.

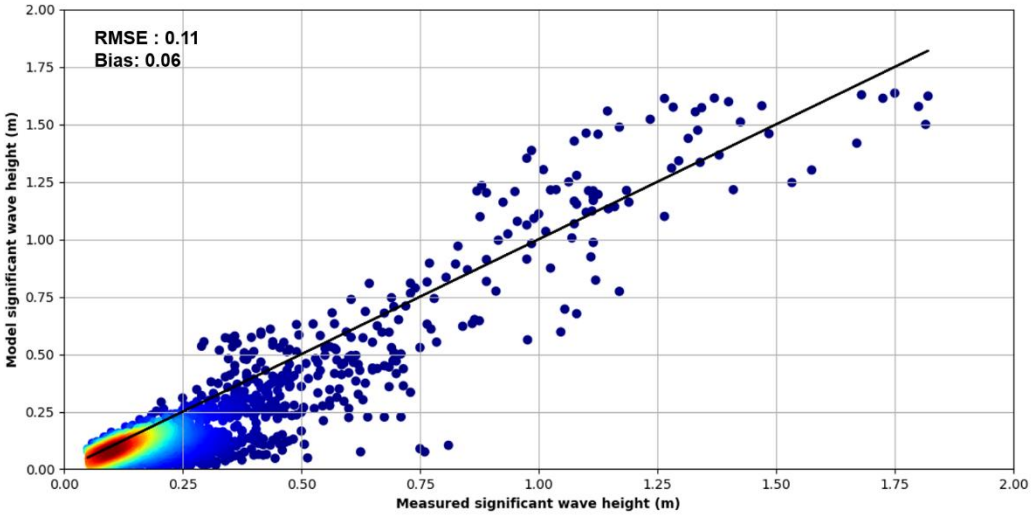

Figure 3-3. Scatter plot produced from measured (X-axis) and model (Y-axis) significant wave heights at Position AK1 at the entrance to Karepiro Bay.

3.2 Water Elevation

Comparisons between model and measured water elevation at Position AK2 (Figure 3-4) between March and May 2018 highlights a good level of agreement (Figure 3-5). The maximum difference in water elevation does not exceed 25 cm over the calibration period which corresponds to ~10% of the tidal amplitude. This illustrates the capability of the model to realistically simulate the flooding and drying of the inter-tidal areas where significant sediment fluxes occur between the Okura estuary and Wēiti river and Karepiro Bay.

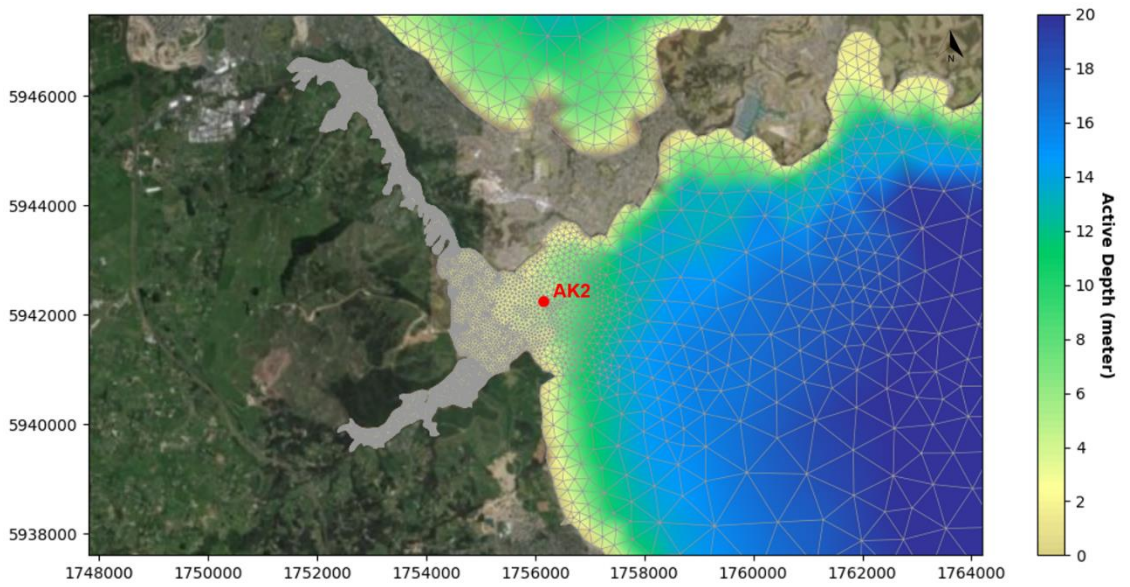

Figure 3-4. Bathymetry map with the location of the instrument deployed at Position AK2 to measure water elevation.

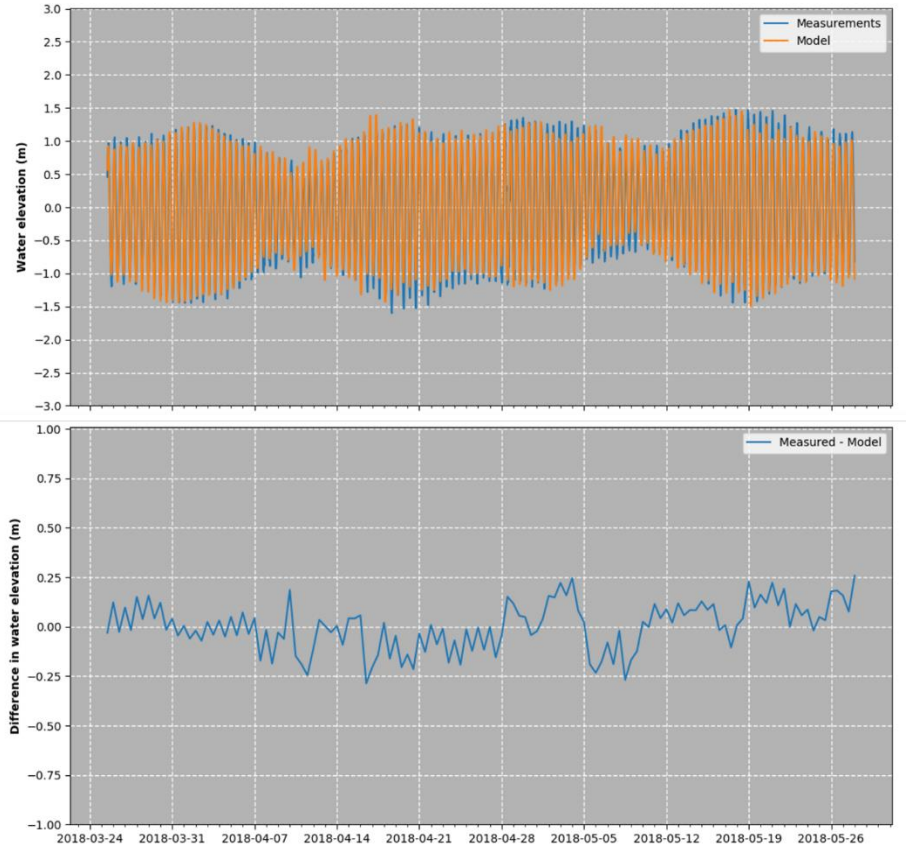

Figure 3-5. Measured and model water elevations (top panel) and differences in water elevation (bottom panel) at Position AK2.

3.3 Currents

Near-surface, mid-depth and near-bottom currents were compared against the measured data at position AK1 between March and July 2018. Current speeds and directions were examined at these levels to ensure the model allows capturing the combining effect of tides, winds and bed roughness on the local hydrodynamics. Timeseries, Quantile-Quantile (QQ) plot and current roses are provided for each level in Figure 3-6, Figure 3-7 and Figure 3-8.

The validation results indicate the model satisfactorily simulate the hydrodynamics in Karepiro Bay. The QQ plots highlight close distributions of current speed through the water column. Velocities are somewhat under-estimated in surface (<20%) and at mid-depth (<10%), and over-estimated near bottom (<10%). Model current directions are also consistent with the measurements. We can, however, note a ~10 – 20° shift in the tidal ellipse which is not expected to significantly modify the sediment transport patterns.

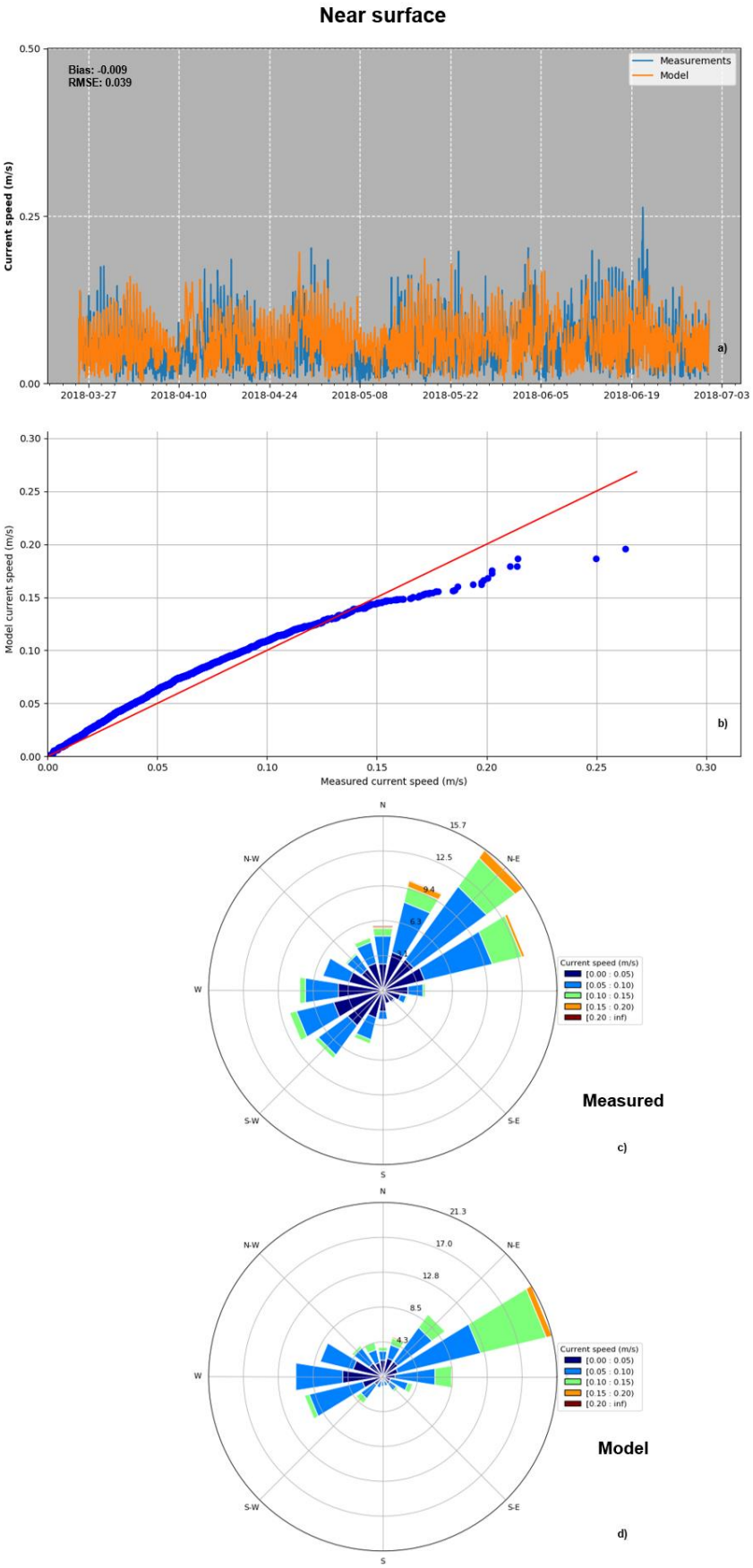

Figure 3-6. Measured and model near-surface current timeseries, Quantile-Quantile plot and roses.

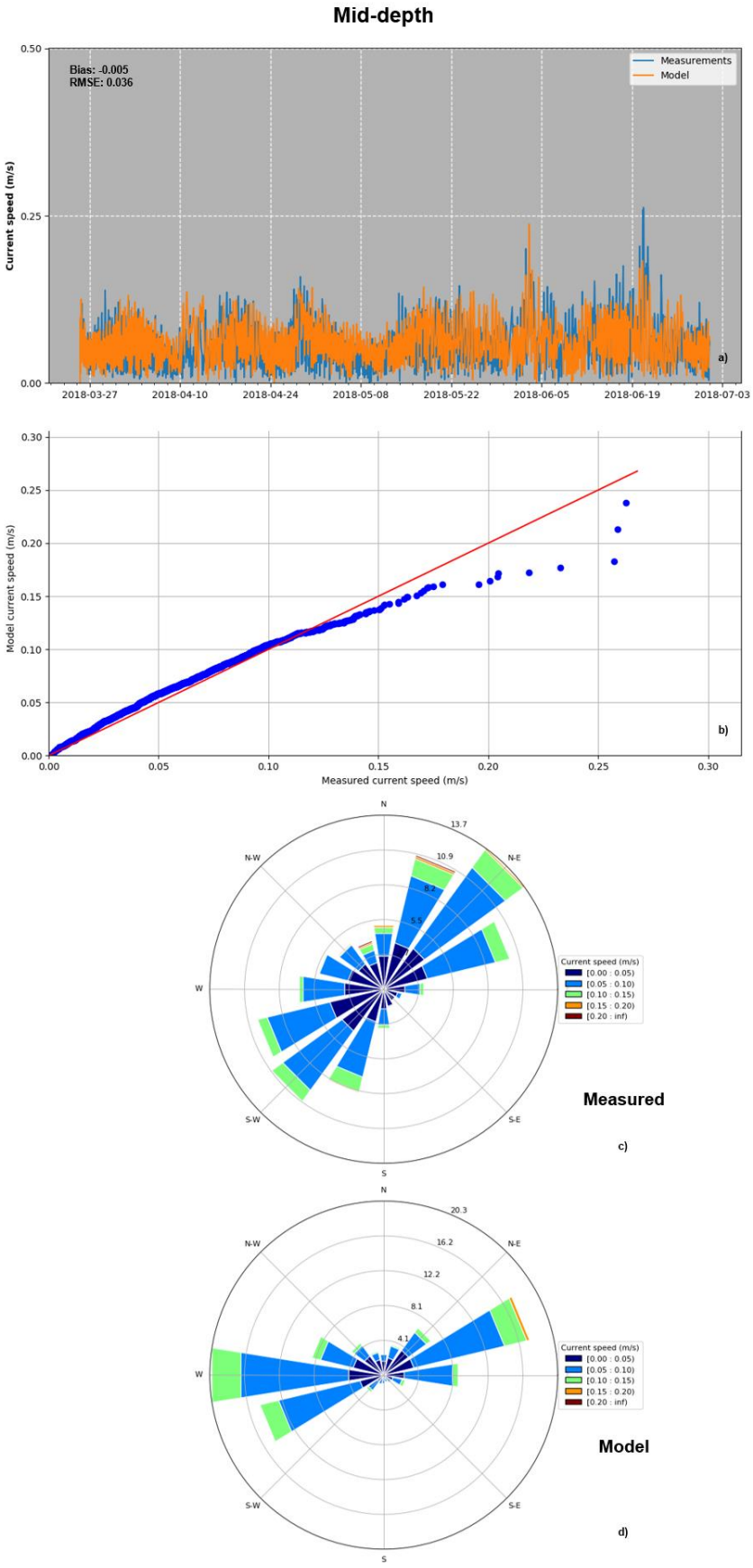

Figure 3-7. Measured and model mid-depth current timeseries (a), Quantile-Quantile plot (b) and roses (c, d).

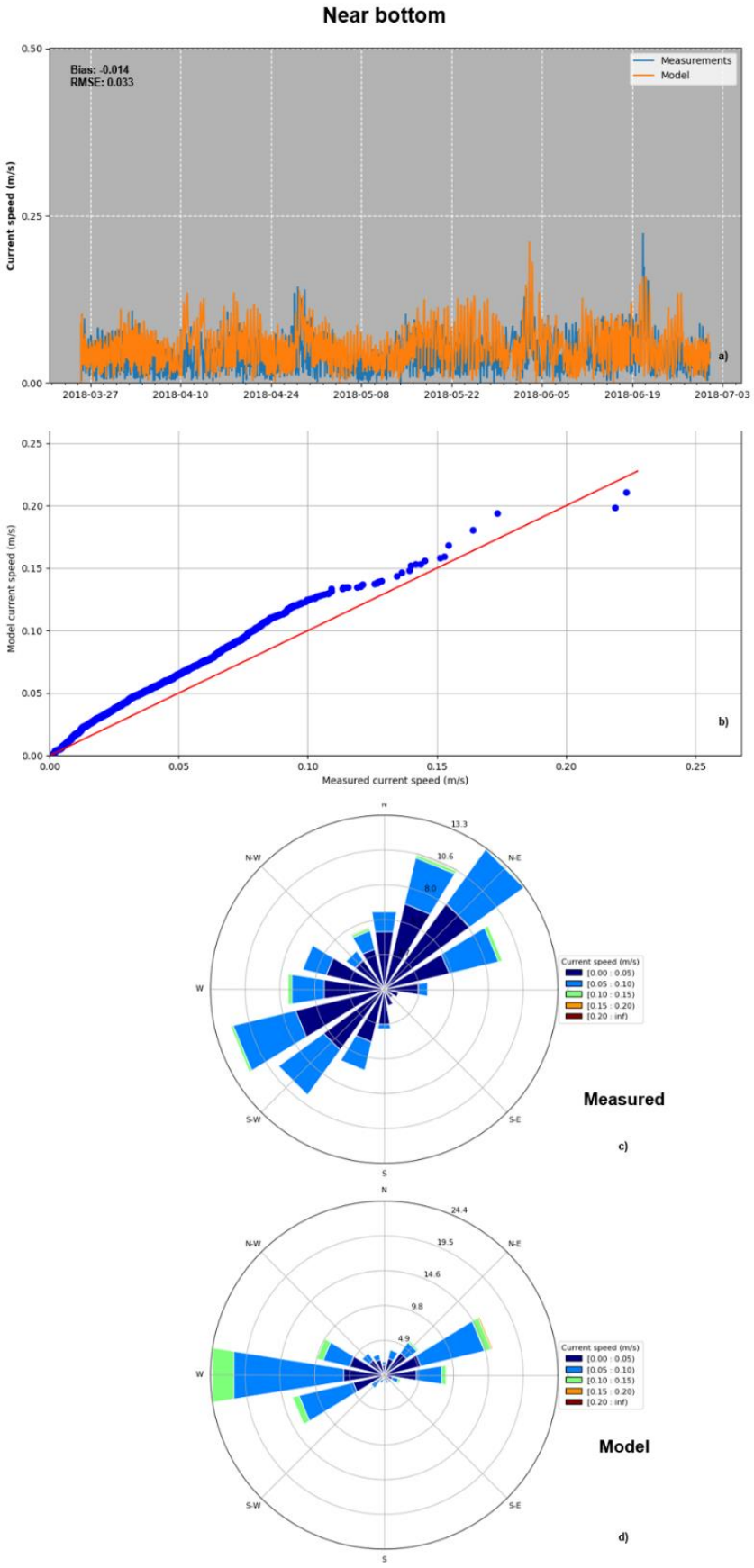

Figure 3-8. Measured and model near-bottom current timeseries (a), Quantile-Quantile plot (b) and roses (c, d).

3.4 SSC/Turbidity

Measurements of turbidity were carried out by VE at Positions AK2A, AK3A and AK2AMR in Karepiro Bay. However, the turbidity does not provide a direct measure of suspended sediment and there is no formula or set of conversion factors that can allow calculating suspended sediment concentrations (SSC) from turbidity (NTU). The relationship between SSC and NTU depends on near infrared reflectivity (NIR), refraction index, shape and size of particles. One of the most important factors is the particle size that can considerably vary in the environment. During wave-dominated events, the size of particles in suspension tends to be higher than during tide-dominated periods due to increasing bed shear stresses. In absence of calibration during the measurement process, it has not been possible to validate the model SSC against measured data to quantify the accuracy of the MIKE 3 MT predictions. Model normalized SSCs and measured normalized NTUs at positions AK2A, AK3A and AK2AMR are presented in Figure 3-9, Figure 3-10 and Figure 3-11.

The secondary peaks in the measured turbidity timeseries are caused by the combined effect of tidal currents and river discharges. Back and forth movement of sediments occur through both Okura estuary and Wēiti river mouths at ebb and flood tidal stages. During strong wave events as described in Section 3.1, enhanced bed shear stresses cause the suspension of a substantial amount of material highlighted by the primary peaks in the measured NTUs data. Both measured and model data indicate a greater influence of the wave climate on sediment transport than any other factors such as river discharges or tidal currents in Karepiro Bay.

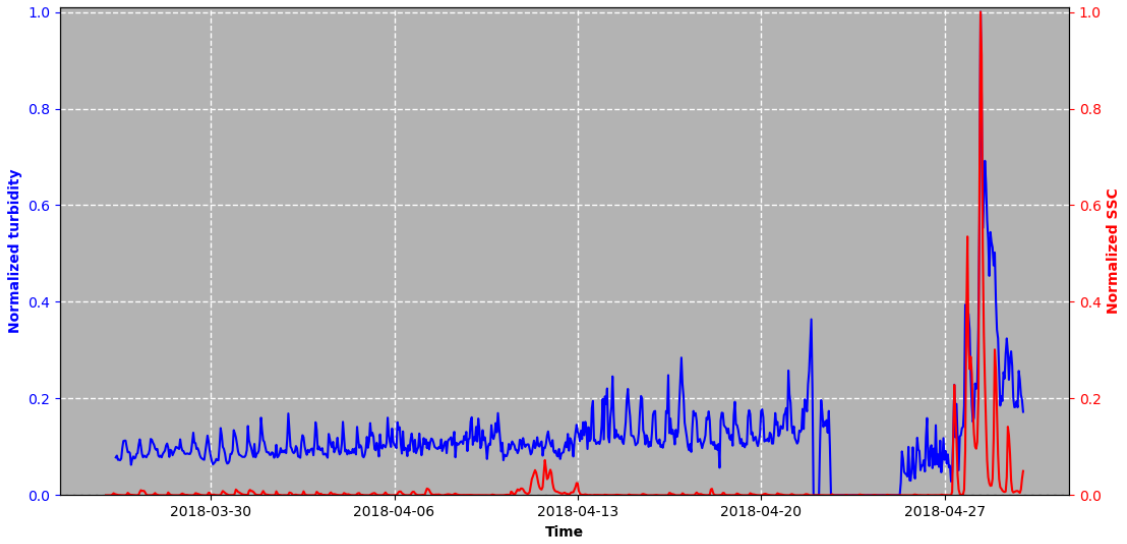

Figure 3-9. Normalized measured turbidity and model suspended-sediment concentration at Position AK2AMR during one event characterised by significant deposition. In absence of calibrated NTU:SSC relationship, timeseries were normalized using the maximum value.

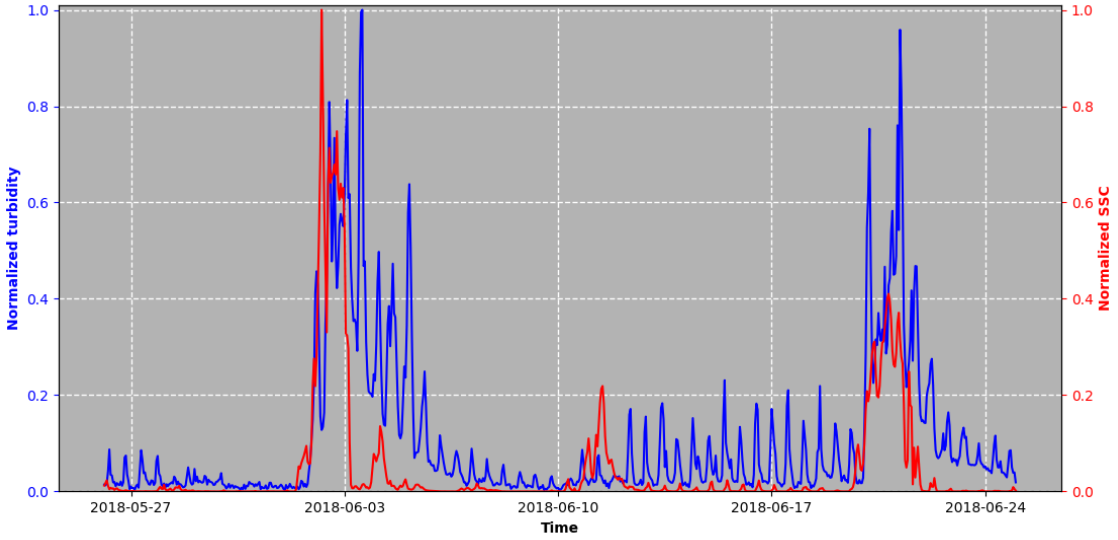

Figure 3-10. Normalized measured turbidity and model suspended-sediment concentration at Position AK3A over a one-week period. In absence of calibrated NTU:SSC relationship, timeseries were normalized using the maximum value.

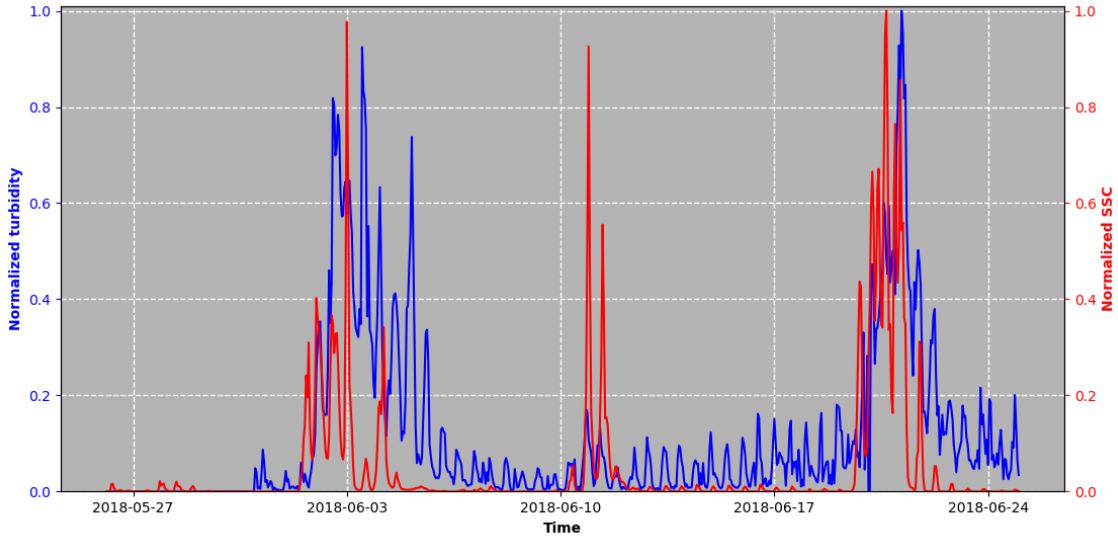

Figure 3-11. Normalized measured turbidity and model suspended-sediment concentration at Position AK2AMR during one event characterised by significant deposition. In absence of calibrated NTU:SSC relationship, timeseries were normalized using the maximum value.

3.5 Bed Level Changes

Comparisons between model and measured bed level changes were performed at Positions AK2A, AK3A and AK2AMR to investigate the morphodynamics of the Karepiro Bay. For this purpose, interconnections between bed level changes, wave heights and total bed shear stresses are examined in Figure 3-12, Figure 3-13 and Figure 3-14. The measurements of bed level changes indicate several periods of strong sedimentation (i.e. 04/27/2018, 03/06/2018, 05/06/2018) of 3 – 15 cm which are not represented in the model. Most of these events are, however, characterised by high wave conditions with bed shear stress higher than 3 – 5 N/m^2.

According to the numerous relationships established in laboratory between sediment grain size and critical shear stress (e.g. Figure 3-15, Zuo et al. (2017)), it is not realistic that sedimentation occurs with such high values of bed shear stress. Given that the model wave heights have been successfully validated against measurements, the discrepancy between model and measured bed level changes can be attributed to potential errors relating to the acoustic transducers during periods of elevated suspended sediment concentrations. Moulton et al. (2014) determined that altimeter estimates of the seabed can be biased by 0.04 – 0.10 m, particularly in the case of noisy acoustic returns caused by waves and dense near-bed turbid plumes. Although few events are relatively well captured in the model, it has not been possible to identify valid measured periods for the calibration of the space-varying critical bed shear stress field for erosion, critical shear stress for deposition and bed thickness in the mud transport model.

While the successful validation of both wave and current components of the model provide a solid basis for qualitatively investigating the behaviour of the suspended sediments over the study area, the lack of information for the calibration of the morphological model means that the estimates of suspended sediment concentrations induced by wave action have some degree of uncertainty. However, model results in areas dominated by wave action can still be used to provide estimates of the relative importance of wave driven resuspension of existing seabed sediments and the role of catchment derived sediments.

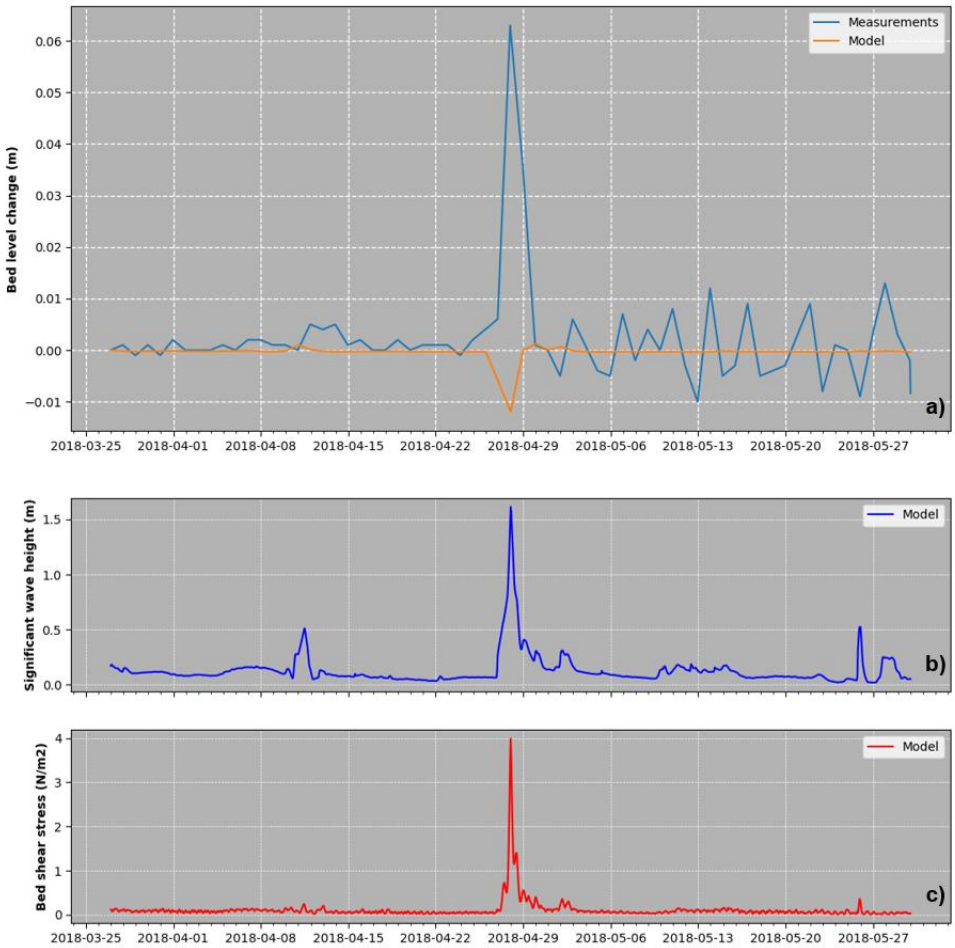

Figure 3-12. Measured and model daily bed level changes (a), significant wave height (b) and bed shear stress (c) at Position AK2A.

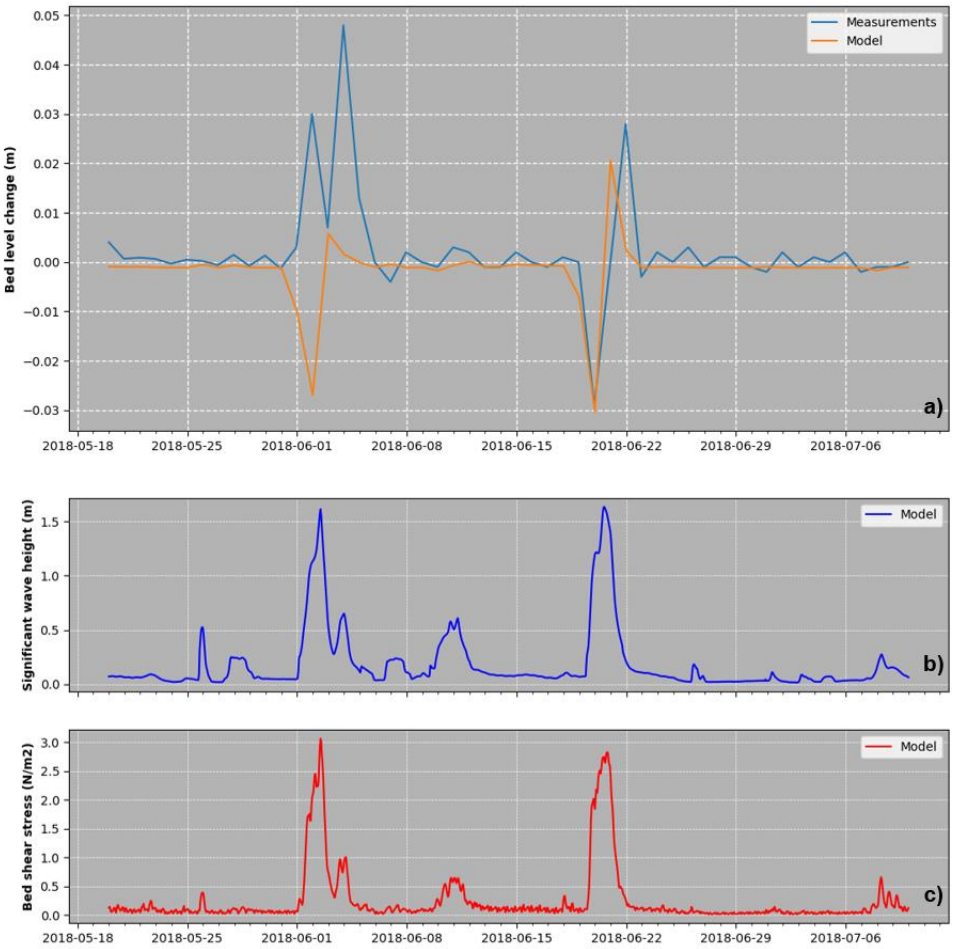

Figure 3-13. Measured and model daily bed level changes (a), significant wave height (b) and bed shear stress (c) at Position AK3A.

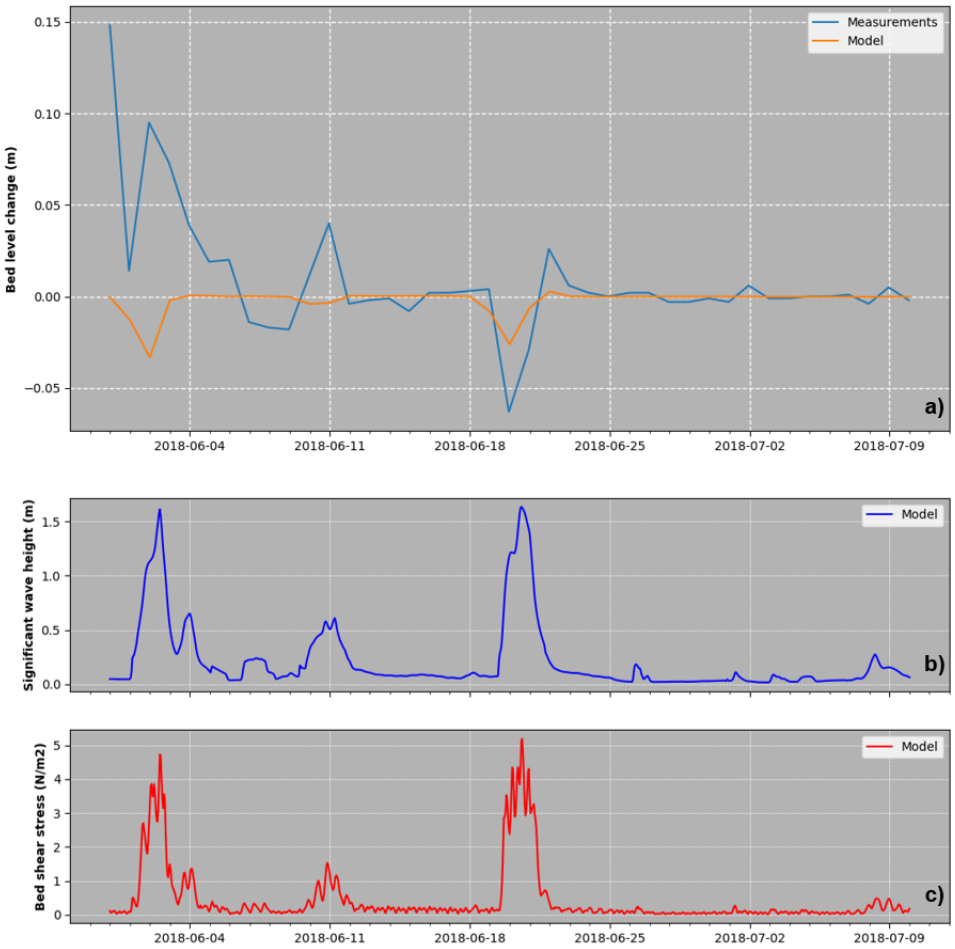

Figure 3-14. Measured and model daily bed level changes (a), significant wave height (b) and bed shear stress (c) at Position AK2AMR.

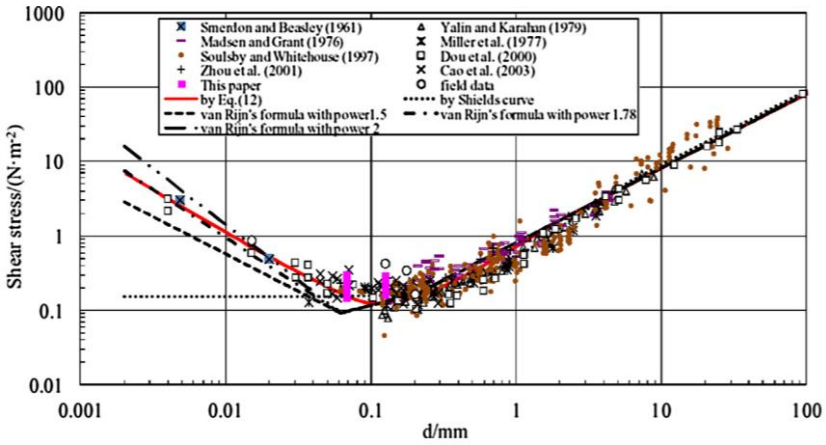

Figure 3-15. Critical shear stress versus sediment grain size (source: Zuo et al. 2017).

3.6 Metal Accumulation Model

The calibration of the metal model is based on the available monitoring data at five sites. These are the State of the Environment (SoE) sites at Long Bay, Awaruku (1998-2013) and Wēiti (1998-2016) plus one-off sampling within the Okura estuary in 2010.

Data from the Okura sites are consistent with data presented in Reed (2008) across similar catchments in the Auckland Region and with the data presented in Green (2016).

Data at the Long Bay and Awaruku sites show very little trend in metal accumulation (Mills, 2016) and show the predominance of coarser grained sediments at these sites.

Figure 3-16 show the overlapping Zinc monitoring data from the Wēiti SoE site and the predicted annual sediment loads from the Silverdale catchment from the FWMT for the period 2002-2016. This figure illustrates that the observed downward trend in Zinc concentrations is driven, in part, by variations in load generation within the catchment.

The calibration of the model was achieved by assumed a spatially varying SML of 15 cm for inter-tidal areas to a minimum of 5 cm in the deeper parts of the model domain. Initial background levels of Zinc and Copper were assumed to be 25 mg/kg and 5 mg/kg respectively.

The calibration against the monitoring data is shown in Figure 3-17.

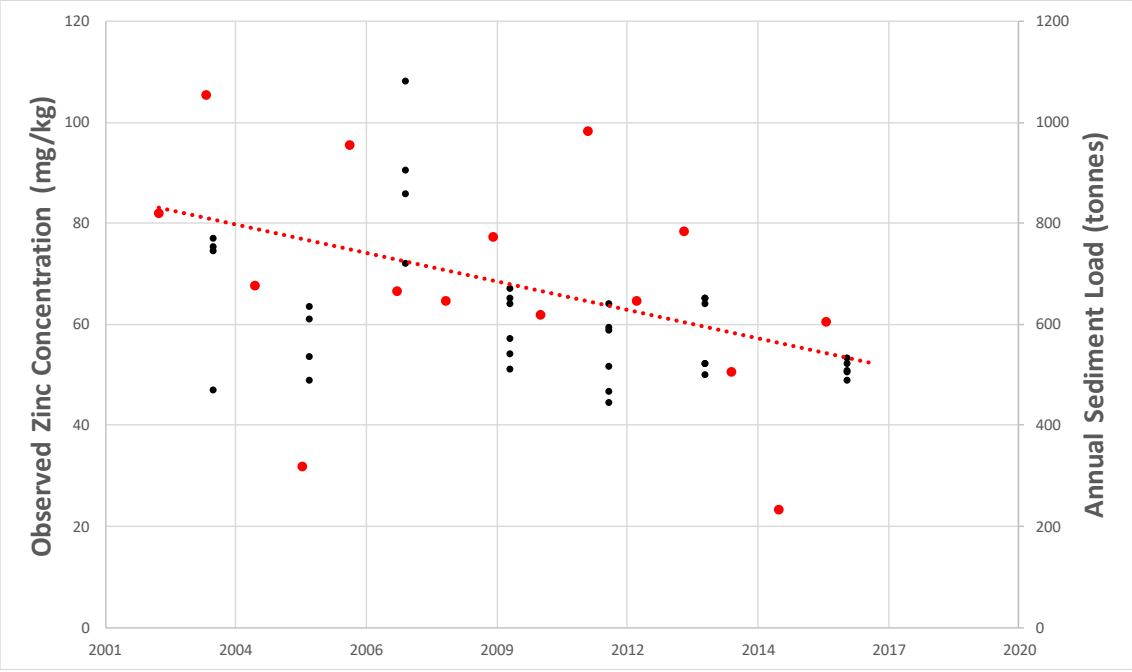

Figure 3-16. Zinc monitoring data (mg/kg) from the Wēiti State of Environment site (black symbols)and predicted FWMT sediment loads (tonnes/year) from the Silverdale catchment (red symbols).

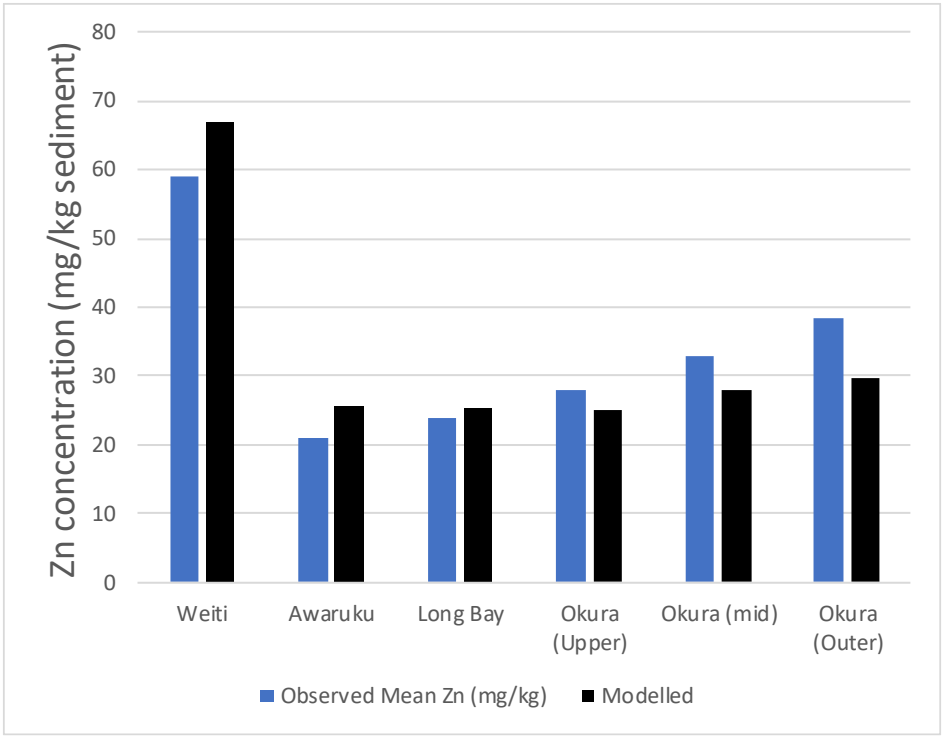

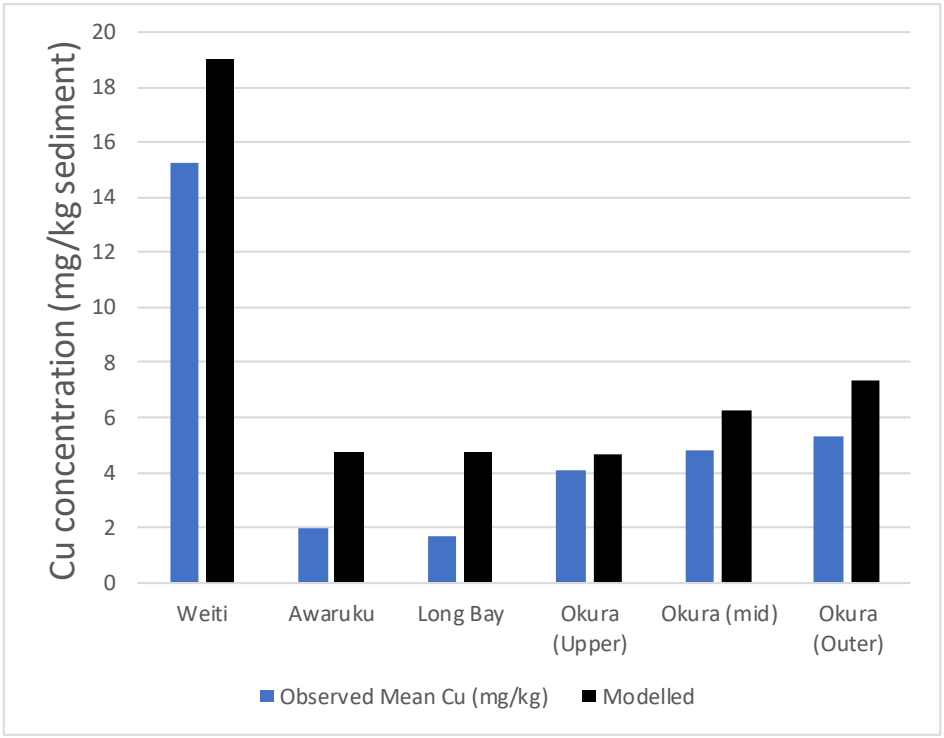

Figure 3-17. Current day observed and predicted sediment metal concentrations (mg/kg) at the metal monitoring sites.

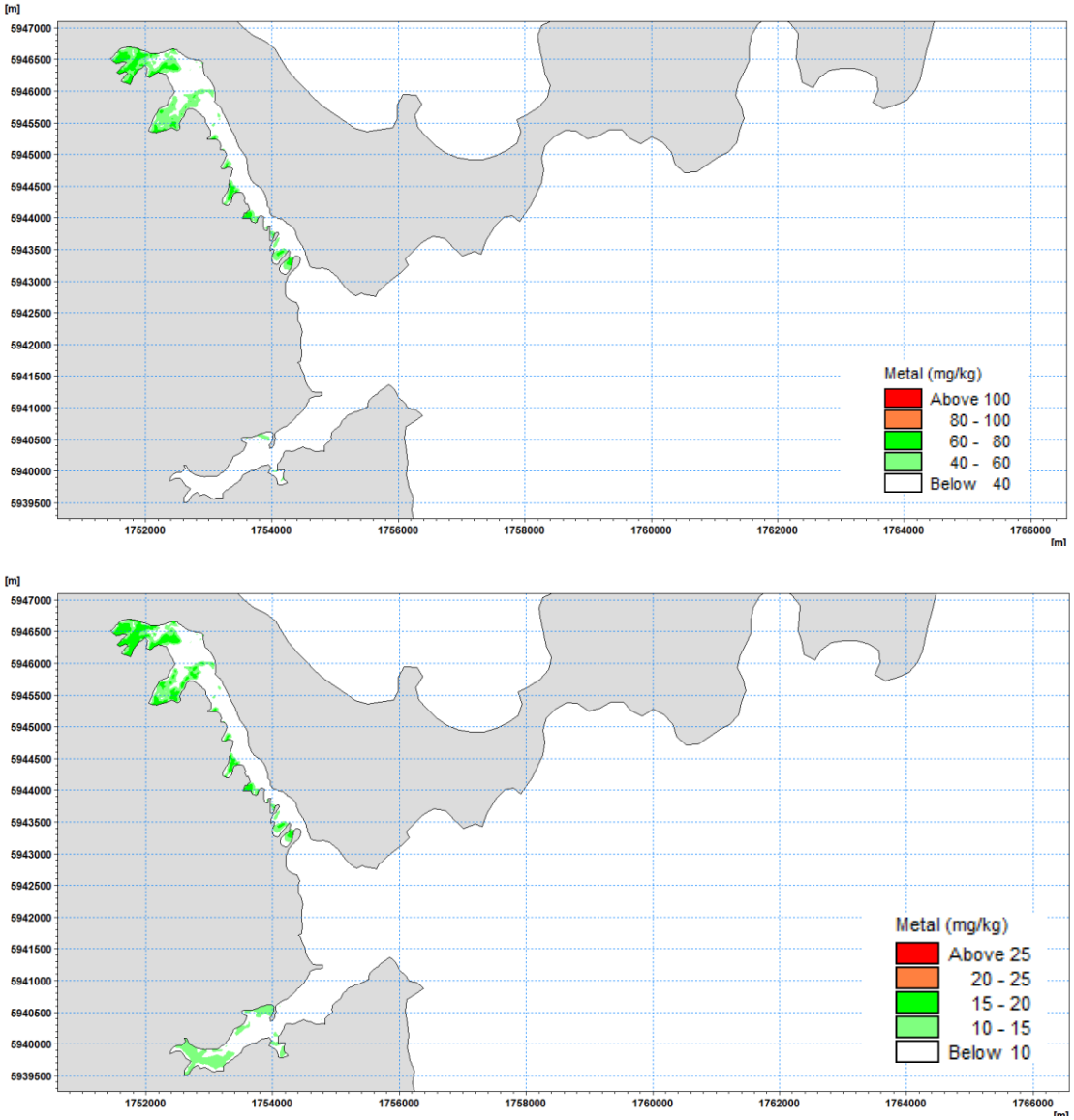

Figure 3-18. Current day predicted Zinc (top) and Copper (bottom) concentrations (mg/kg).

4 Model Results

The following section of the report provides an overview of the model predictions based on catchment inputs from Scenario 0 with existing sea bed sediments (as per Section 2.7).

Current and sediment transport patterns have been investigated in both Wēiti and Okura Estuaries, and Karepiro Bay over the full calibrated period (25/03/2018 – 12/07/2018).

The effect of tidal currents on local bed shear stress at Neap and Spring tides is presented in Figure 4-1 to Figure 4-4.

Bed shear stress fields induced during high wave events (i.e. 20/06/2018) are shown in Figure 4-5.

While the tide-induced shear stresses are relatively low in Karepiro Bay (< 0.3 N/m^2 at Spring tide), tidal flows generate high shear stresses in the more constricted sections of Wēiti and Okura estuaries, particularly near the river mouths. The upper stream areas are, however, subjected to low currents and bed shear stresses which favour the deposition of catchment derived sediments as shown in Figure 4-6. The finest particles are transported toward the channels (see Figure 4-7) and transported into the wider Karepiro Bay depositing mostly in water depths higher than 8 – 10 m. During calm conditions, deposition of material can happen immediately in the river mouths. However, the lack of sediment consolidation in the sediment transport model means that sediments can be resuspended during wave events.

Over the inter-tidal areas, the model results suggest a slow erosion of the sea bed. Consolidation effects due to organic contents and sand bed-load transport are, however, likely to prevent the long-term erosion of the sea bed.

Without any inter-annual bathymetry survey of this area, it has not been possible to determine the correct space-varying sediment transport patterns in this area.

However, a key finding of the modelling is the relative importance of wave processes and the much higher potential for sediment transport in Karepiro Bay compared to the tidally driven sediment transport in the Wēiti River and Okura Estuary.

In this context, the focus of the assessment of the future development scenarios will be on the relative changes in deposition and suspended sediment due to just the catchment derived sediments with model results with existing seabed sediments used to provide context of the overall pattern of deposition and erosion in the wider Karepiro Bay and the relative role of wave induced resuspension of sediments.

In the following sections of the report model results from key sites are presented (Section 4.1), quantification of the connectivity of the system is discussed (Section 4.2) and result from the metal accumulation model are presented (Section 4.3).

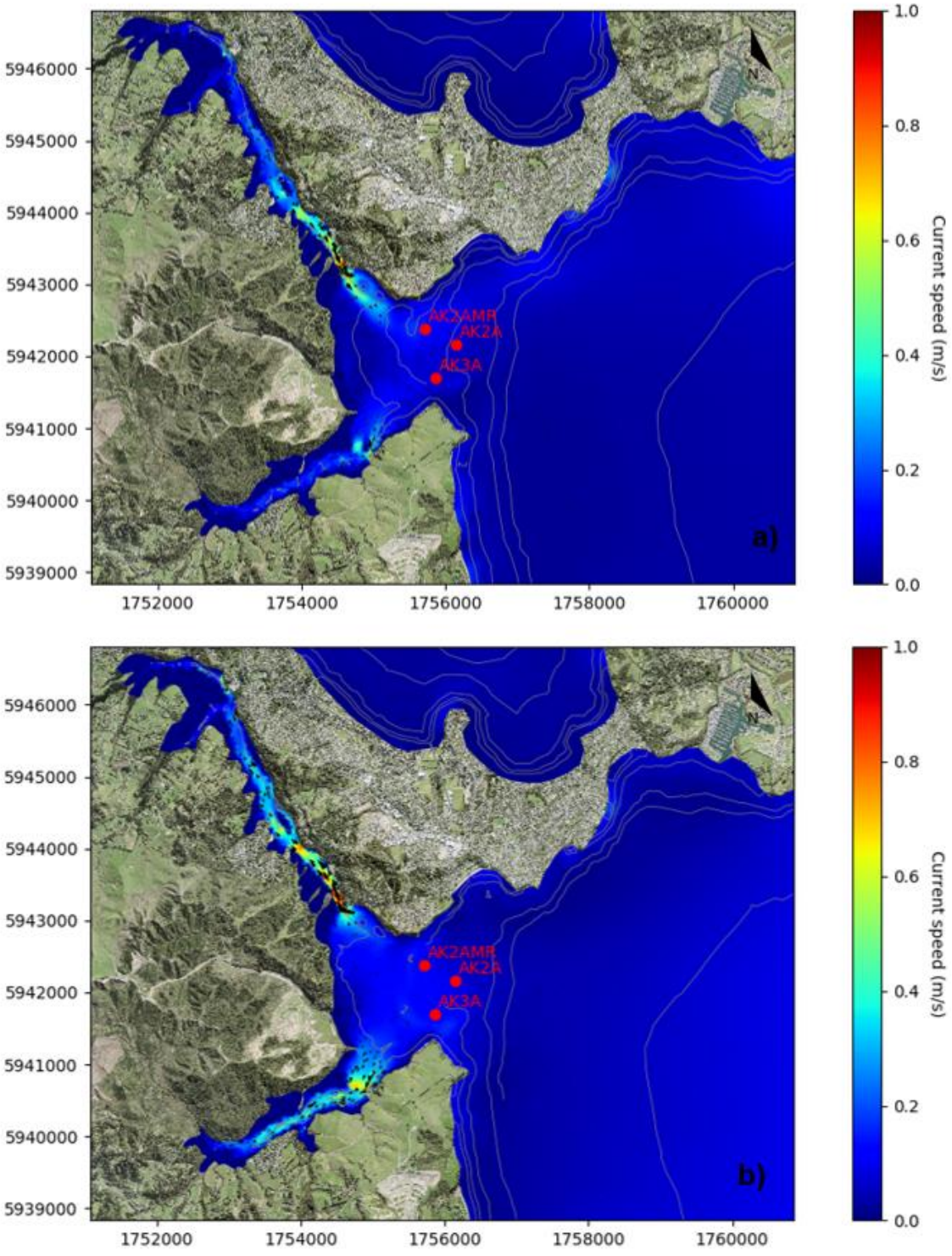

Figure 4-1. Peak ebb (a) and flood (b) currents at Neap tide.

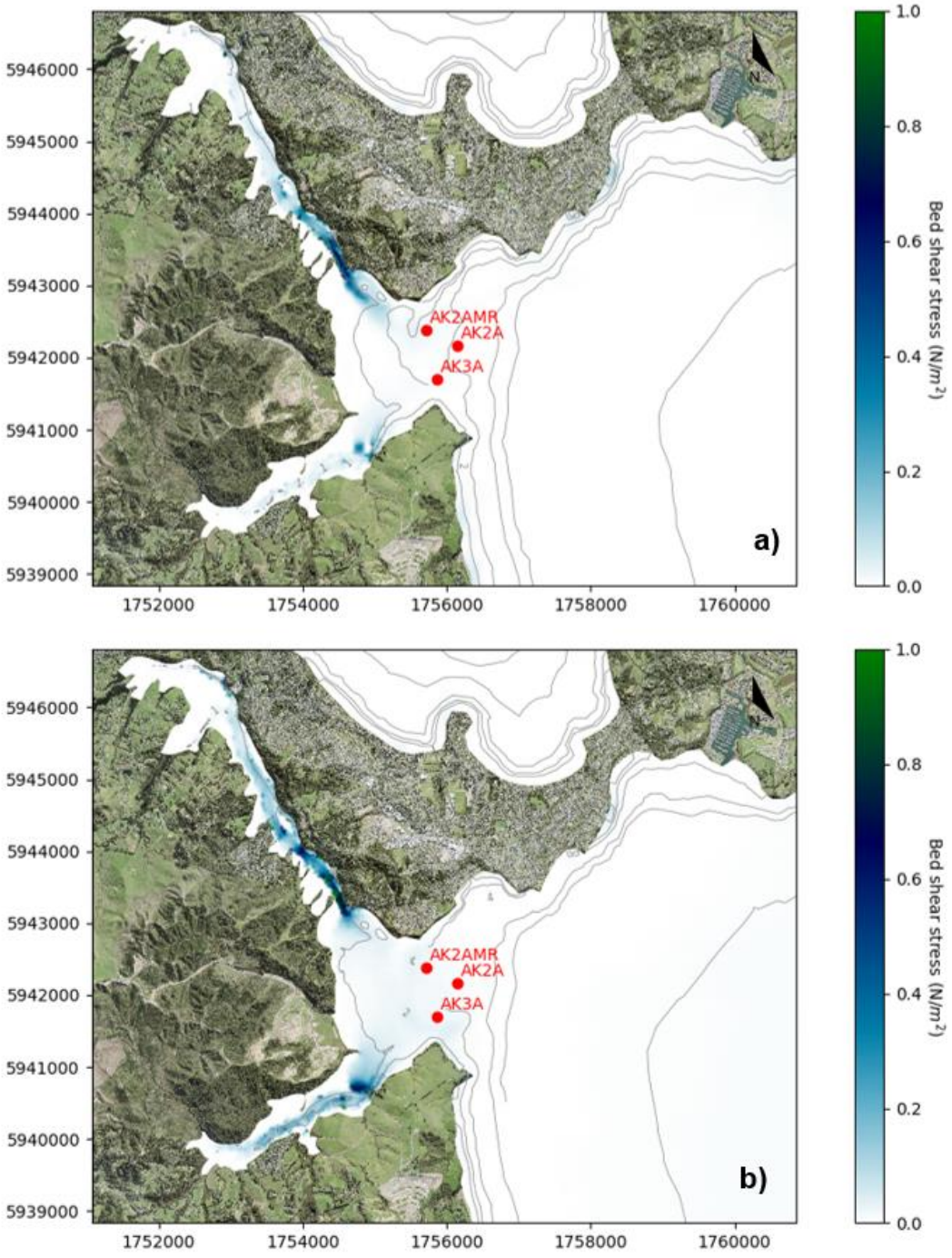

Figure 4-2. Peak ebb (a) and flood (b) bed shear stress at Neap tide.

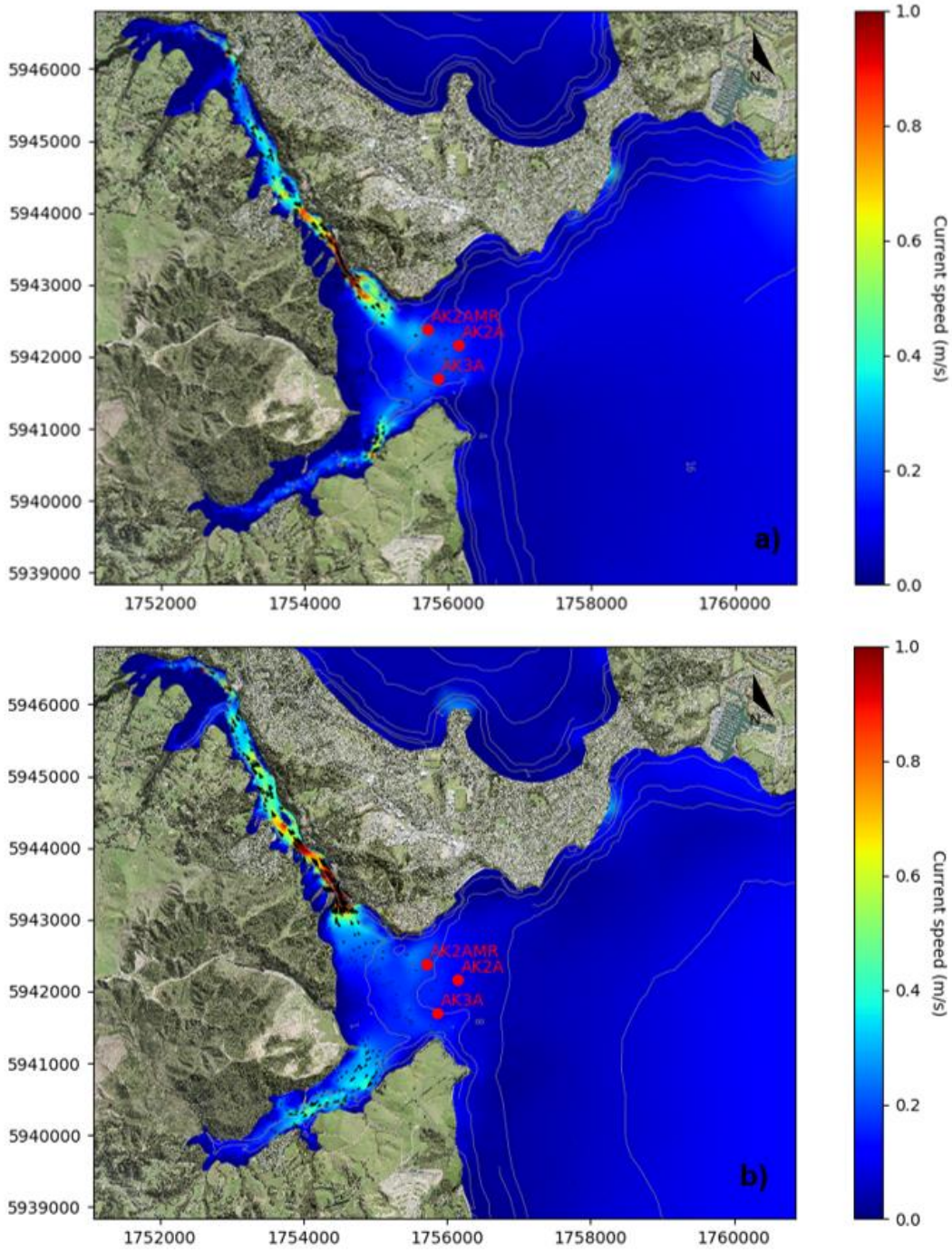

Figure 4-3. Peak ebb (a) and flood (b) currents at Spring tide.

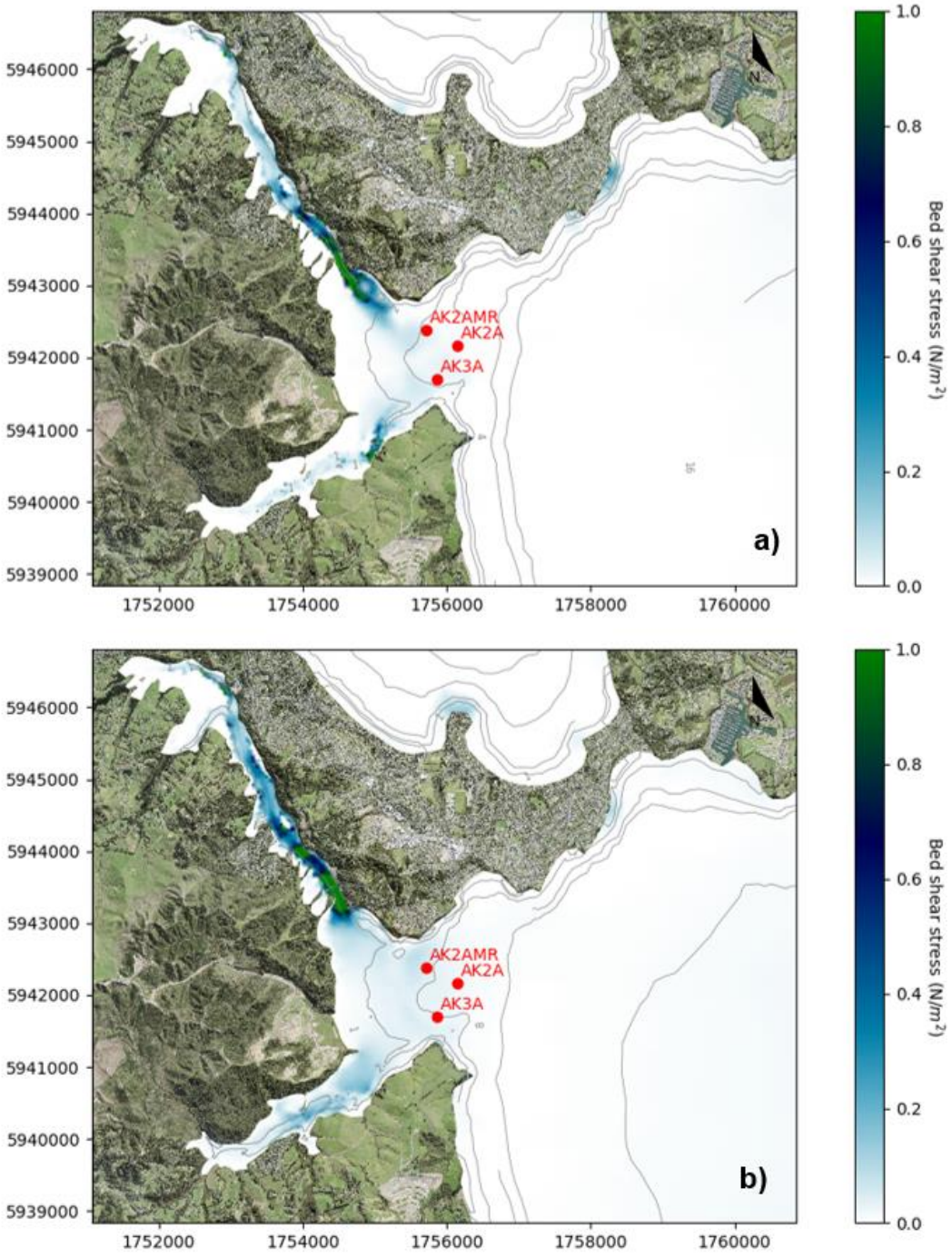

Figure 4-4. Peak ebb (a) and flood (b) bed shear stress at Spring tide.

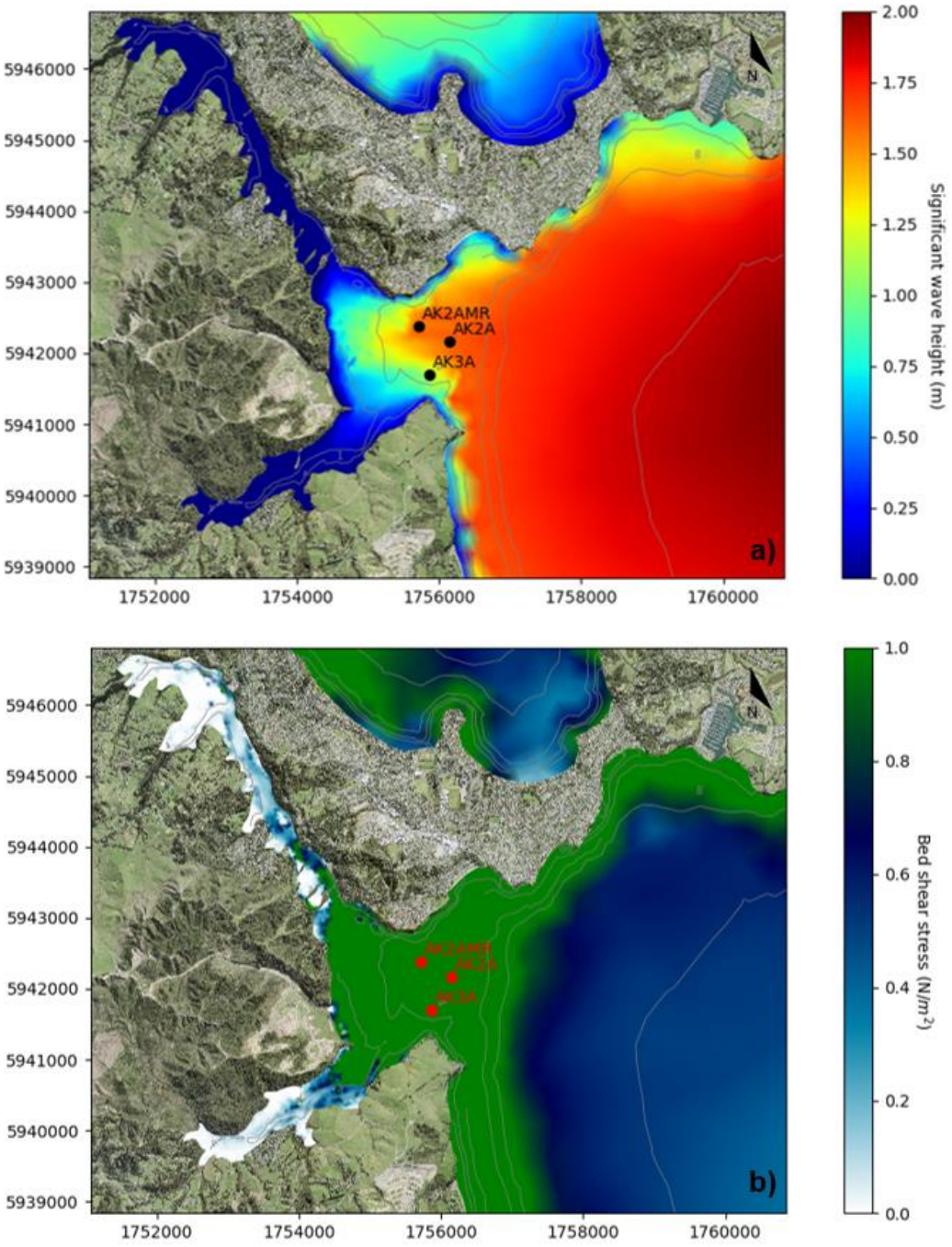

Figure 4-5. Significant wave height (a) and bed shear stress (b) for a high-wave event on 20/06/2018 at 14:00.

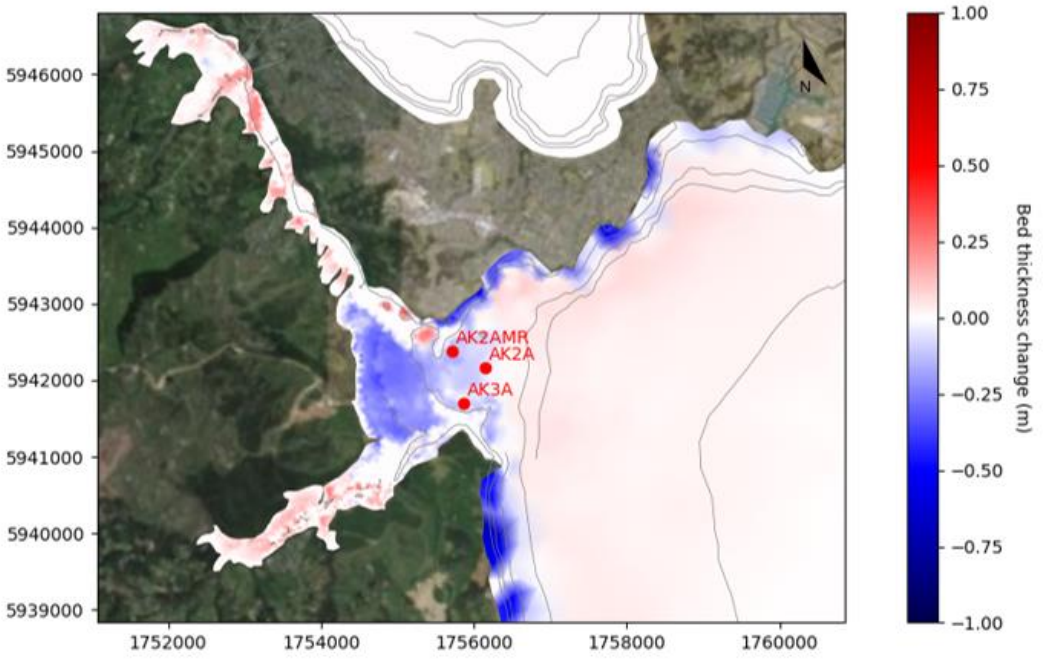

Figure 4-6. Bed thickness change over the calibration period (25/03/2018 – 12/07/2018). Positive (red colours) and negative (blue colours) values indicate sedimentation and erosion, respectively.

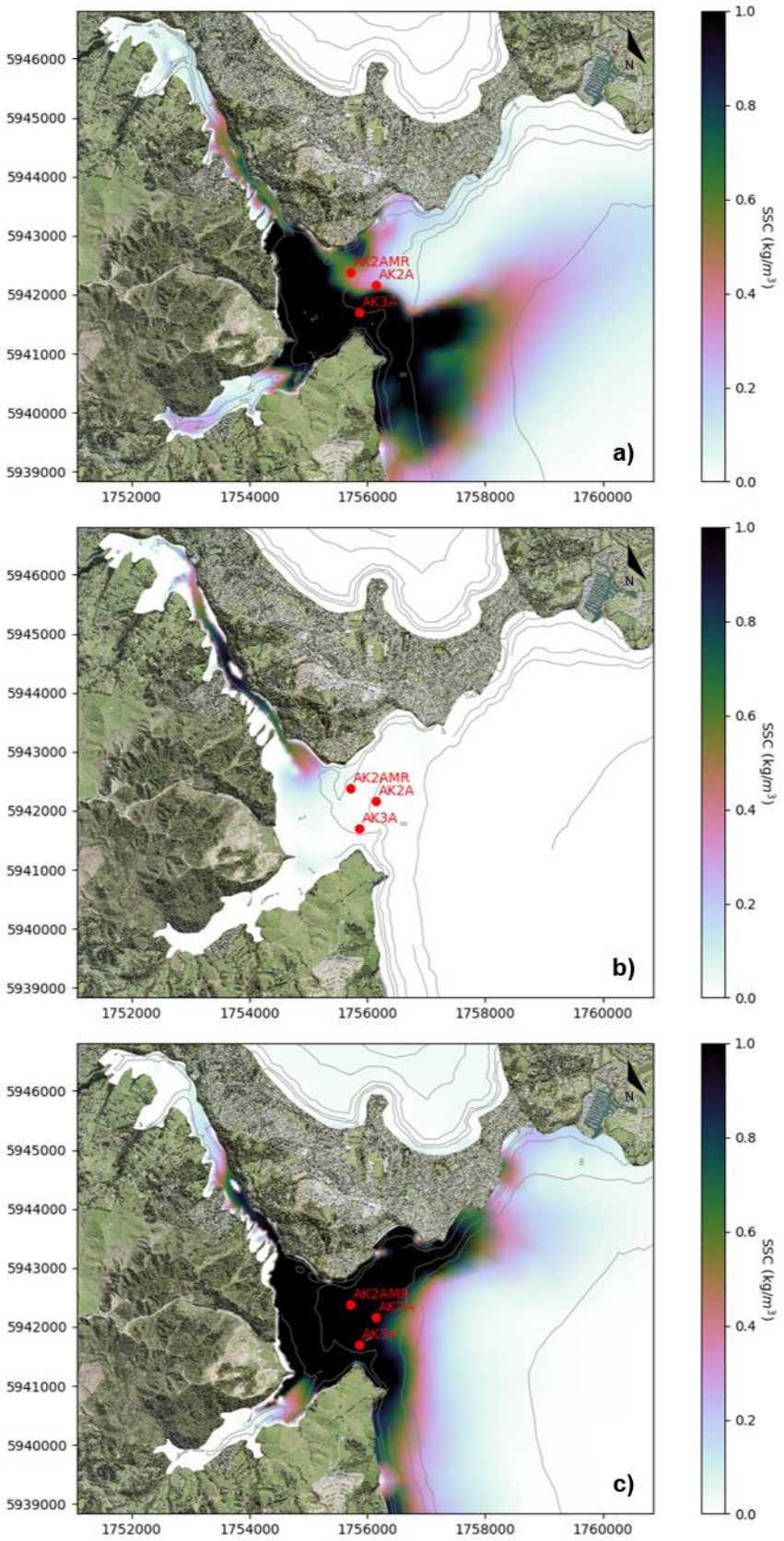

Figure 4-7. Suspended-sediment concentrations in the model top layer during (a) a large wave event combined with a large discharge into the Okura River (24/05/2018 10:00), (b) a large river discharge only into the Wēiti River (02/06/2018 23:00) and (c) a large wave event only described in Figure 4-5 (20/06/2018 14:00) .

4.1 Key Sites

Data at the eight key sites shown in Figure 4-8 are presented in Table 4-1 and Figure 4-9 to Figure 4-12.

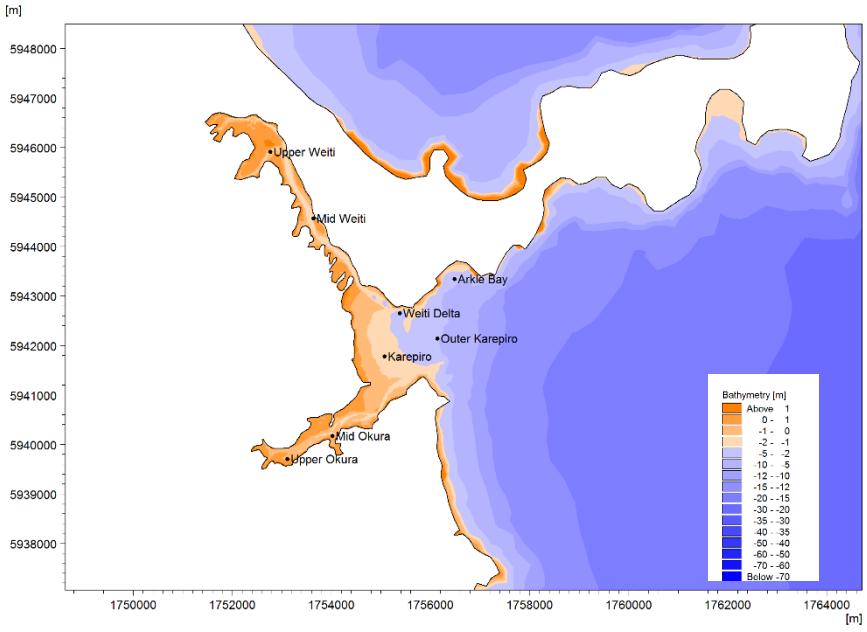

Figure 4-8. Eight key sites in different settings

Table 4-1. Key model outputs at the eight key sites (Figure 4-8).

	Upper Wēiti	Mid Wēiti	Upper Okura	Mid Okura	Karepiro	Wēiti Delta	Outer Karepiro	Arkle Bay
Time above > 80 mg/L	11.68%	17.04%	4.53%	9.65%	18.36%	22.05%	15.26%	13.59%
Time above > 310 mg/L	1.67%	8.10%	0.12%	3.69%	14.30%	14.42%	8.94%	6.44%
Time above > 400 mg/L	1.31%	7.51%	0.12%	3.22%	13.11%	11.68%	7.39%	5.36%
Maximum Bed Level Change (mm)	8.2	3.3	3.8	2.1	0.7	2.9	0.1	0.3

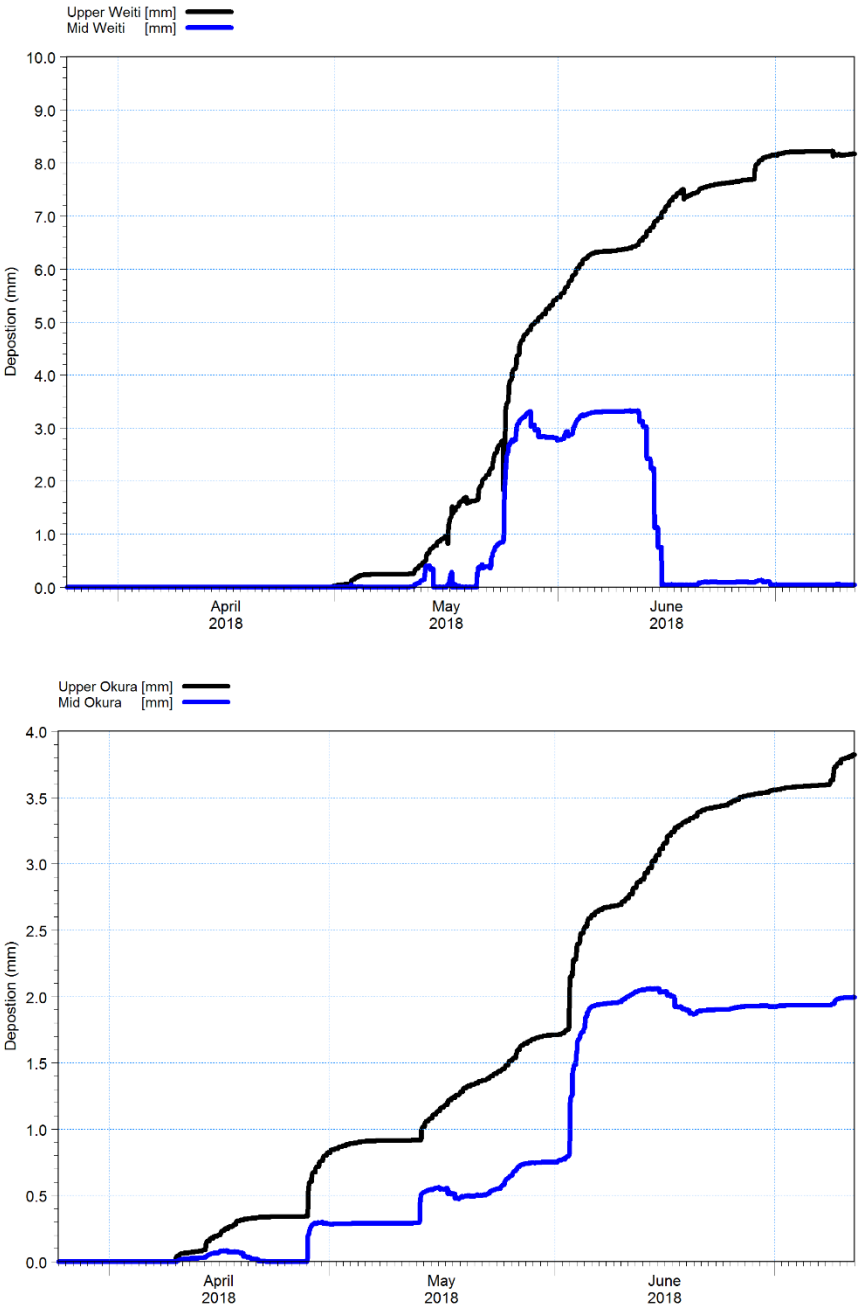

Figure 4-9. Predicted bed level change (mm) at the key sites within the Okura estuary and Wēiti river (Figure 4-8).

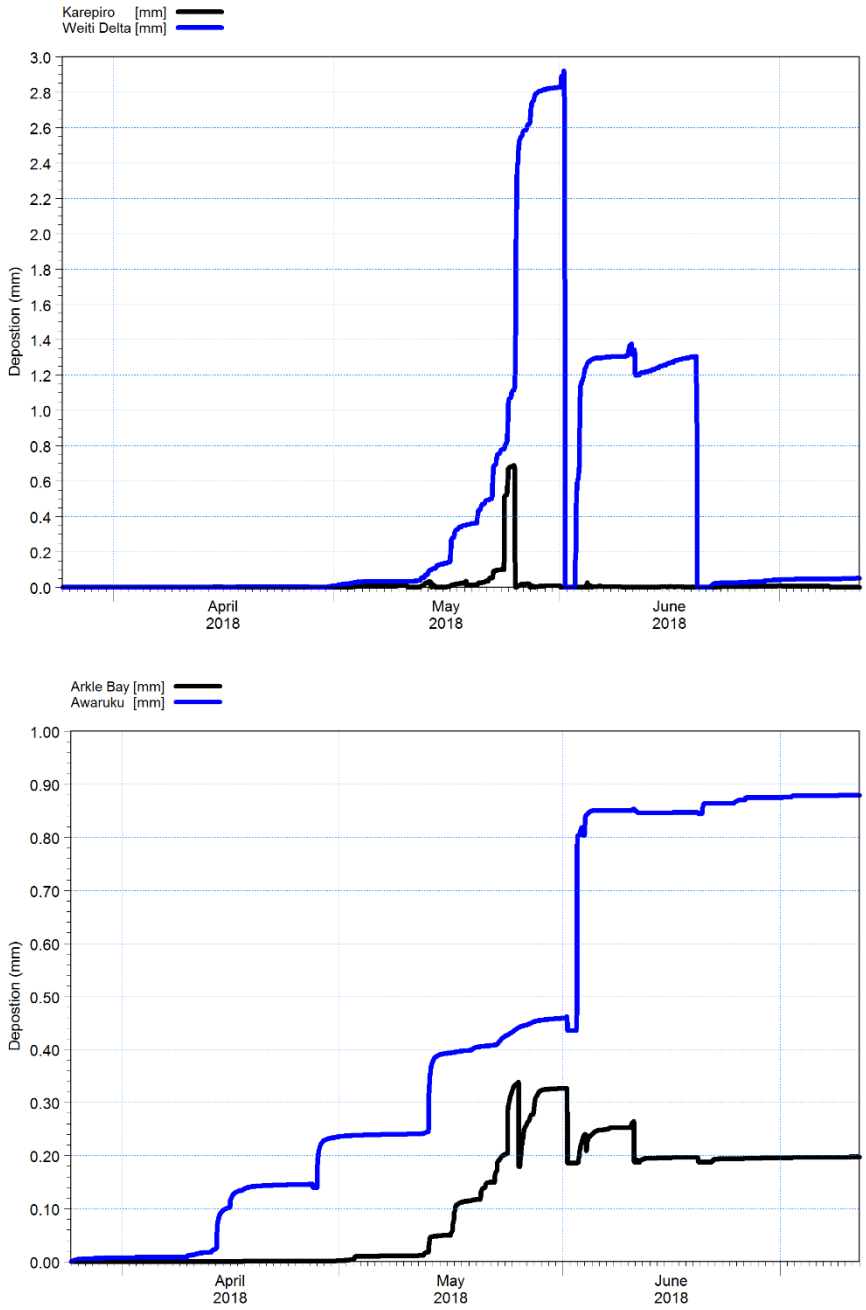

Figure 4-10. Predicted bed level change (mm) at the key sites within Karepiro Bay (Figure 4-8).

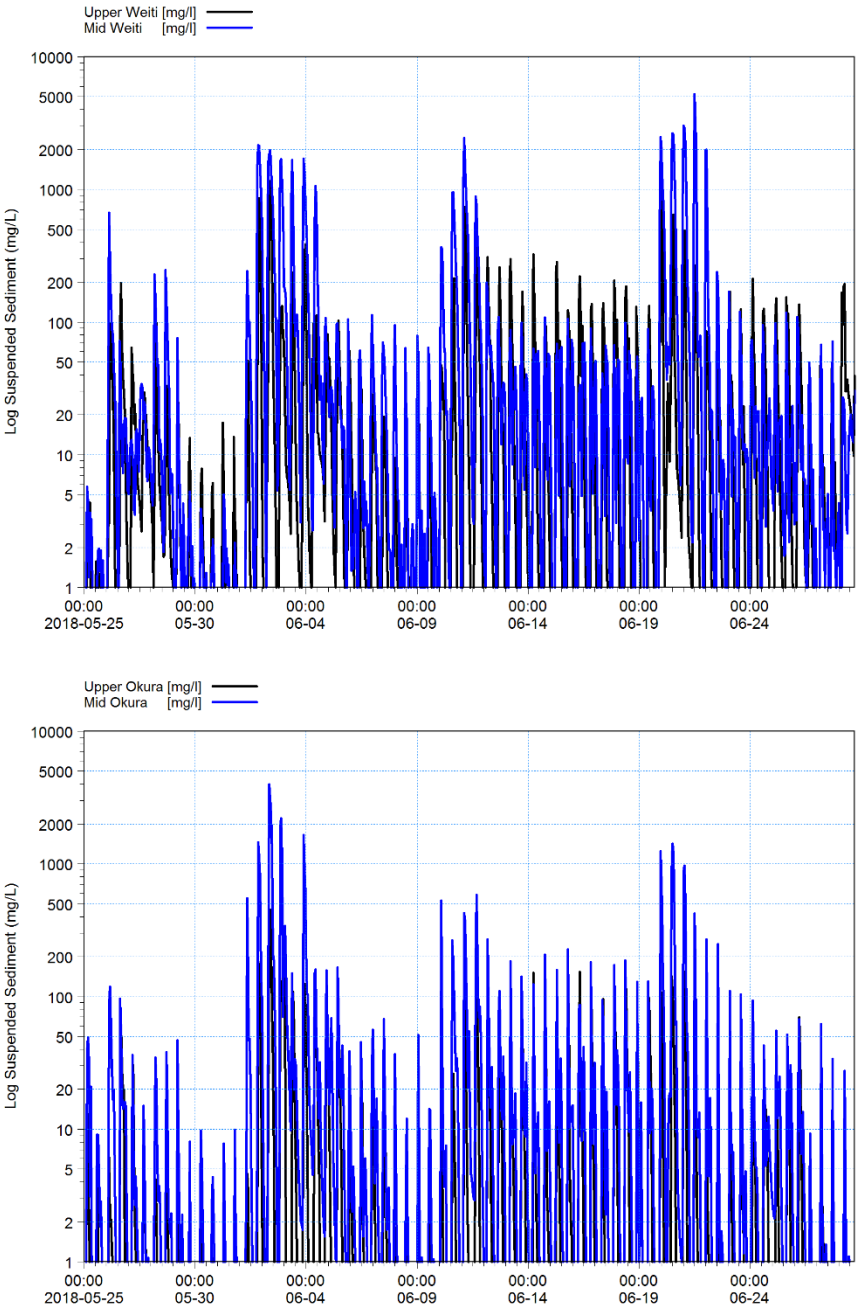

Figure 4-11. Predicted near-surface suspended sediment concentrations (mg/L) at the key sites within the Okura estuary and Wēiti river (Figure 4-8). Note the vertical axis has a log scale.

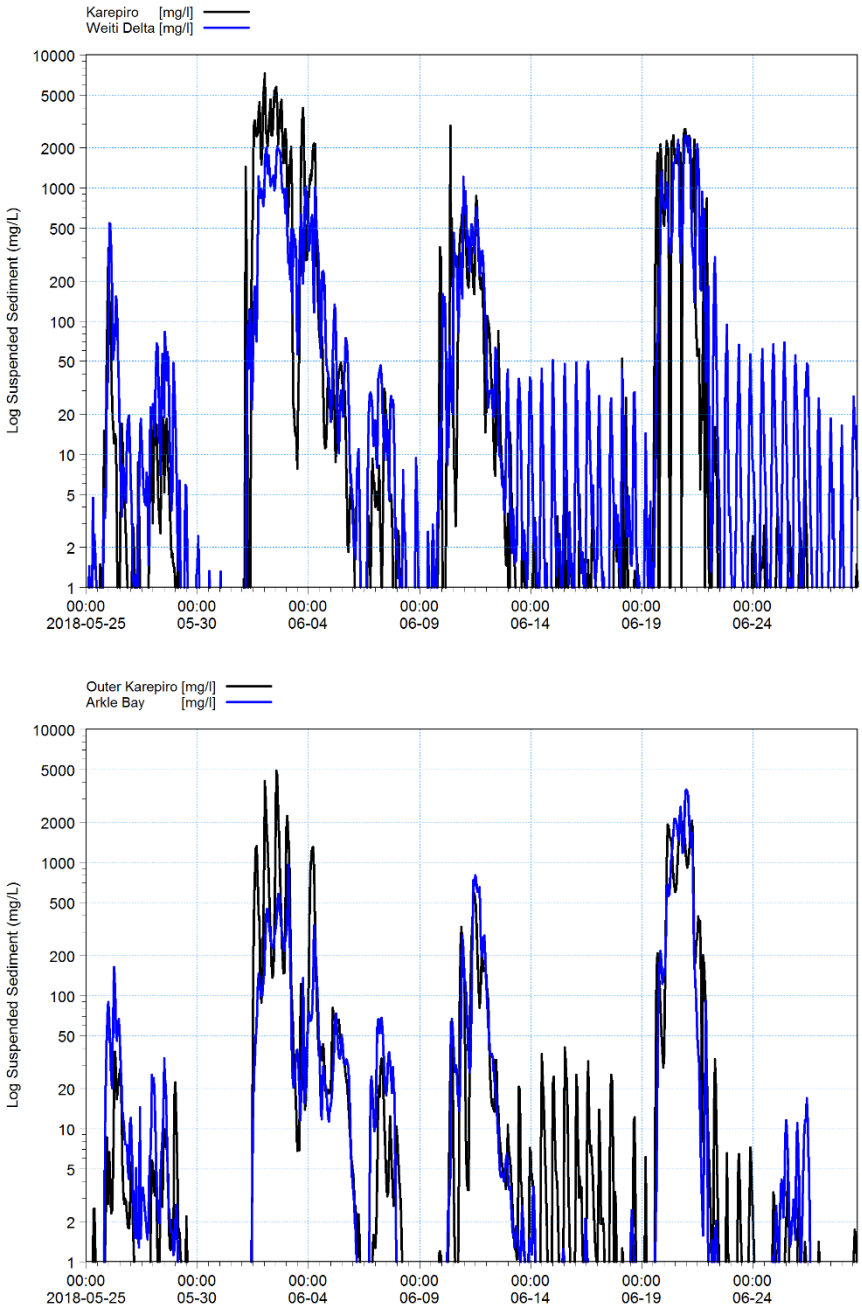

Figure 4-12. Predicted near-surface suspended sediment concentrations (mg/L) at the key sites within Karepiro Bay (Figure 4-8). Note the vertical axis has a log scale.

4.2 Connectivity

To provide an understanding of the connectivity of the system a series of model runs were carried out where silts from individual catchment outlets were tracked independently so that the contribution each catchment outlet makes to the overall predicted deposition could be quantified.

Sands will predominantly be deposited within the subestuary adjoining the catchment outlet and clays will be more widely dispersed.

The subdivision of the model domain into subestuaries (Figure 4-13) was done based on the broad scale setting of the area (e.g. tidally dominated or wave dominated) and the overall predicted pattern of deposition (highest in the upper Okura estuary and Wēiti river) and lower rates in the wider Karepiro Bay.

Appendix A.3 provides spatial maps of the predicted distribution of deposited silts for each of the individual sources. Data from this spatial distribution is used to develop connectivity matrices linking catchment sources with subestuaries.

This data can be used in two ways.

Firstly, the contribution that each catchment makes to the predicted level of deposition in each of the subestuaries can be quantified - summarised in Table 4-2 to Table 4-5.

For example, in Table 4-2 we see that the majority of the deposition in the Upper Okura can be attributed to the Redvale catchment (which has the highest sediment load, Table 2-2) and the other Okura subcatchments. Catchments outside of Okura estuary do contribute to the predicted deposition in the Okura estuary depending on their relative catchment loads and proximity to the subestuary being considered.

For the Karepiro South subestuaries (Table 4-3) the majority of the predicted deposition occurs due to the Redvale and Silverdale catchments with less than 25% of the predicted deposition due to the Karepiro catchments directly. For the Karepiro North subestuary the Karepiro Beach catchment contributes the majority of the deposition (although as noted above this area is dominated by erosional processes) and so has very low deposition rates.

Within the Wēiti River the deposition is dominated by the Silverdale catchment (Table 4-4) with contributions from all the other Wēiti catchments and some connectivity to catchment outside the Wēiti river.

Within the wider Karepiro Bay (Table 4-5) the deposition is dominated by the Silverdale catchment.

Secondly, the data can be used to determine what portion of sediment from a particular catchment ends up in each subestuary – summarised in Table 4-6.

For example, we see that the majority (> 70%) of the Silverdale silt load is deposited in the Upper Wēiti and less than 10% of the Silverdale silt load deposited in the Mid and Lower Wēiti. We also see that just over 3% of the Silverdale silt load is deposited in the Okura subestuaries.

A similar pattern is seen for the Redvale catchment with the majority of the silt load (>87%) deposited in the Okura estuary and around 7% being deposited in the Wēiti river.

Also, of note is the high degree (> 80%) of loss of silt loads from the Arkle Bay, North Outlet Awaruku and Long Bay catchments to the “Outer Gulf” (defined as the area outside the defined subestuaries in Figure 4-13).

Of interest is the relatively high portion of the Karepiro and Karepiro Beach sediment loads that deposit in the Okura and Weiti subestuaries and higher losses to the Outer Gulf.

In summary we see that

- around 70% of the Okura catchment silt load is deposited within the Okura estuary with nearly 15% deposited in the Wēiti river
- around 70% of the Wēiti catchment silt load is deposited within the Wēiti river with less than 15% deposited in the Okura estuary
- nearly 40% of the silt load from the Karepiro subcatchments is deposited in the Okura estuary and just over 30% of the silt load from the Karepiro subcatchments is deposited in the Wēiti river

Figure 4-13. Extent of the subestuaries within the Okura/Wēiti marine receiving environment.

Table 4-2 Connectivity for Okura estuary. Column is percentage contribution to predicted deposition within the given subestuary (Figure 4-13). Colour coding indicates strong connectivity in red, intermediate connectivity in yellow and low connectivity in green.

	Okura (Upper)	Okura (Mid)	Okura (Outer)
Awaruku	0.03%	0.05%	0.09%
Long Bay	0.16%	0.29%	2.50%
SS Outer	0.56%	1.10%	2.28%
SS Mid East	1.55%	3.28%	8.00%
SS Mid West	1.93%	3.91%	7.09%
SS Inner	3.14%	2.83%	2.71%
Redvale	57.89%	40.66%	35.41%
North Arm	16.88%	11.88%	8.83%
NorthShore	1.08%	2.95%	6.43%
Karepiro	5.21%	10.88%	5.73%
Karepiro Beach	3.21%	6.90%	12.36%
Stillwater	1.10%	1.95%	0.66%
Wēiti South	1.15%	2.10%	0.89%
Silverdale	5.14%	9.41%	4.42%
Arkle Bay	0.45%	0.86%	1.20%
Whangaparaoa	0.21%	0.38%	0.38%
Wēiti North	0.14%	0.25%	0.15%
North Outlet	0.05%	0.10%	0.75%
Duck Creek	0.11%	0.20%	0.12%

Table 4-3 Connectivity for Karepiro Beach. Column is percentage contribution to predicted deposition within the given subestuary (Figure 4-13). Colour coding indicates strong connectivity in red, intermediate connectivity in yellow and low connectivity in green.

	Karepiro (S)	Karepiro (N)
Awaruku	0.45%	0.08%
Long Bay	1.21%	0.18%
SS Outer	1.43%	1.16%
SS Mid East	2.96%	3.54%
SS Mid West	2.72%	2.63%
SS Inner	1.97%	1.05%
Redvale	27.98%	13.32%
North Arm	7.09%	3.32%
NorthShore	2.30%	2.38%
Karepiro	10.04%	3.71%
Karepiro Beach	13.81%	35.34%
Stillwater	2.01%	2.42%
Wēiti South	3.51%	4.17%
Silverdale	18.50%	21.86%
Arkle Bay	1.05%	1.42%
Whangaparaoa	1.27%	1.68%
Wēiti North	0.86%	0.95%
North Outlet	0.26%	0.05%
Duck Creek	0.59%	0.75%

Table 4-4 Connectivity for Wēiti river. Column is percentage contribution to predicted deposition within the given subestuary (Figure 4-13). Colour coding indicates strong connectivity in red, intermediate connectivity in yellow and low connectivity in green.

	Wēiti (Upper)	Wēiti (Mid)	Wēiti (Outer)
Awaruku	0.02%	0.03%	0.06%
Long Bay	0.06%	0.14%	0.26%
SS Outer	0.08%	0.20%	0.37%
SS Mid East	0.24%	0.56%	1.03%
SS Mid West	0.23%	0.51%	0.89%
SS Inner	0.10%	0.21%	0.40%
Redvale	1.55%	3.37%	6.15%
North Arm	0.39%	0.84%	1.54%
NorthShore	0.18%	0.41%	0.72%
Karepiro	0.91%	1.93%	3.29%
Karepiro Beach	2.12%	3.91%	7.78%
Stillwater	4.41%	12.96%	12.19%
Wēiti South	15.41%	12.68%	12.32%
Silverdale	69.71%	56.75%	45.35%
Arkle Bay	0.57%	1.26%	2.51%
Whangaparaoa	0.95%	1.68%	2.47%
Wēiti North	1.43%	1.38%	1.51%
North Outlet	0.02%	0.06%	0.11%
Duck Creek	1.63%	1.10%	1.08%

Table 4-5 Connectivity for wider Karepiro Bay. Column is percentage contribution to predicted deposition within the given subestuary (Figure 4-13). Colour coding indicates strong connectivity in red, intermediate connectivity in yellow and low connectivity in green.

	Long Bay	Karepiro Bay	Whangaparaoa	Outer Karepiro Bay
Awaruku	10.73%	3.99%	3.50%	8.20%
Long Bay	12.16%	5.25%	4.72%	9.47%
SS Outer	0.78%	1.05%	0.65%	0.95%
SS Mid East	1.48%	2.48%	1.36%	1.59%
SS Mid West	1.08%	2.04%	1.05%	1.05%
SS Inner	0.55%	0.78%	0.55%	0.48%
Redvale	8.48%	11.31%	8.57%	7.84%
North Arm	2.24%	2.98%	2.18%	2.22%
NorthShore	0.82%	1.70%	0.77%	0.62%
Karepiro	8.70%	4.97%	4.79%	6.39%
Karepiro Beach	3.88%	10.71%	11.82%	6.22%
Stillwater	7.29%	4.79%	5.70%	5.53%
Wēiti South	6.54%	6.51%	7.41%	6.43%
Silverdale	26.16%	29.49%	33.28%	28.89%
Arkle Bay	5.05%	7.08%	8.79%	9.42%
Whangaparaoa	1.05%	1.90%	1.96%	1.51%
Wēiti North	0.66%	1.08%	1.11%	0.95%
North Outlet	1.85%	1.05%	0.90%	1.55%
Duck Creek	0.50%	0.84%	0.89%	0.69%

Table 4-6. Percentage of each catchment sediment load deposited within each of the subestuaries (Figure 4-13). Row is the percentage of each individual catchment load deposited within the given subestuary (Figure 4 13). Colour coding indicates in red, intermediate connectivity in yellow and low connectivity in green.

	Subestaury												
Catchment	Okura (Upper)	Okura (Mid)	Okura (Outer)	Karepiro (S)	Karepiro (N)	Wēiti (Upper)	Wēiti (Mid)	Wēiti (Outer)	Long Bay	Karepiro Bay	Whangaparaoa	Outer Karepiro Bay	Outer Gulf
Awaruku	0.77%	0.26%	0.00%	0.02%	0.01%	0.87%	0.22%	0.14%	3.15%	0.66%	3.27%	4.24%	86.37%
Long Bay	2.32%	1.00%	0.07%	0.04%	0.02%	2.23%	0.62%	0.40%	2.35%	0.57%	2.90%	3.21%	84.28%
SS Outer	34.78%	15.47%	0.27%	0.19%	0.43%	12.81%	3.53%	2.35%	0.63%	0.47%	1.67%	1.34%	26.06%
SS Mid East	39.50%	19.04%	0.39%	0.16%	0.54%	14.82%	4.15%	2.70%	0.49%	0.46%	1.44%	0.92%	15.39%
SS Mid-West	46.98%	21.60%	0.33%	0.14%	0.38%	13.45%	3.58%	2.23%	0.34%	0.36%	1.05%	0.58%	8.97%
SS Inner	71.92%	14.76%	0.12%	0.10%	0.14%	5.39%	1.40%	0.93%	0.16%	0.13%	0.52%	0.25%	4.18%
Redvale	75.71%	12.10%	0.09%	0.08%	0.10%	4.96%	1.27%	0.82%	0.14%	0.11%	0.46%	0.23%	3.90%
North Arm	76.49%	12.25%	0.08%	0.07%	0.09%	4.32%	1.10%	0.71%	0.13%	0.10%	0.41%	0.23%	4.02%
NorthShore	39.67%	24.69%	0.46%	0.18%	0.53%	16.23%	4.33%	2.70%	0.39%	0.46%	1.16%	0.52%	8.68%
Karepiro	31.58%	15.02%	0.07%	0.13%	0.14%	13.53%	3.39%	2.05%	0.68%	0.22%	1.20%	0.88%	31.12%
Karepiro Beach	20.37%	9.98%	0.15%	0.19%	1.35%	33.06%	7.18%	5.07%	0.32%	0.50%	3.10%	0.90%	17.84%
Stillwater	4.92%	1.98%	0.01%	0.02%	0.06%	48.17%	16.67%	5.57%	0.42%	0.16%	1.05%	0.56%	20.41%
Weiti South	2.34%	0.97%	0.00%	0.02%	0.05%	76.45%	7.40%	2.56%	0.17%	0.10%	0.62%	0.30%	9.03%
Silverdale	2.32%	0.97%	0.00%	0.02%	0.06%	77.21%	7.40%	2.10%	0.15%	0.10%	0.62%	0.30%	8.75%
Arkle Bay	4.35%	1.90%	0.02%	0.02%	0.08%	13.54%	3.53%	2.50%	0.64%	0.50%	3.52%	2.09%	67.30%
Whangaparaoa	4.85%	1.98%	0.02%	0.06%	0.23%	53.37%	11.11%	5.80%	0.31%	0.32%	1.85%	0.79%	19.31%
Weiti North	2.96%	1.20%	0.01%	0.04%	0.12%	73.05%	8.29%	3.24%	0.18%	0.16%	0.95%	0.45%	9.35%
North Outlet	3.97%	1.80%	0.11%	0.04%	0.02%	4.70%	1.33%	0.86%	1.88%	0.60%	2.94%	2.78%	78.96%
Duck Creek	2.26%	0.92%	0.00%	0.03%	0.09%	80.20%	6.39%	2.22%	0.13%	0.12%	0.74%	0.32%	6.58%

4.3 Metal Accumulation Model

Based on the calibrated metal model, the predicted metal concentrations (mg/kg) 50 years from present are presented in Table 4-7 for each of the sub-estuaries (Figure 4-13).

Predicted concentrations at the SoE monitoring sites are shown in Figure 4-14.

Spatial plots of the predicted future metal concentrations are shown in Figure 4-14 and Figure 4-16.

Table 4-7. Predicted subestuary wide current day and future (50 year) metal concentrations (mg/kg) under Scenario 0 (Table 1-1).

Subestuary	Current Day Zn (mg/kg)	Future Zn (mg/kg)	Current Day Cu (mg/kg)	Future Cu (mg/kg)
Upper Okura	35.1	80.5	10.0	23.9
Mid Okura	29.3	47.9	6.8	12.6
Outer Okura	25.2	26.0	4.7	5.0
Karepiro Beach (S)	25.1	26.0	4.7	5.0
Karepiro Beach (N)	25.3	26.7	4.8	5.2
Upper Wēiti	43.5	91.3	11.1	24.9
Mid Wēiti	35.1	60.2	7.7	14.4
Outer Wēiti	34.3	58.3	7.4	13.7
Marine Reserve	25.4	26.5	4.7	5.0
Karepiro Bay	25.4	26.6	4.7	5.0
Whangaparaoa	26.1	29.6	4.9	5.8

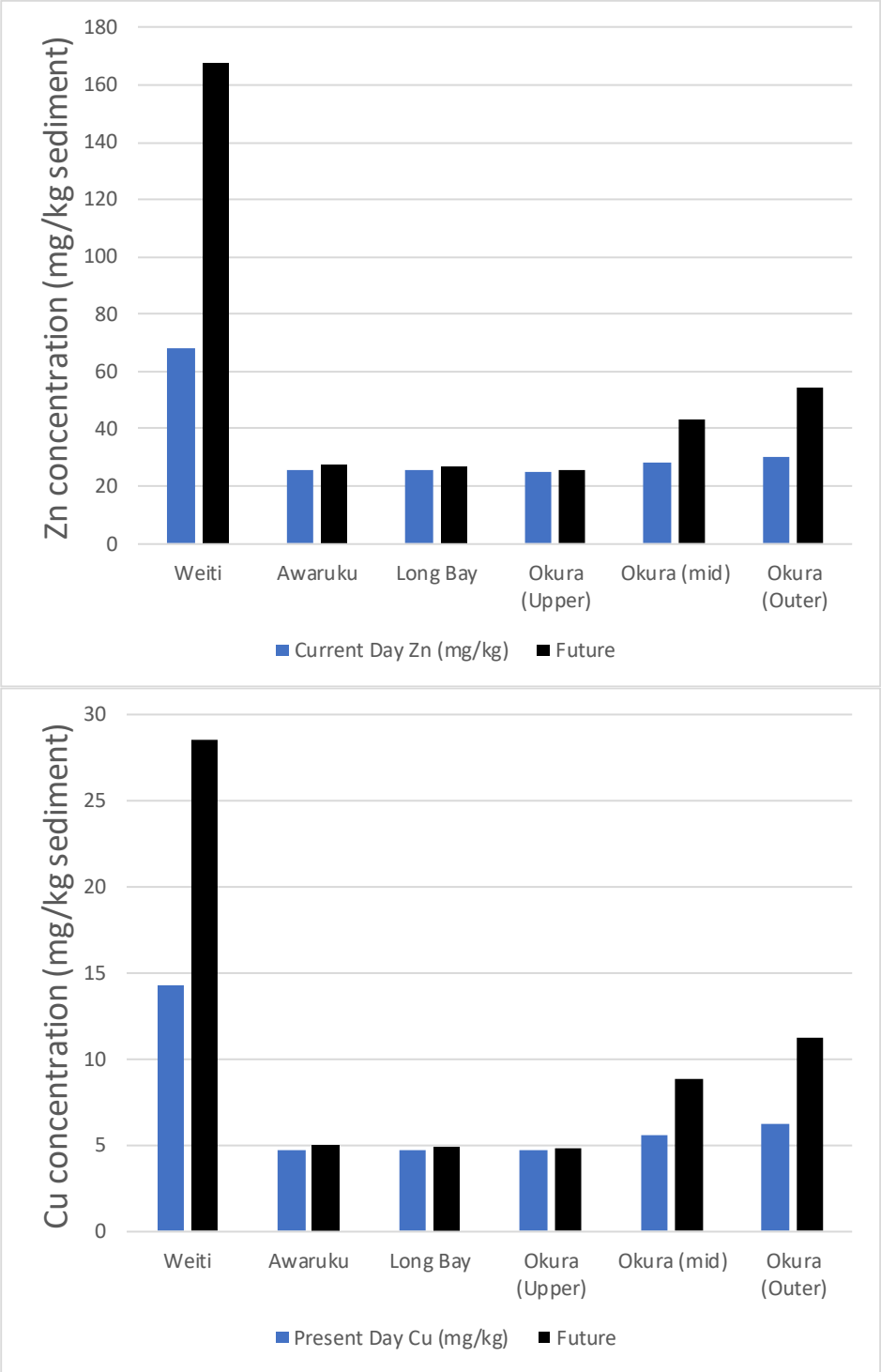

Figure 4-14. Predicted future Zinc (top) and Copper (bottom) concentrations (mg/kg) under Scenario 0 land use at the metal monitoring sites compared to the present-day predictions from the metal accumulation model.

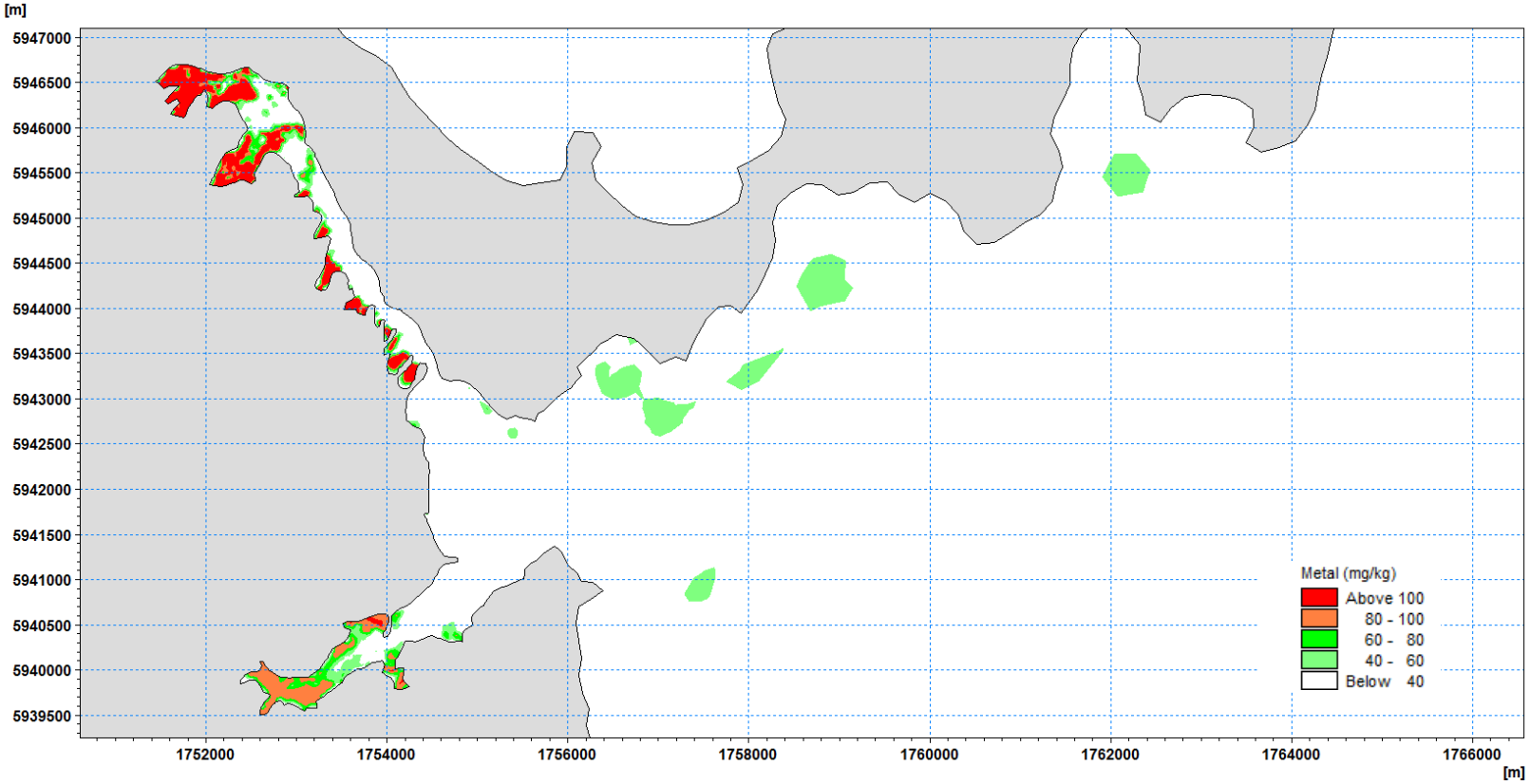

Figure 4-15. Future Zinc concentrations (mg/kg) under Scenario 0 land use.

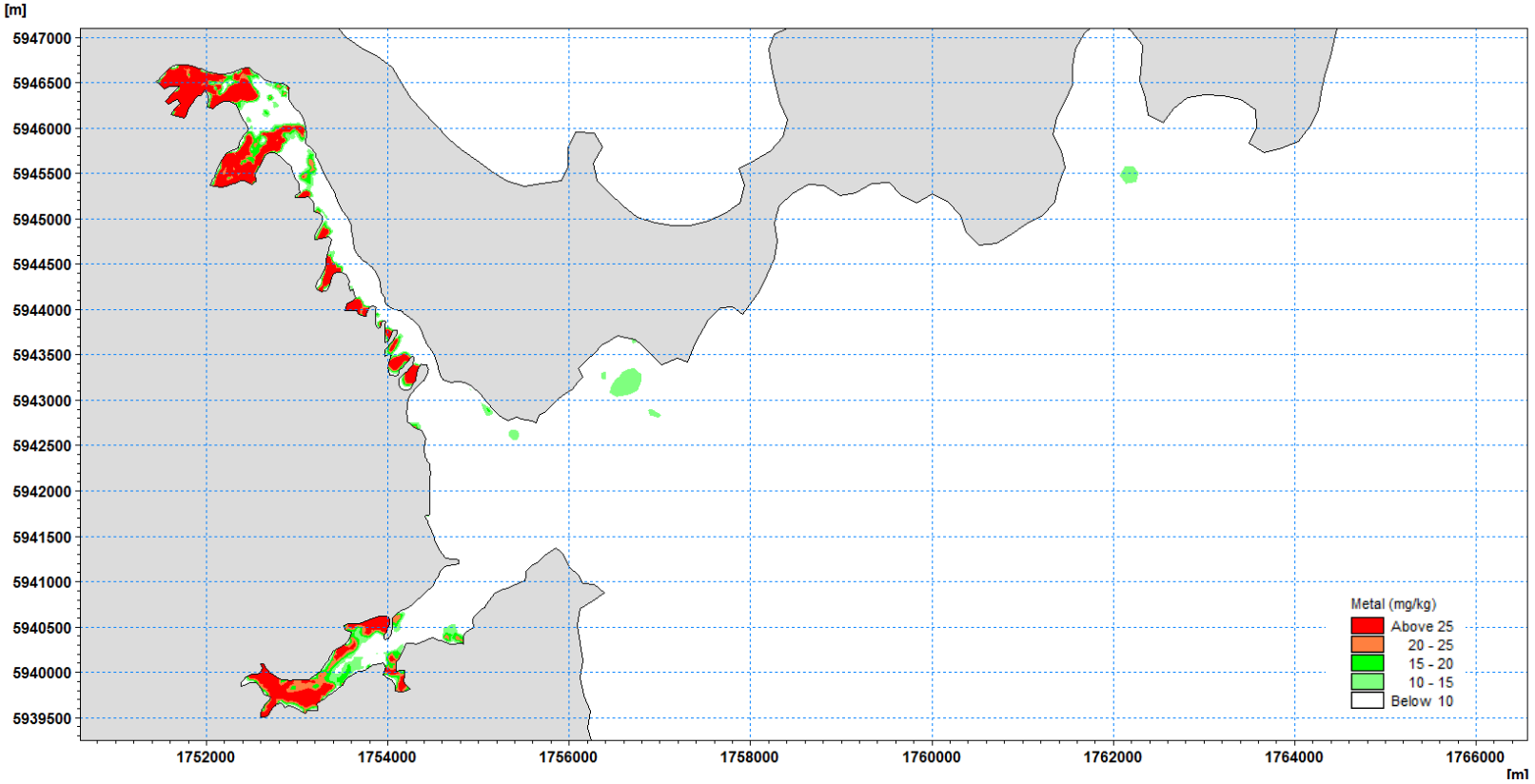

Figure 4-16. Future Copper concentrations (mg/kg) under Scenario 0 land use.

5 Conclusions

Future development within the catchments which surround the Wēiti and Okura estuaries may have accumulative effect on the marine receiving environment which, to date, has not been studied in detail.

Previous modelling studies have focused on development within the Okura catchment and potential ecological effects within Okura estuary itself. There has been limited work to date to assess the potential for the combined effects of sediment and contaminant loads from all of the catchments surrounding the Wēiti river and Okura estuary.

This report provides details of the calibration of a marine receiving environment model which uses predicted sediment and metal load inputs for current land use within the Wēiti-Okura-Long Bay catchments from the Freshwater Management Tool (FWMT) being developed for the Auckland Region.

The marine receiving environment model includes a coupled hydrodynamic model, wave model and sediment transport model which has been validated against field data collected with Karepiro Bay between March and July 2018 and a metal accumulation model which uses outputs from the sediment transport model and estimates of annual metal loads from the FWMT to estimate the long-term build-up of metal in surface sediments.

Both the wave and hydrodynamic components of the model are well calibrated and, as such, provide good predictions of the relative influences of tidally driven sediment transport (which dominants sediment transport processes with the Wēiti river and Okura estuary) and wave induced sediment transport (which is the key driver of sediment transport within Karepiro Bay).

Limited information on the variability of offshore sediment meant that the calibration of the observed bed level changes was problematic, but the calibrated sediment transport model still provides the basis for investigating the behaviour of catchment derived sediments in the context of existing bed sediment behaviour under a range of wind, tide and wave conditions.

Predicted bed level changes and suspended sediment concentrations at key sites have been extracted from a long-term model simulation to provide benchmark estimates to be compared to results from model predictions under future land use change scenarios.

Both the spatial and temporal variability of model results need to be considered when quantifying the potential impacts of catchment derived sediments on the marine receiving environment particularly when comparing the predictions for the different scenarios.

In addition, the calibrated models have been used to quantify the connectivity of the system. That is, to define the fate of sediment from each of the individual catchments.

Results from the modelling have shown that;

- The Upper Okura estuary and Wēiti River are the major sinks for catchment derived sediments with the area immediate offshore of Wēiti River and the deeper area of Karepiro Bay being secondary sinks,
- Around 70% of the Okura catchment silt load is deposited within the Okura estuary with nearly 15% deposited in the Wēiti river,
- Around 70% of the Wēiti catchment silt load is deposited within the Wēiti river with less than 15% deposited in the Okura estuary,
- Nearly 40% of the silt load from the Karepiro subcatchments is deposited in the Okura estuary and just over 30% of the silt load from the Karepiro subcatchments is deposited in the Wēiti river,

- There is no long-term deposition of catchment derived sediments on Karepiro Beach with this area dominated by the dynamics of offshore sediments, and
- Fine sediments from the Arkle Bay, Long Bay, Awaruku and North Outlet catchments are widely dispersed in the marine receiving environment and tend to settle in the deeper waters in the wider Karepiro Bay.

Outputs from the sediment transport model have been used as the basis for calibrating a metal accumulation model which replicates current day levels of both Zinc and Copper in surface sediments. The metal accumulation model has been used to forecast future levels of Zinc and Copper in surface sediments and identifies areas within the marine receiving environment where a combination of higher deposition rates and high ratios of metal to sediment load lead to the highest increases in metal concentrations in surface sediments.

6 References

DHI, 2018. Okura Wēiti Sediment Transport Modelling - Data report 44801163/01 prepared for Auckland Council.

DHI, 2017a. MIKE 21 Flow Model FM, Hydrodynamic Module, User Guide.

DHI, 2017b. MIKE 21 SW, Spectral Wave FM Module, User Guide.

DHI, 2017c. MIKE 3 Flow Model FM, Mud Transport Module, User Guide.

DHI, 2017d. MIKE C-MAP, Extraction of World Wide Bathymetry Data and Tidal Information, User Guide.

Green, M.O. 2008. Central Waitemata Harbour Contaminant Study. Predictions of Sediment, Zinc and Copper Accumulation under Future Development Scenario 1. Prepared by NIWA Ltd for Auckland Regional Council. Auckland Regional Council Technical Report 2008/043.

Green, M.O. 2016. Assessment of Potential Effects of Land Development on Okura Estuary. Estimates of Metal Accumulation in the Estuary. Extension of Model and Review of Model Parameters. Report TOD1601–1, Streamlined Environmental.

Greig, M.J., 1990. Circulation in the Hauraki Gulf, New Zealand. N. Z. J. Mar. Freshw. Res. 24, 141–150.

Mills, G N 2016. Long Bay sediment contaminant monitoring: a review of data collected from 1998 to 2013. Prepared by Diffuse Sources Ltd for Auckland Council. Auckland Council Technical Report, TR2016/037

Morphum Environmental 2019. Long Bay/ Okura Freshwater Management Tool Study.

Moulton, M., Elgar, S., Raubenheimer, B., 2014. Improving the time resolution of surfzone bathymetry using in situ altimeters. Ocean Dyn. 64, 755–770.

NIWA, 2008. Sediment in the Okura-Wēiti-Karepiro Bay System.

Partheniades, E., 1965. Erosion and deposition of cohesive soils. J. Hydraul. Div. 91, 105–139.

Pritchard, M.E., Reeve, G., Swales, A., 2009. Modelling storm-load sediment deposition thresholds for potential ecological effects in Okura Estuary / Karepiro Bay: Model development and calibration. NIWA Client Report No. HAM2009–106.

Reed, J. 2008. Central Waitemata Harbour Study. Background Metal Concentrations in Soils: Methods and Results. Auckland Regional Council Technical Report 2008/033.

Swales, A., Gibbs, M., Ovenden, R., Budd, R., Hermansphan N. 2008. Sedimentation in the Okura-Weiti-Karepiro Bay system. Auckland Regional Council Technical Report 2008/026.

Stroud, M.J., Cooper, A.B., Bottcher, A.B., Hiscock, J.G., Pickering, N.B., 1999. Sediment Runoff from the Catchment of Okura Estuary. ARC90241/1.

Yalden, S. and Moores, J. 2014. Assessment of Potential Effects of Land Development on Okura Estuary. Report prepared for Todd Property Group.

Zuo, L., Roelvink, D., Lu, Y., Li, S., 2017. On incipient motion of silt-sand under combined action of waves and currents. Appl. Ocean Res. 69, 116–125.

Appendix A.1: Linkages between the FWMT catchment (ME) outlets on the marine receiving environment inputs.

MIKE 3 Sites	Morphum Environmental Sites	Catchment Area (ha)
North Outlet	100823, 100284	82.6
Awaruku	100291, 100292	97.2
Long Bay	100285, 100286, 100290	120.9
SS Outer	100282	69.3
SS Mid-East	100279, 100280	93.8
SS Mid-West	100278	93.3
SS Inner	100277	105.1
Redvale	100260, 100270, 100274, 100275, 100276	204.6
North Arm	100251, 100252, 100257, 100258	235.6
North Shore	100250	85.9
Karepiro	100244, 100249	186.8
Karepiro Beach	100245	31.7
Stillwater	100240, 100241, 100242, 100243	161.5
Wēiti South	100233	44.9
Silverdale	100205, 100206, 100225, 100226, 100227, 100228, 100230, 100231, 100232	451.5
Arkle Bay	100201, 100202	45.5
Whangaparaoa	100204*	167.6
Wēiti North	100204*	
Duck Creek	100239	154.7

* River flows at the Whangaparaoa and Wēiti North locations in MIKE 3 were extracted from Site 100204 applying 50% of the original river flow.

Appendix A.2: Summary of NIWA (2009) and DHI (2019) Model Setups

DHI MIKE3 FM	Parameters	Pritchard et al. (2009)	DHI (2019)
Model Simulation time		10 days	6 months
Bed roughness	Z0	0.05	
Horizontal mixing **Lower limit** **Upper limit**	Smagorinsky coefficient	0.28 1.8e-006 m^2/s 10 m^2/s	0.28 0.1 100
Vertical mixing	C_{my} C_{1e} C_{2e} C_{3e} Prandtl number Turbulent kinetic energy Dissipation of turbulent kinetic energy	0.09 1.44 1.92 0 0.9 1.0 1.2	0.09 1.44 1.92 0 0.9 1.0 1.3
Salinity scaling factor		1.1	1.0
Bed erosion	Erosion rate ($kg/m^2/s$) Power term	6e-005 4.3	5e-005 4.3
Erosion critical shear stress	ρ_e	Constant 0.2 N/m^2	Spatially varying 0.125 N/m^2 Inter-tidal areas 0.150 N/m^2 Sub-tidal areas 0.425 N/m^2 Offshore
Deposition critical shear stress	ρ_d	0.1 N/m^2	0.1 N/m^2
Number of catchment sources		4	20
		Scaled flow and SSC from Awanohi data Trapezoidal hydrograph and associated SSC time-series	Calibrated FWMT outputs (flow and three grain size SSC) at 15 minute interval,

DHI MIKE3 FM	Parameters	Pritchard et al. (2009)	DHI (2019)
Grain sizes considered		Three grain sizes modelled independently (assuming all load is associated with an individual grain size) with a constant fall velocity 4 µm (“washload”) 15 µm (fine silt, 0.0002 m/s fall velocity) 40 µm (coarse silt)	Three grain sizes modelled together accounting for flocculation processes Clay 0.000021 m/s Silt 0.0002 m/s Fine sand 0.01 m/s
Wave forcing		None	Full spectral wave model
Tidal boundary condition		Sinusoidally varying synthetic tide representing a spring or neap tide	Broad scale tidal forcing from tidal analysis of Port Charles tide record with inclusion of wind effects
Wind Conditions		Fixed wind of 7.5 m/s from the south-west and calm winds	Spatially varying wind speed and direction validated against observations
Existing bed sediments		None	Spatially varying bed thickness representative of observed sediments in the surface mixed layer

Appendix A.3: Depostional footprints for individual subcatchments

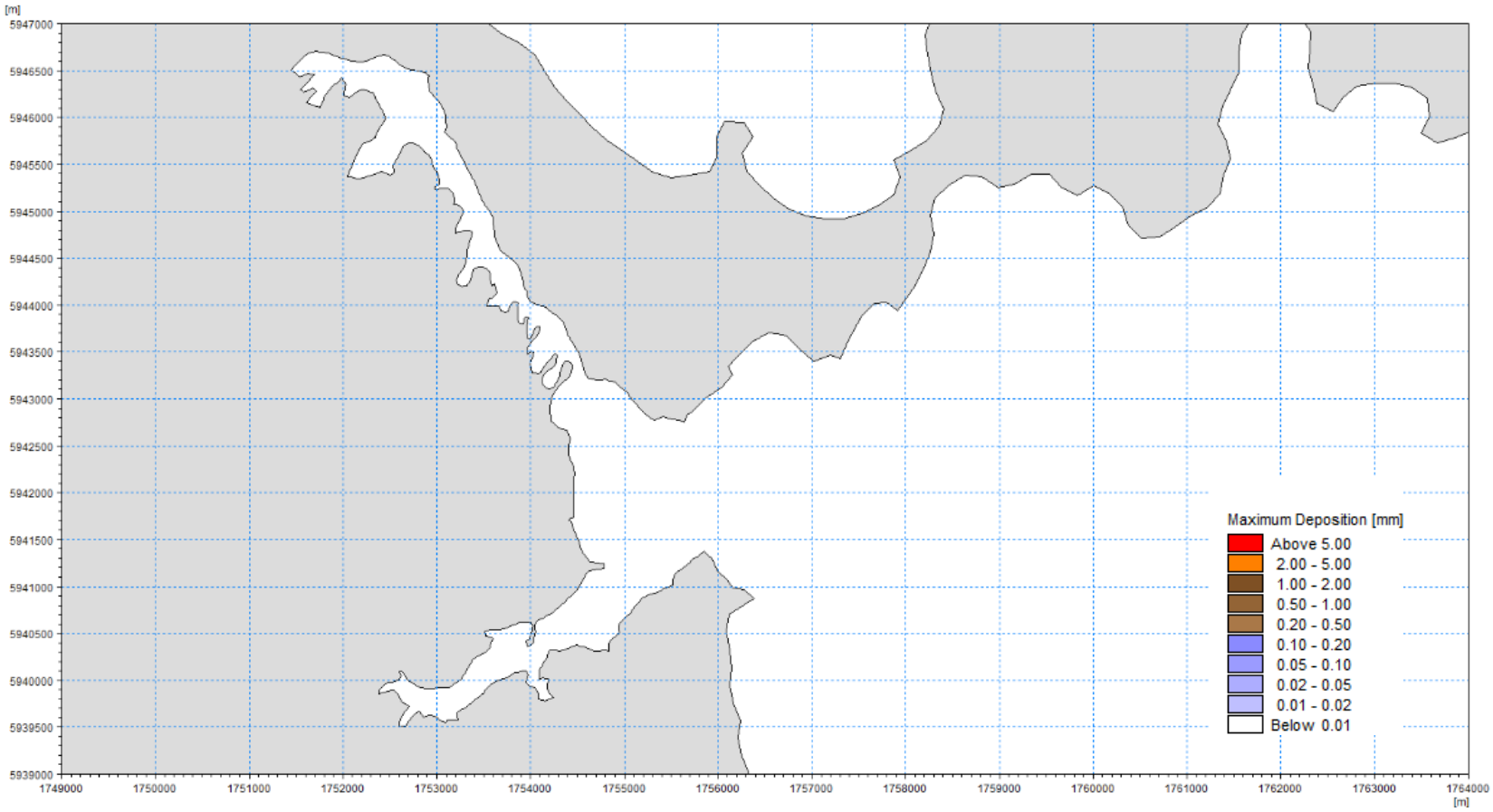

Figure 6-1. Predicted maximum deposition (mm) over the period January-June 2018 from catchment derived silts from the Awaruku catchment. Predictions indicate very low deposition rates (< 0.01 mm) across the model domain.

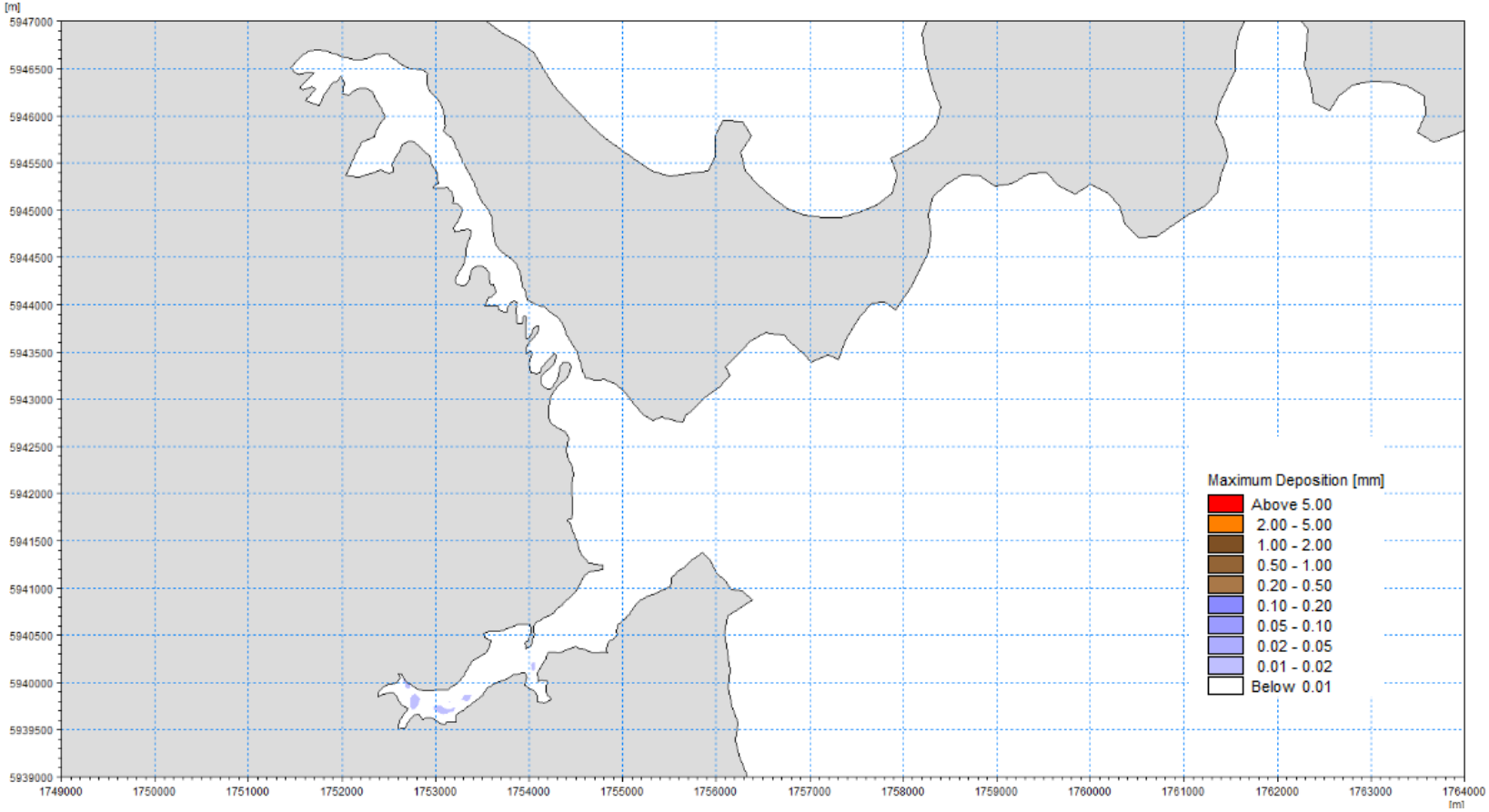

Figure 6-2. Predicted maximum deposition (mm) over the period January-June 2018 from catchment derived silts from the Long Bay catchment. Predictions indicate very low deposition rates (< 0.01 mm) across the model domain.

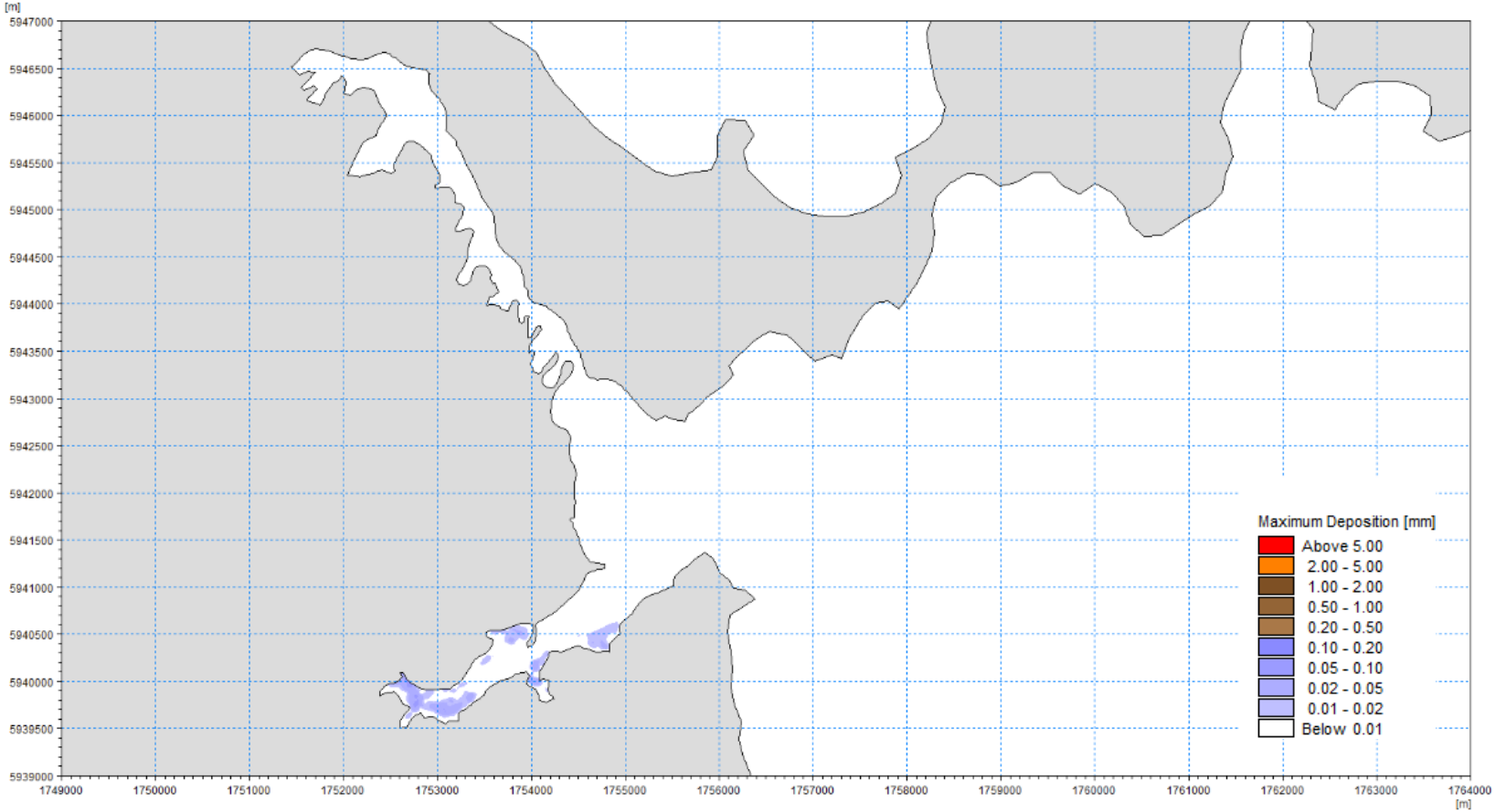

Figure 6-3. Predicted maximum deposition (mm) over the period January-June 2018 from catchment derived silts from the SS Outer catchment.

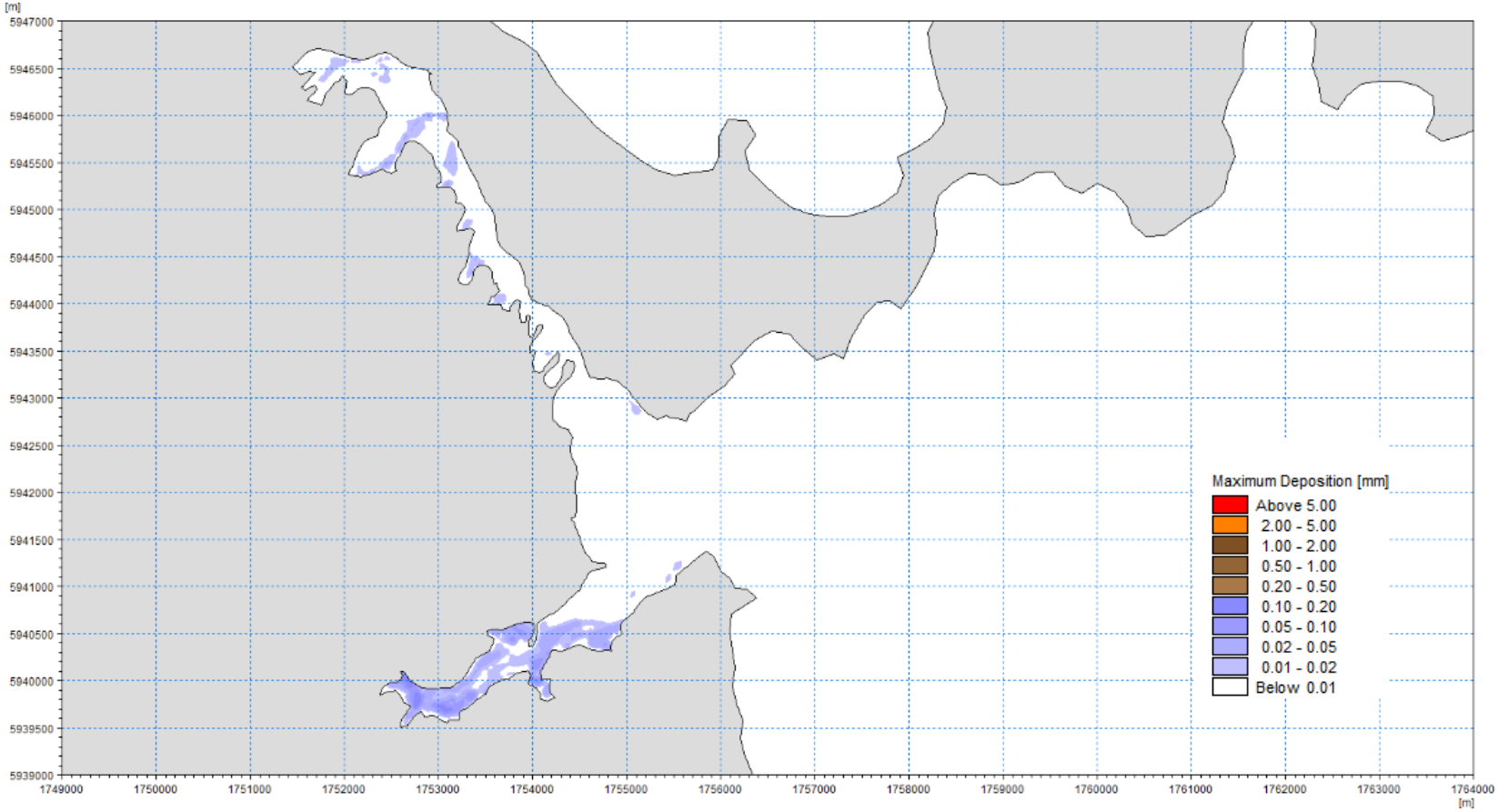

Figure 6-4. Predicted maximum deposition (mm) over the period January-June 2018 from catchment derived silts from the SS Mid-East South catchment.

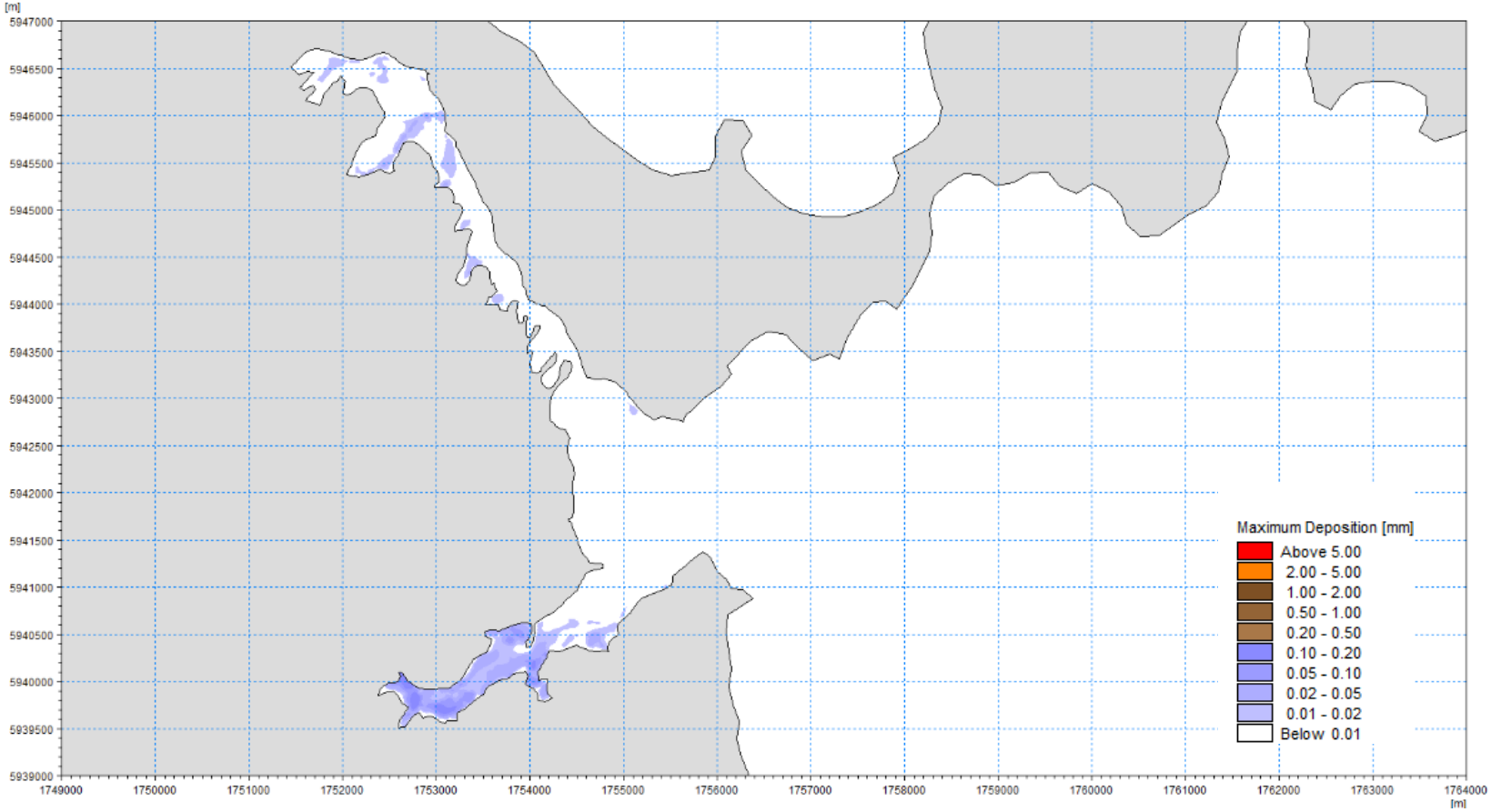

Figure 6-5. Predicted maximum deposition (mm) over the period January-June 2018 from catchment derived silts from the SS Mid-West catchment.

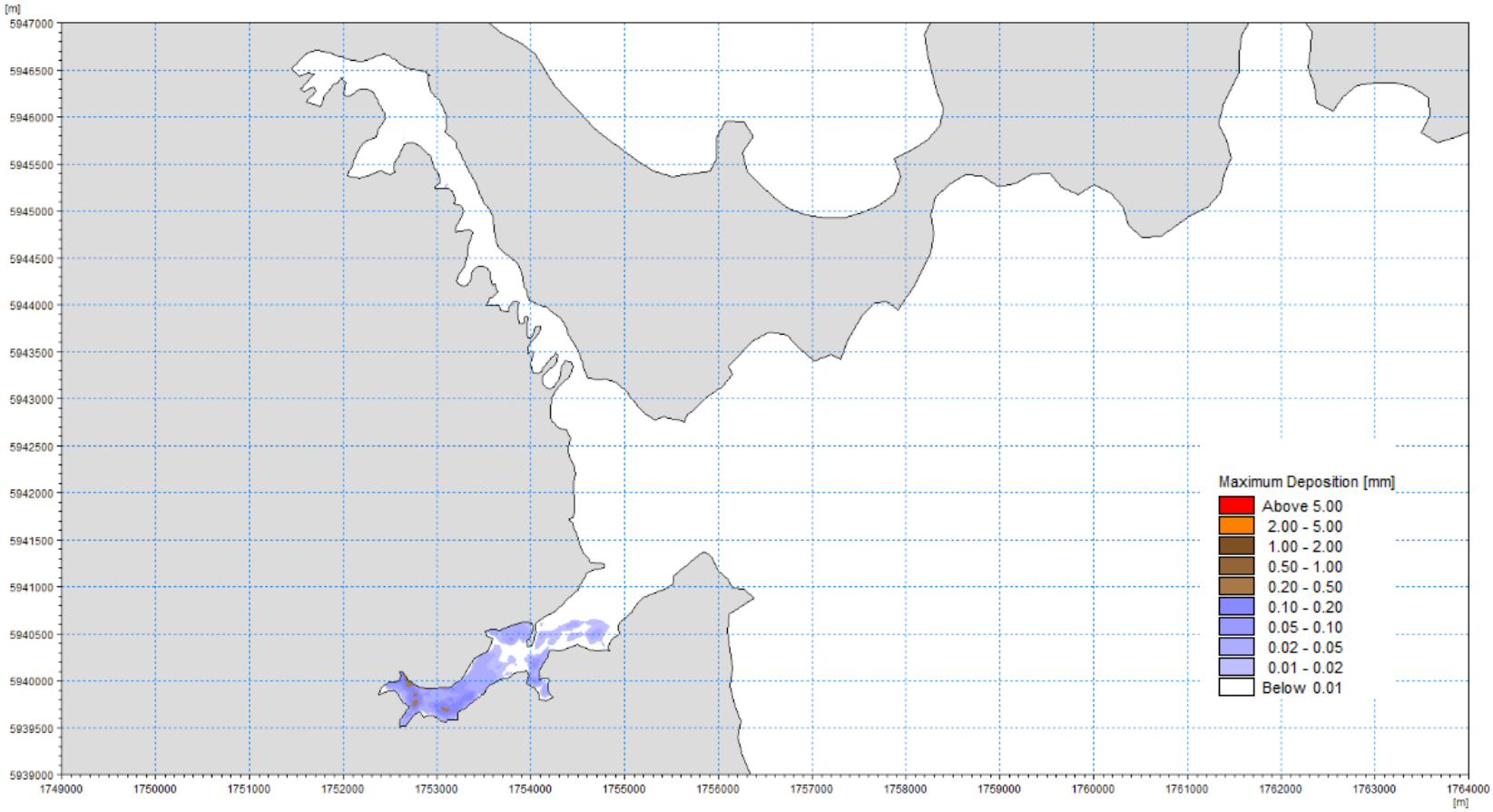

Figure 6-6. Predicted maximum deposition (mm) over the period January-June 2018 from catchment derived silts from the SS Inner catchment.

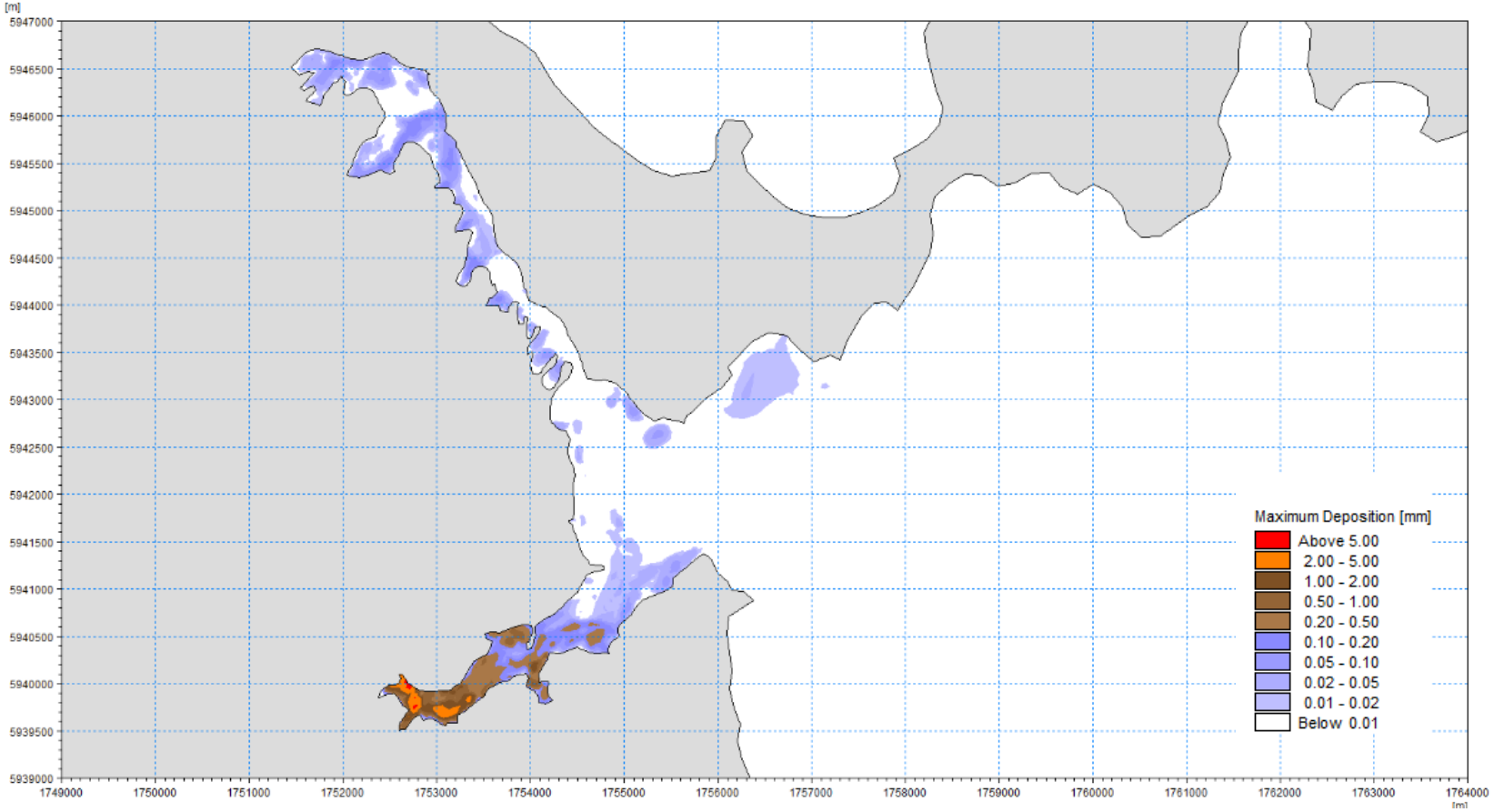

Figure 6-7. Predicted maximum deposition (mm) over the period January-June 2018 from catchment derived silts from the Redvale catchment.

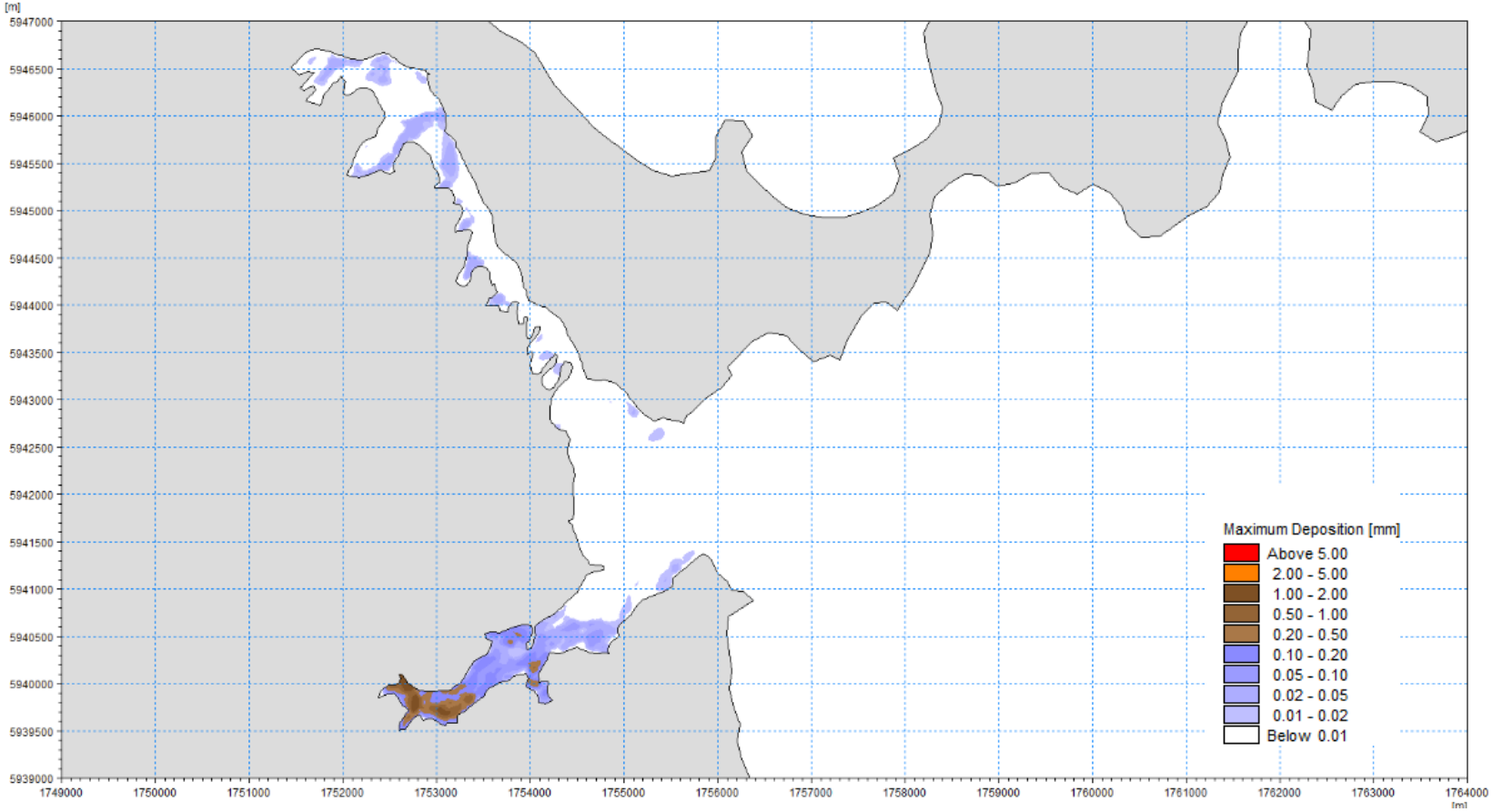

Figure 6-8. Predicted maximum deposition (mm) over the period January-June 2018 from catchment derived silts from the North Arm catchment.

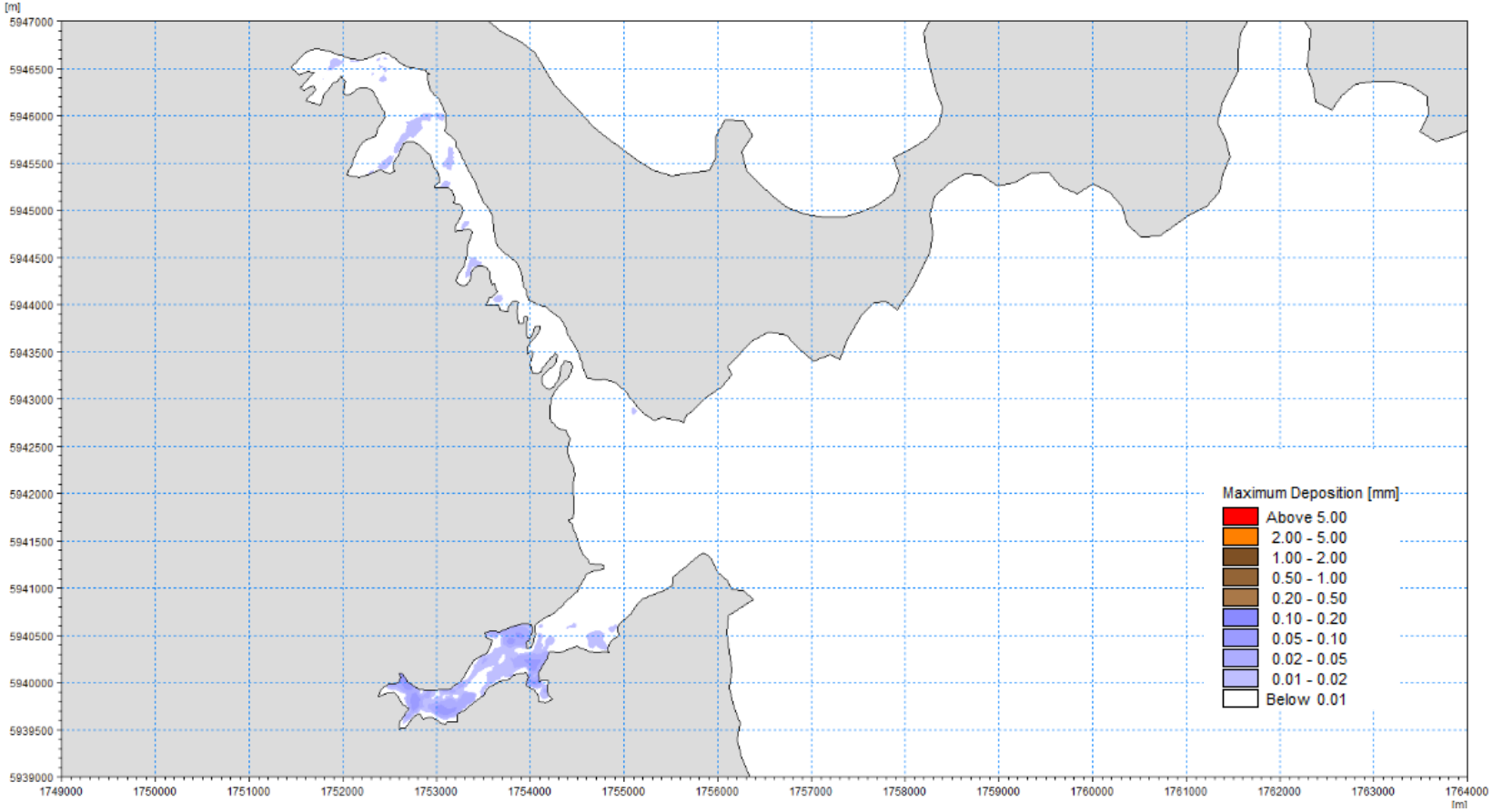

Figure 6-9. Predicted maximum deposition (mm) over the period January-June 2018 from catchment derived silts from the North Shore catchment.

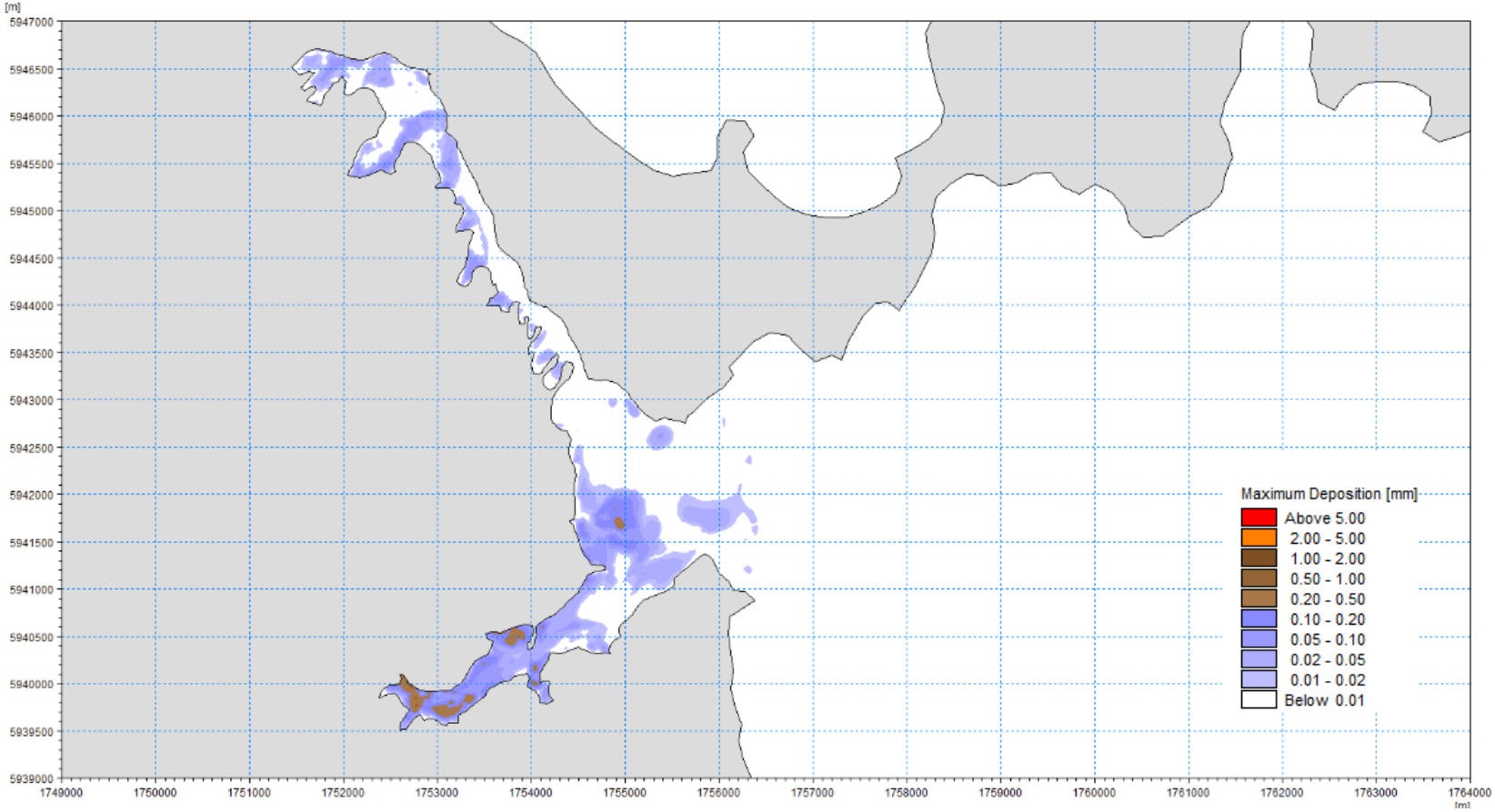

Figure 6-10. Predicted maximum deposition (mm) over the period January-June 2018 from catchment derived silts from the Karepiro catchment.

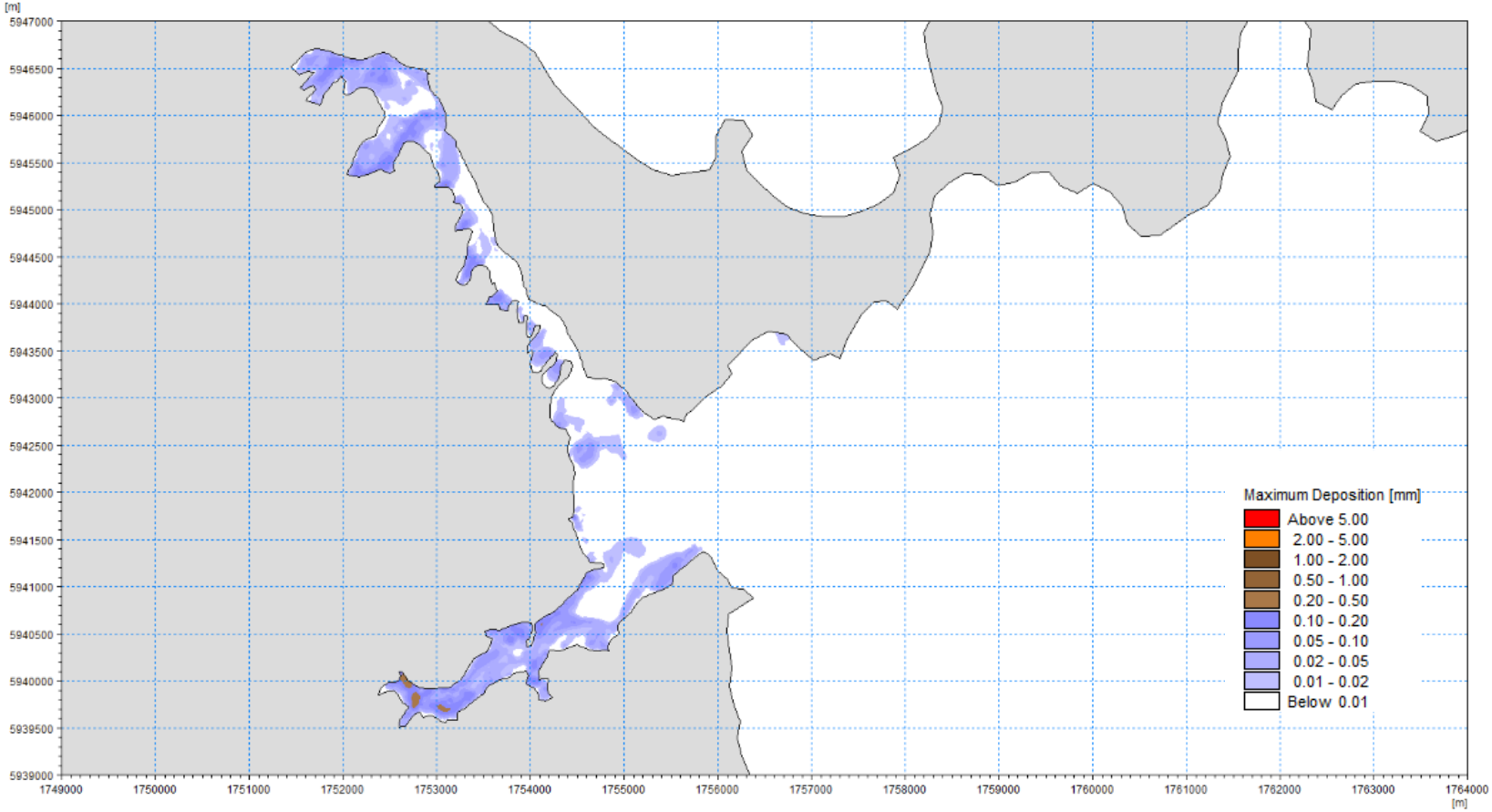

Figure 6-11. Predicted maximum deposition (mm) over the period January-June 2018 from catchment derived silts from the Karepiro Beach catchment.

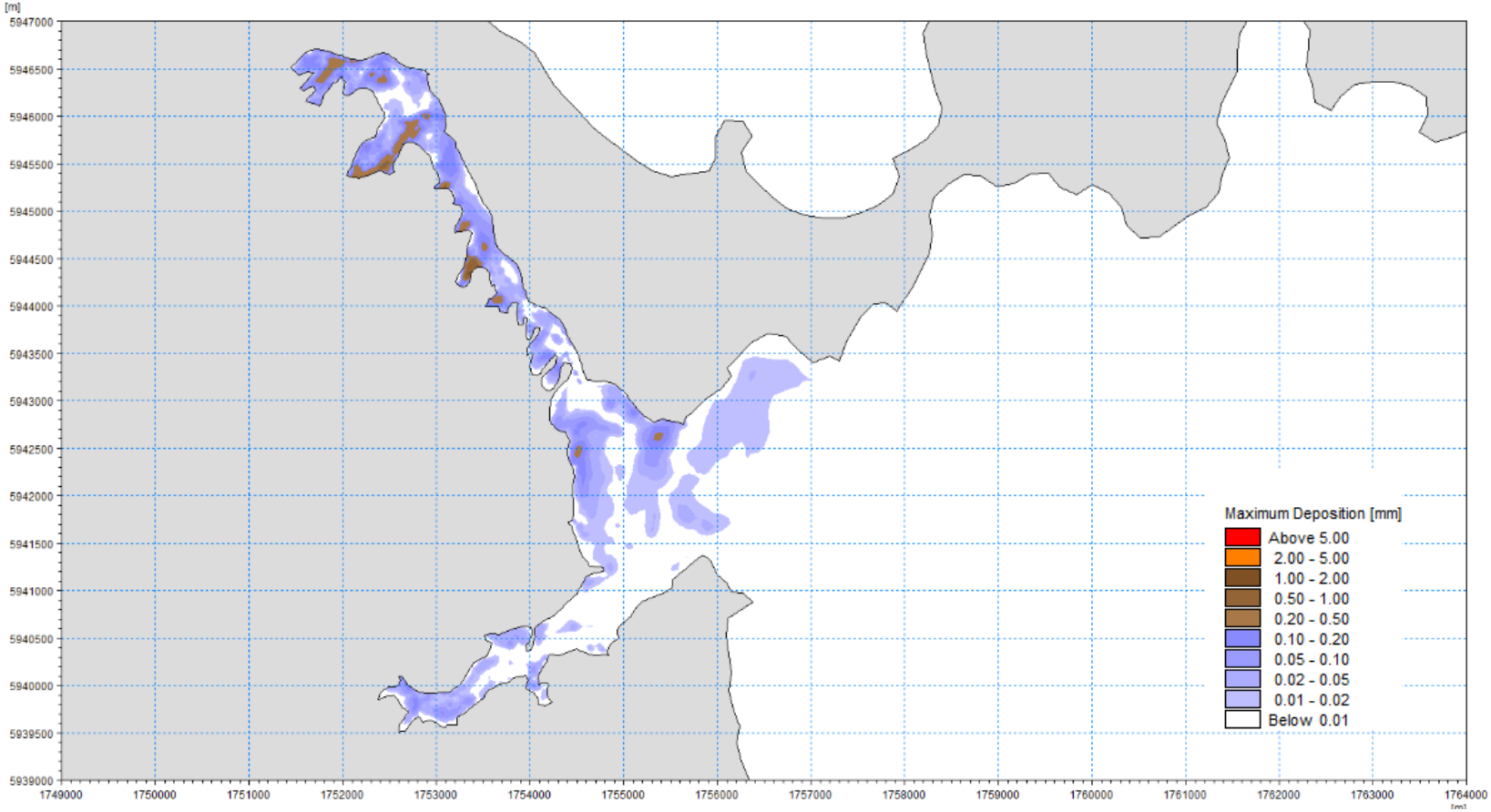

Figure 6-12. Predicted maximum deposition (mm) over the period January-June 2018 from catchment derived silts from the Stillwater catchment.

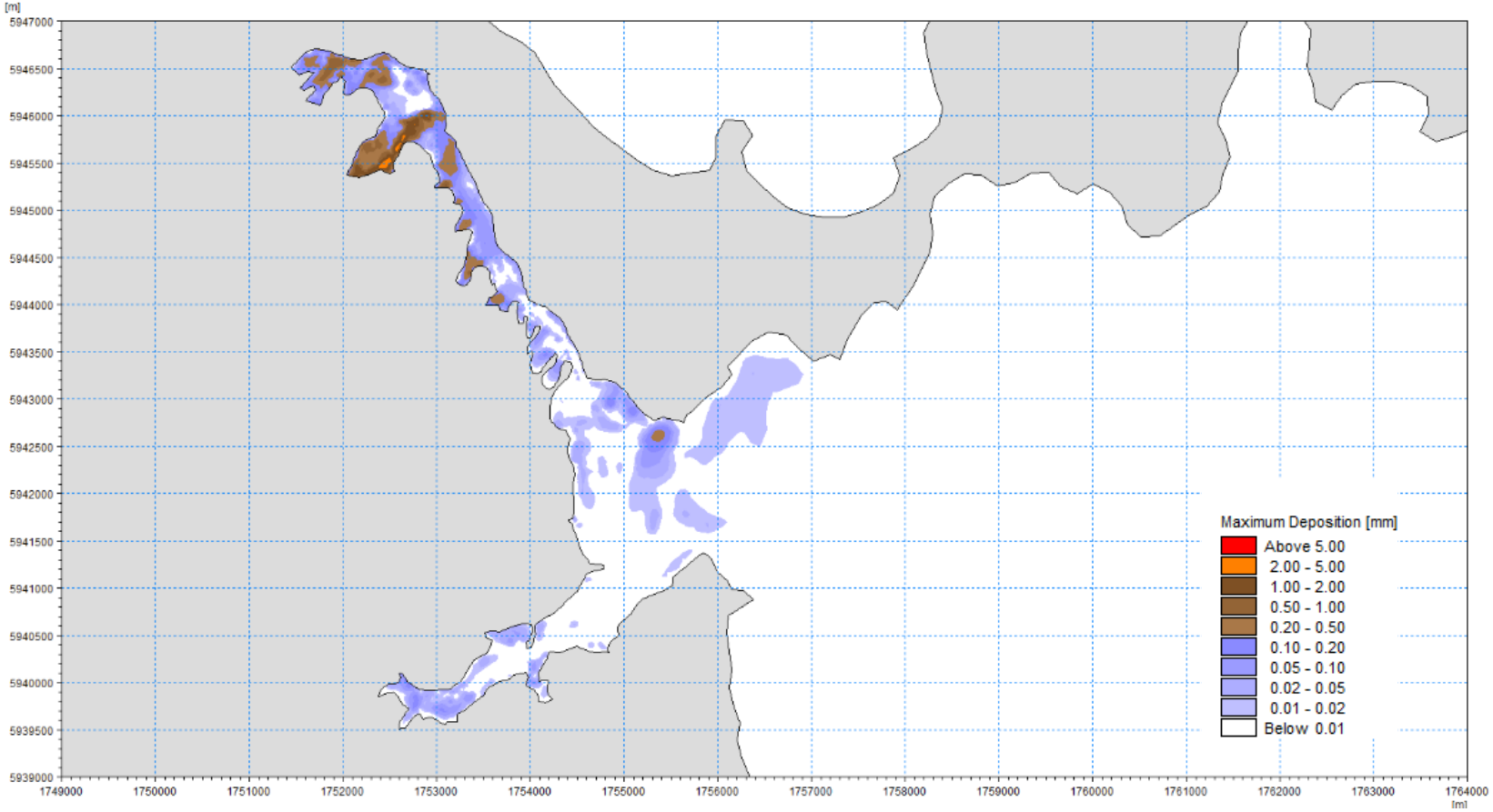

Figure 6-13. Predicted maximum deposition (mm) over the period January-June 2018 from catchment derived silts from the Wēiti South catchment.

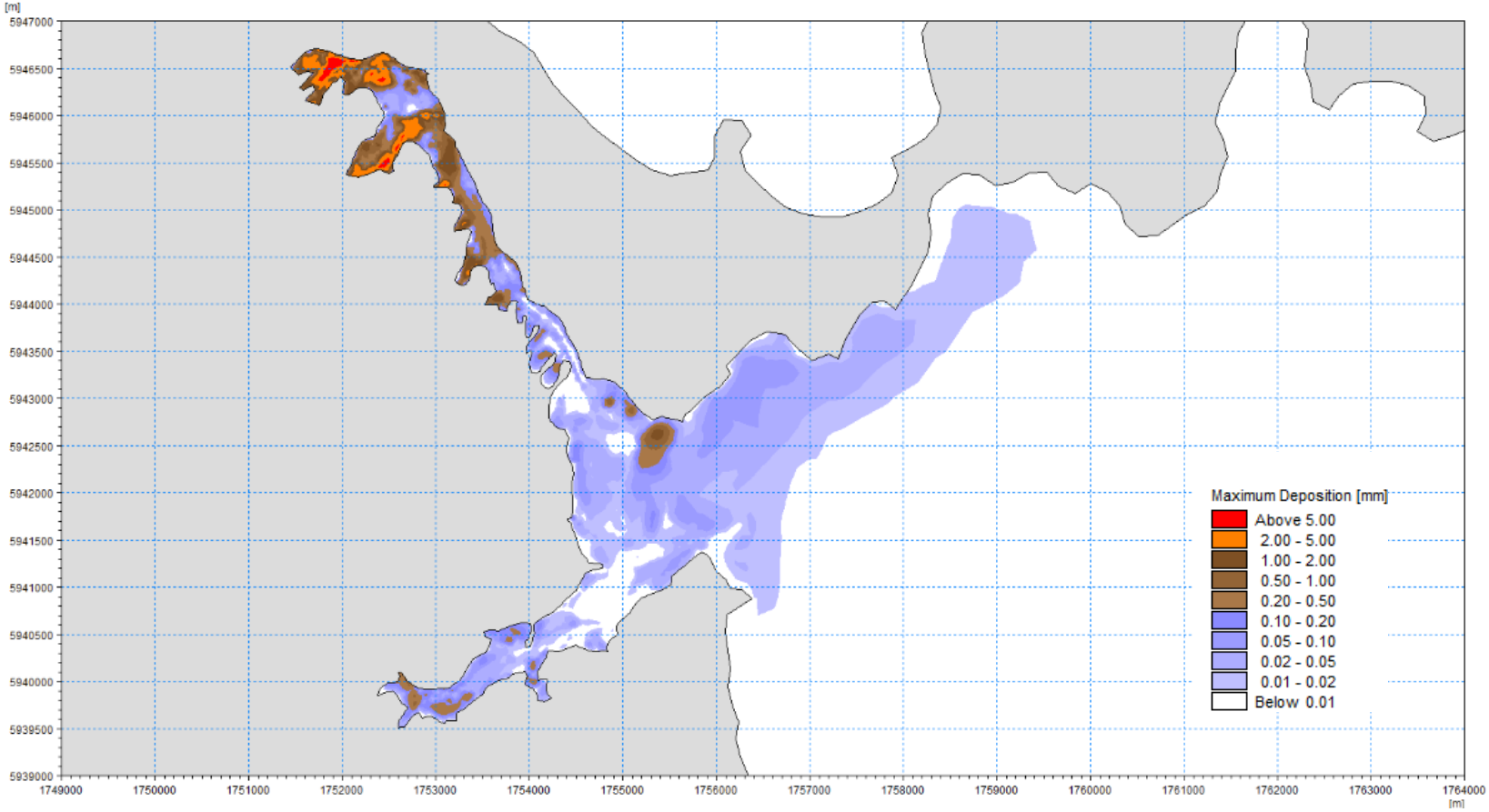

Figure 6-14. Predicted maximum deposition (mm) over the period January-June 2018 from catchment derived silts from the Silverdale catchment.

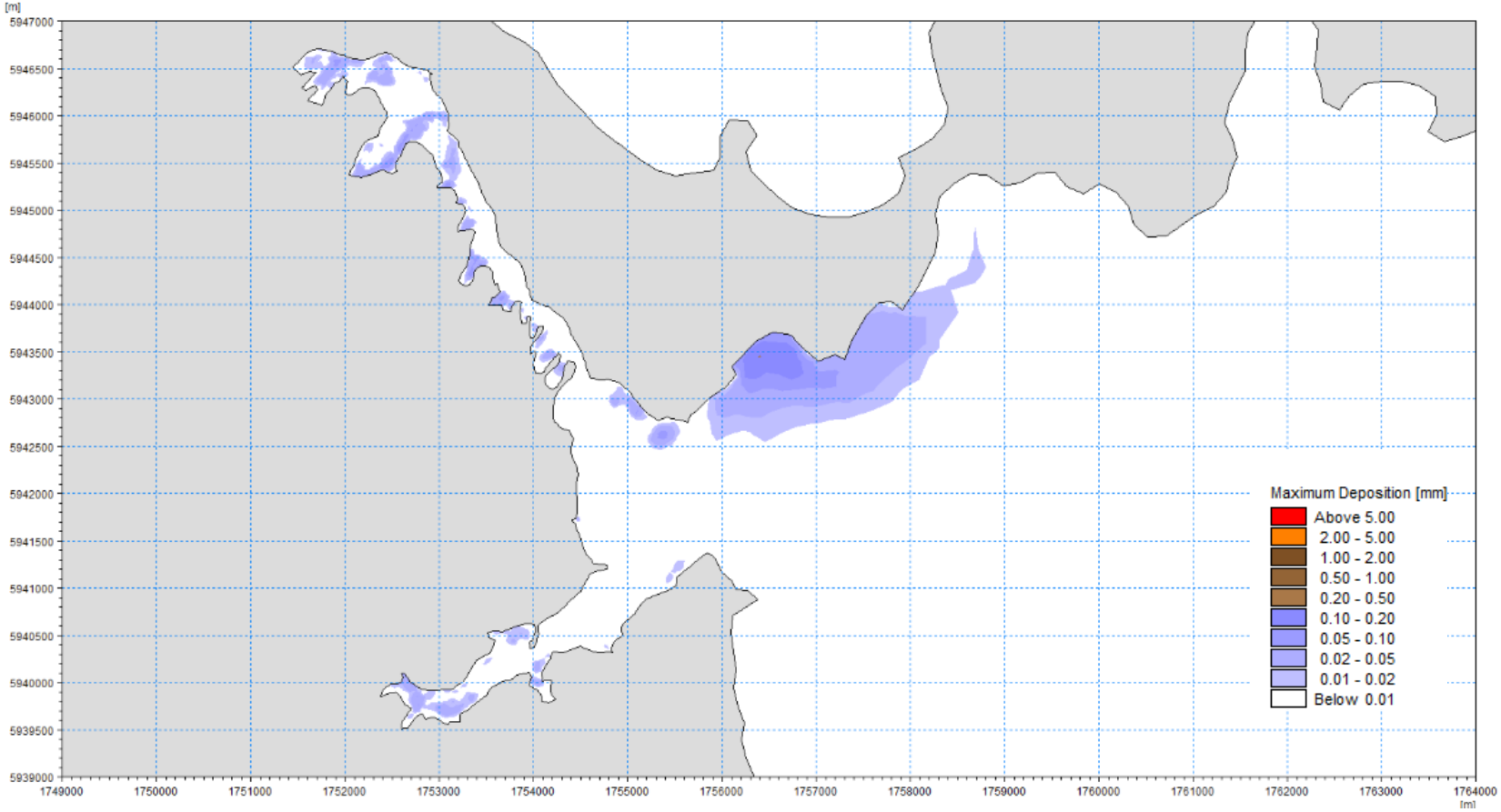

Figure 6-15. Predicted maximum deposition (mm) over the period January-June 2018 from catchment derived silts from the Arkle Bay catchment.

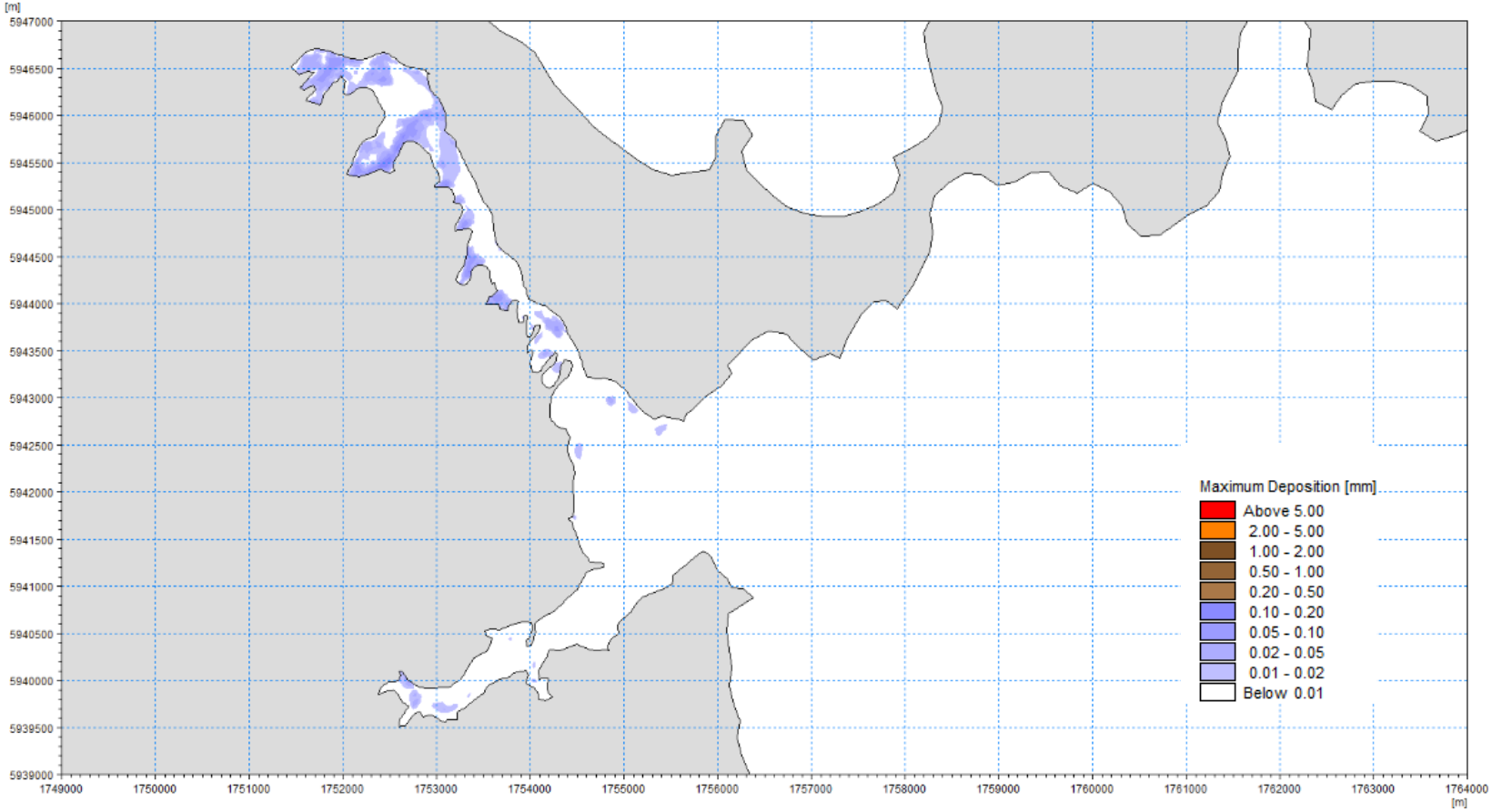

Figure 6-16. Predicted maximum deposition (mm) over the period January-June 2018 from catchment derived silts from the Whangaparaoa catchment.

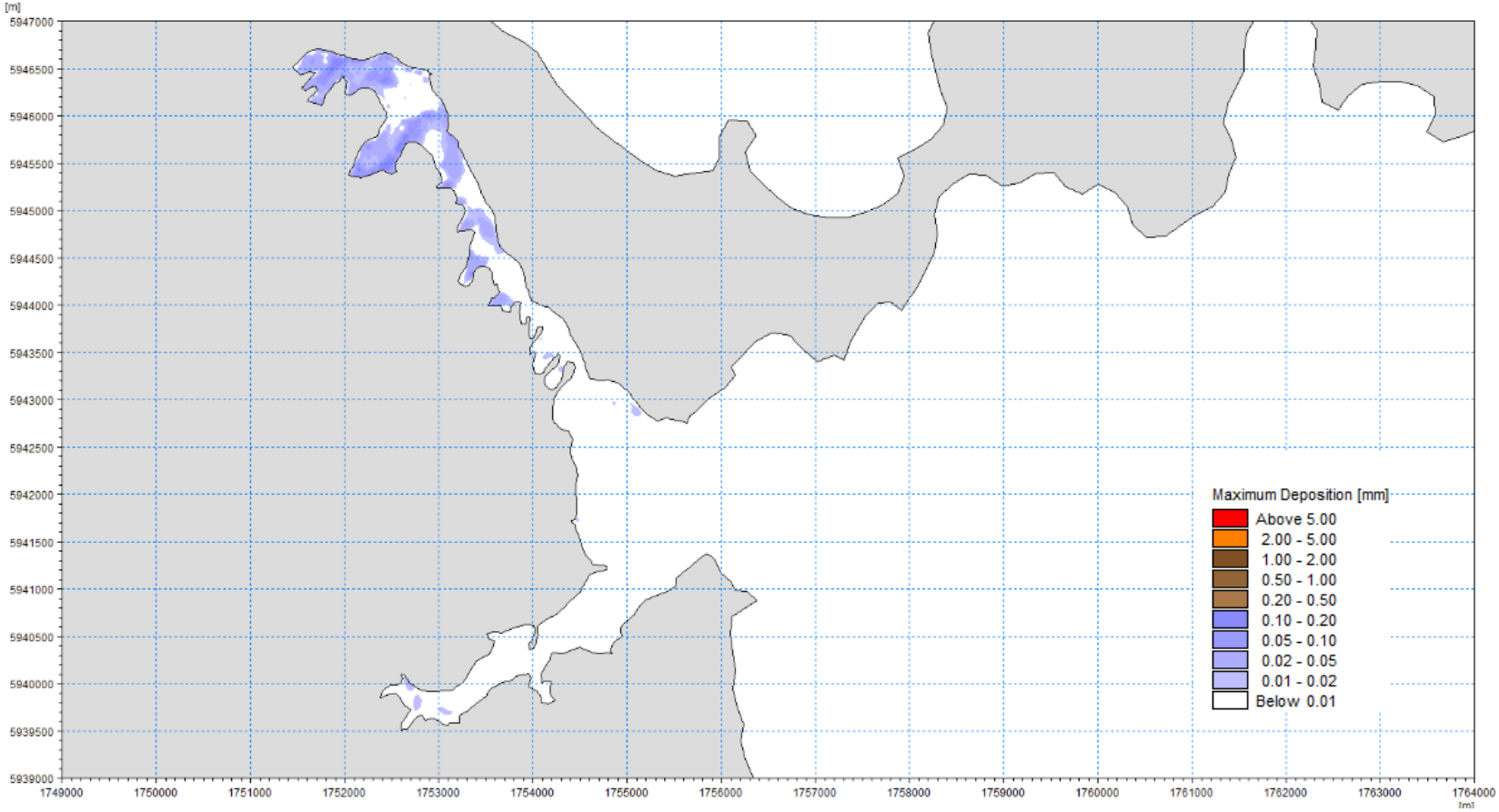

Figure 6-17. Predicted maximum deposition (mm) over the period January-June 2018 from catchment derived silts from the Wēiti North catchment.

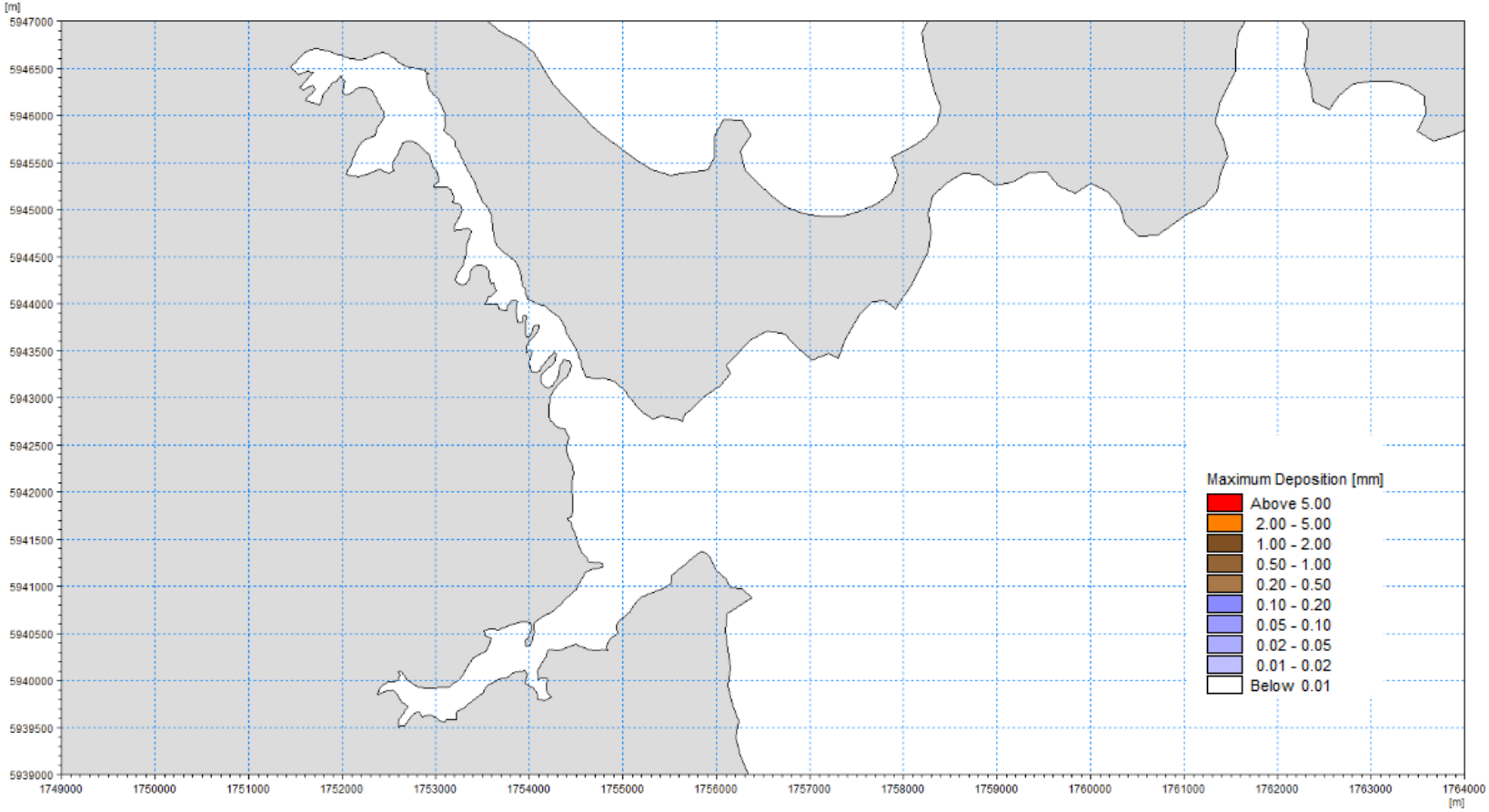

Figure 6-18. Predicted maximum deposition (mm) over the period January-June 2018 from catchment derived silts from the North Outlet catchment. Predictions indicate very low deposition rates (< 0.01 mm) across the model domain.

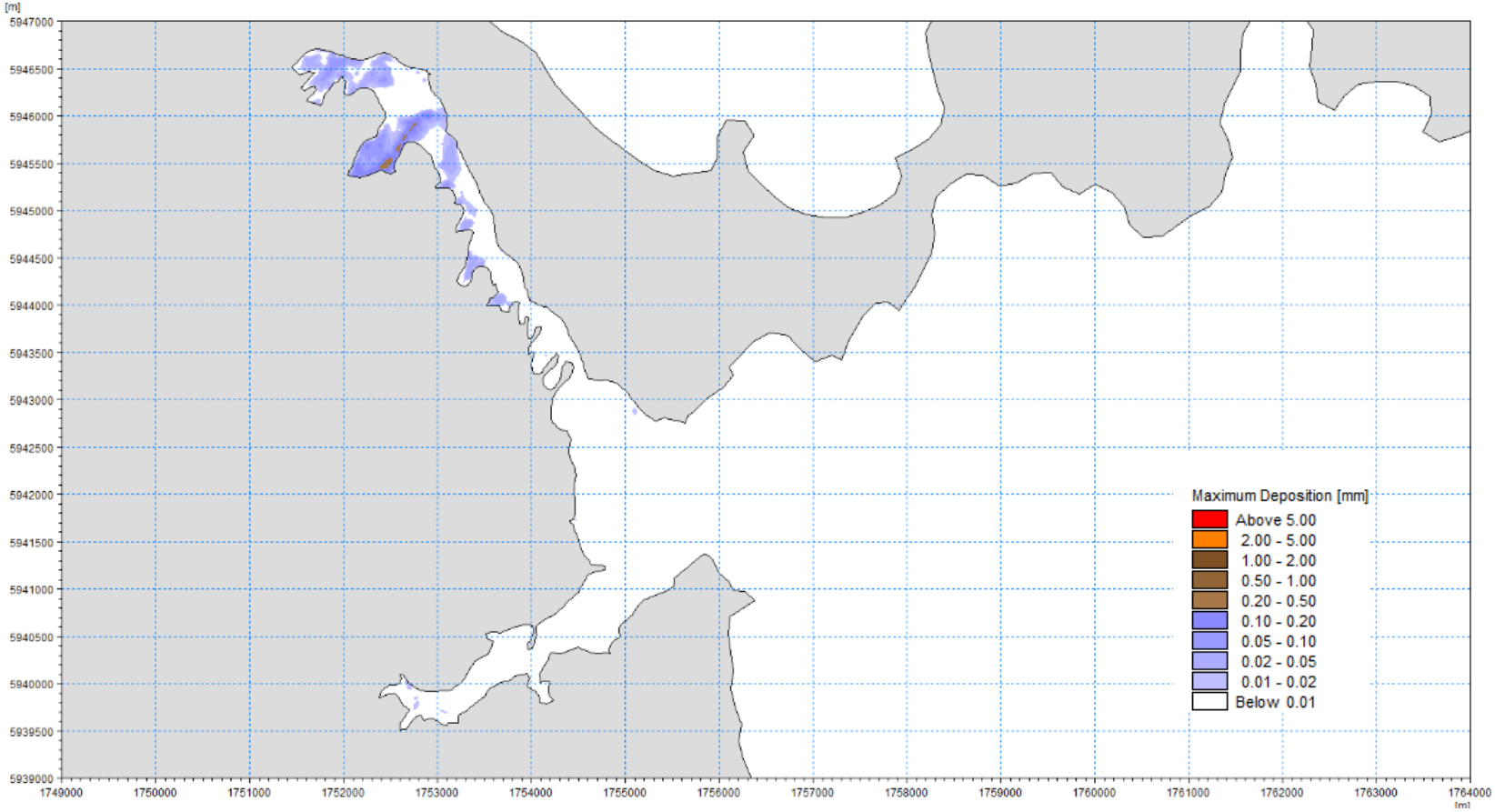

Figure 6-19. Predicted maximum deposition (mm) over the period January-June 2018 from catchment derived silts from the Duck Creek catchment.

Appendix A.4: Metal Accumulation Model Methodology

The metal accumulation model works at a subestuary scale to derive an equilibrium metal concentration. Thus, for each subestuary the following methodology is applied.

It is assumed that there is a surface mixed layer on seabed that is uniformly mixed to a depth of λ (m) during each year by a combination of physical and bioturbation processes. Thus, at the end of each year, the sediment in the surface mixed layer consists of the sediment deposited from the catchment mixed uniformly with the existing bed sediments.

The mass of catchment derived sediment that accumulates on the seabed (*S*) over the course of a year is given by:

$$S_c = \rho\eta \text{ (kg/m}^2\text{)} \quad (1)$$

where η is the sediment deposition rate (m/y) derived from the sediment transport model and ρ is the density (kg/m^3) of the bed sediments (assumed to be 1200 kg/m^3).

At the end of the year (t = 1) the sediment in the surface mixed layer consists of the catchment derived sediment deposited during the year mixed uniformly to a depth of $(\lambda - \eta)$ metres with pre-existing sediments. Hence, at the end of the year, the mass of sediment per unit area of seabed exhumed to a depth of $(\lambda - \eta)$, metres given by:

$$S_e = \rho(\lambda - \eta) \text{ (kg/m}^2\text{)} \quad (2)$$

The total mass of sediment per unit area of seabed in the surface mixed layer at the end of the year (S_t) is given by the sum of sediment deposited (S_c) and sediment exhumed (S_e):

$$S_t = \rho\eta + \rho(\lambda - \eta) \text{ (kg/m}^2\text{)} \quad (3)$$

Assuming that the catchment derived sediment deposited during the course of the year carries metal at a concentration of C_c (kg metal / kg sediment), the mass of catchment derived metal that accumulates on the seabed per unit area of seabed over the year is:

$$M_c = \rho\eta C_c \text{ (kg)} \quad (4)$$

At the beginning of the simulation period (time = 0) the metal concentration in the seabed surface mixed layer is C_0 (kg metal / kg sediment). The mass of metal per unit area of seabed that is exhumed from below during the year is:

$$M_e = \rho(\lambda - \eta)C_0 \text{ (kg)} \quad (5)$$

Hence, the total mass of metal in the surface mixed layer at the end of the year is:

$$M_t = \rho[\eta C_c + (\lambda - \eta)C_0] \text{ (kg)} \quad (6)$$

The metal concentration in the surface mixed layer at the end of the year, C_1, is given by the total mass of metal in the surface mixed layer (M_t) divided by the total mass of sediment in the surface mixed layer:

$$C_1 = \frac{\rho[\eta C_c + (\lambda-\eta)C_0]}{\rho\lambda} \text{ (kg metal/kg sediment)} \quad (7)$$

Which reduces to:

$$C_1 = \frac{[\eta C_c + (\lambda-\eta)C_0]}{\lambda} \text{ (kg metal/kg sediment)} \quad (8)$$

For the following year, the initial concentration (C_0) becomes the predicted concentration at the end of year C_1, hence:

$$C_2 = \frac{[\eta C_c + (\lambda - \eta) C_1]}{\lambda} \text{ (kg metal/kg sediment)} \quad (9)$$

Catchment sediment and metal load data is used to define the source concentration for each of the subcatchments (Table 2-3). Outputs from the sediment transport model are used to determine the contribution that each subcatchment makes to the overall deposition in each subestuary (Table 4-2 through to Table 4-5). For each subestuary (Figure 4-13), C_c can then be derived by summing the percent contribution to the overall deposition of each subcatchment by the predicted subcatchment source concentration.

Repeating this calculation for each subestuary we derive C_c for each subestuary.

Data from the sediment transport model is used to define η for each subestuary and global values of C_o and λ are assumed based on observations.

Zinc and Copper concentrations in the surface mixed layer of each subestuary are then derived starting with equation 8 and iterating equation 9 over a 50-year interval.